UNIVERSITÉ DU QUÉBEC

THESIS PRESENTED TO THE
UNIVERSITY OF QUEBEC AT CHICOUTIMI
IN PARTIAL FULFILMENT OF
THE REQUIREMENT FOR THE DEGREE
OF DOCTOR OF PHYLOSOPHY IN ENGINEERING

BY
SAYYED MAHDI ALE-EMRAN

DESIGN OF BOOSTER SHED PARAMETERS FOR IMPROVING THE ELECTRICAL PERFORMANCE OF POST INSULATORS UNDER ICING CONDITIONS

DECEMBER 2013

UNIVERSITÉ DU QUÉBEC

THÈSE PRÉSENTÉE À
L'UNIVERSITÉ DU QUÉBEC À CHICOUTIMI
COMME EXIGENCE PARTIELLE
DU DOCTORAT EN INGÉNIERIE

PAR
SAYYED MAHDI ALE-EMRAN

CONCEPTION DES PARAMÈTRES DES JUPES AUXILIAIRES POUR AMÉLIORER LES PERFORMANCES ÉLECTRIQUES DES ISOLATEURS DE POSTE DANS DES CONDITIONS DE GIVRAGE

DÉCEMBRE 2013

ABSTRACT

The optimized design of outdoor insulators that consider heavy icing and pollution conditions is a significant concern for the reliability of power networks. Based on field observations, the probability of flashover of EHV post insulators is higher than line insulators under the same heavy icing conditions. The flashover along the insulators is caused mainly by the presence of a water film on the ice surfaces (melting period) and partial arcs in ice-free zones (air gaps).

One of the mitigation options is the use of booster sheds (BSs) to create air gaps along the iced insulator. A booster shed (BS) is a flexible c-shape device made of high-quality insulating materials. Since BSs are easy to use, they seem to be simpler alternatives to upgrading insulators to those designed for cold climate regions. Despite the promising results of BS applications, still an important work must be achieved to propose optimized design of BS configurations.

This project aims to provide a generic design approach to the use of BSs by optimizing their main parameters (number, diameter, inclination angle, position, and permittivity) on post insulators under heavy icing conditions. This approach is based on analyzing previous BS tests in CEGELE, an improved hypothesis of BS effects, numerical analysis using commercial software (e.g. Comsol Multiphysics™, Matlab, and Minitab), geometric modeling of ice-covered post insulator with BSs, and finally experimental validation tests.

The improved hypothesis states that the major effect of BSs is the creation of air gaps and their minor effect is the increase in dry arcing distance. Moreover, among total length of the air gaps, dry arcing distance, and total ice-free leakage distance ($IFLD_{tot}$), the $IFLD_{tot}$ is a good indicator to quantify the BS effects on standard post insulators. Simulation analyses of BS configurations during the melting period demonstrate that the optimized relative permittivity of BS is an arbitrary value in its feasible variation range (2-15). The proper positions of BSs close to the HV electrode should be determined based on the probability of electrical breakdown. In contrast, the positions close to the ground electrode are determined based on ice-bridging effect. The geometric model and Taguchi method analysis show that the optimized value of BS inclination angle is equal to the upper shed angle of the insulator. Also, it indicates that generally the maximum feasible values for diameter and number of BSs are the best options. The feasibility in this regard, depends mainly on the minimum required distances between BSs as well as the mechanical forces of heavy ice and strong wind that may deform BSs. PVC sheet was deemed an effective solution for fabricating BS prototypes to perform the final validation tests. The experimental tests completely confirmed the improved hypothesis, the effectiveness of the geometric model, and the simulation analysis.

RÉSUMÉ

La conception optimisée des isolateurs externes sous des conditions sévères de givrage et de pollution est une préoccupation importante, surtout pour la fiabilité des réseaux électriques dans les régions au climat froid. Basée sur la pratique des transporteurs d'énergie électriques, la probabilité de contournement des isolateurs de poste THT est plus élevée que celle des isolateurs de ligne dans les mêmes conditions de givrage. Le contournement le long des isolateurs est essentiellement dû à la présence d'un film d'eau sur les surfaces de glace (période de fonte) et d'arcs partiels le long de zones sans glace (intervalles d'air).

L'une des alternatives pour diminuer la probabilité de contournement des isolateurs recouverts de glace est l'utilisation des jupes auxiliaires (JAs), ce qui permet de créer de plus grands intervalles d'air le long des isolateurs. Une jupe auxiliaire (JA) est un dispositif en forme de C flexible fabriqué à partir de bons isolants. En plus d'être faciles à utiliser, les JAs semblent être une alternative relativement simple, puisqu'elles permettent d'éviter de concevoir des isolateurs spéciaux pour les régions froides. Même si les résultats des applications de JA sont prometteurs, il y a encore un important travail à faire pour proposer une conception optimisée de leur configuration.

Ce projet vise à optimiser les paramètres principaux (nombre, diamètre, l'angle d'inclinaison, la position et la permittivité) des jupes auxiliaires pour fin de leur utilisation sur les isolateurs de poste sous des conditions sévères de givrage. Cette approche est basée sur plusieurs éléments tels que l'analyse des tests précédents des JAs à la CEGELE, une

hypothèse améliorée des effets des JAs, des analyses numériques utilisant des logiciels commerciaux tels que Comsol, MATLAB, et Minitab, ainsi que la modélisation géométrique de l'isolateur glacé avec JAs et sur des tests de validation expérimentaux.

Selon l'hypothèse améliorée, l'effet majeur de JAs est la création d'intervalles d'air et leur effet mineur est l'augmentation de la distance de l'arc. De plus, parmi la longueur totale des intervalles d'air, la distance d'arc et la distance totale de fuite dans les intervalles libres de glace ($IFLD_{tot}$), le $IFLD_{tot}$ est un bon indicateur pour quantifier les effets des JAs sur des isolateurs de poste standard. Les analyses de simulation de configurations des JAs en période de fonte montrent que la permittivité relative optimisée d'une JA est une valeur arbitraire dans sa gamme de variation possible (2-15). Les positions appropriées des JAs proches de l'électrode de haute tension devraient être déterminées à partir de la probabilité de décharge électrique. Par ailleurs, les positions proches de l'électrode reliée à la masse sont déterminées à partir de l'effet de pontage de la glace. Le modèle géométrique et la méthode Taguchi montrent que la valeur optimale de l'angle d'inclinaison des JAs est égale à l'angle de la jupe supérieure de l'isolateur. Ceci indique aussi que les valeurs réalisables maximales pour le diamètre et le nombre de JAs sont généralement les meilleures options. La faisabilité à cet égard, dépend principalement des distances minimales requises entre les JAs, ainsi que des forces mécaniques de la glace et du vent qui peut déformer les JAs. La feuille de PVC a été considérée comme une solution efficace pour fabriquer des prototypes de JA afin d'effectuer les tests de validation finale. Il s'est avéré que les tests ont complètement confirmé l'hypothèse améliorée, l'efficacité du modèle géométrique et les analyses de simulation.

ACKNOWLEDGMENTS

This project was carried out within the framework of the NSERC/Hydro-Quebec/UQAC Industrial Chair on Atmospheric Icing of Power Network Equipment (**CIGELE**) and the Canada Research Chair on Atmospheric Icing Engineering of Power Networks (**INGIVRE**) at Université du Québec à Chicoutimi **(UQAC).** I appreciate all CIGELE partners (**Hydro-Québec**, **Hydro One**, Réseau Transport d'Électricité **(RTE)**, Électricité de France (**EDF**), **Alcan Cable**, **K-Line Insulators**, **Tyco Electronics**, **Dual-ADE**, **CQRDA**, and **FUQAC**) whose financial support made this research possible.

I would like to express my sincere appreciation and admiration to my supervisor, **Prof. Masoud Farzaneh**, for his great experience, admirable support, and trust in me throughout my PhD experience. This dissertation would not have been possible without his patient and continued support.

I am particularly grateful to **Prof. William. A. Chisholm** whose precious comments and professional discussions helped me to improve the quality of this work.

Also, I greatly appreciate **Dr. Hatem Mrad** for the effective discussions and assistance during the last parts of the project.

I would like to express my sincere gratitude to **Prof. Issouf Fofana** for not only his scientific guides, but also valuable advices, human qualities and supports.

I would like to extend my thanks to **Pierre Camirand**, **Xavier Bouchard**, and **Claude Damours** at CIGELE Laboratory for their technical support and to **Denis Masson** for his help with administrative tasks.

I give special thanks to **Dr. Ibrahima Ndiaye** for his precious comments and guides during seminar I and my studies at UQAC. My thanks also go to **Dr. Volat** for his helpful guides and criticisms that helped to enhance the quality of this PhD project.

I am very grateful to the past and present directors of graduate studies, **Prof. Duygu Kocaefe** and **Prof. Mohand Ourouche**, for their valuable comments during my seminar evaluation. Also, I wish to thank their secretaries, **Chantale Dumas** and **Hélène Duchesne**, for her help with administrative tasks.

I also appreciate **Harriette Mostert** for the editorial help in making this dissertation legible.

I would like to thank my **Prof. Behzad Kordi** for carefully reading my thesis and providing useful feedback.

Despite all the ups and downs, I thoroughly enjoyed this PhD period because of having wonderful **friends** and **colleagues** in CIGELE group and in Chicoutimi. I acknowledge all of them for the positive discussions, advices and good humor.

I deeply thank my dear **parents**, **brothers** and **sister** for their invaluable supports and love during my entire life and studies. Although I live far away, I always have them in my heart.

Last, but not least, I would like especially to thank my beloved wife, **Kimia**, whose encouragements and persistent confidence in me gave me the strength to endure the difficult time. I wish one day I will be able to return her dedication and love. This thesis is especially **dedicated** to **her** and my dear **parents**.

TABLE OF CONTENTS

LIST OF FIGURES

LIST OF TABLES

GLOSSARY OF TERMS

Air Gap (AG): an ice-free zone along the insulator.

Applied water conductivity (σ_{20}): the electrical conductivity of water used to simulate ice, snow, or cold-fog accretion on insulators, corrected to 20 ° C.

Booster Shed (BS): a flexible c-shape device usually made of high-quality insulating materials. It can improve the electrical performance of insulators under heavy wetting and icing conditions.

Dry Arcing Distance (DAD): is the shortest distance in air between the high voltage and the ground electrodes.

Dry ice: the ice without water film at its surface.

Flashover: a disruptive discharge through air around or over the surface of solid or liquid insulation, between parts of different potential or polarity, produced by the application of voltage wherein the breakdown path becomes sufficiently ionized to maintain an electric arc.

Glaze ice (clear ice): type of precipitation icing resulting in pure ice accretion of density 0.7 – 0.9 g/cm^3, sometimes with the presence of icicles underneath the wires. It very strongly adheres to objects and is difficult to knock off.

Ice thickness the radial thickness of ice accumulation measured on a rotating monitoring cylinder.

Insulator: an insulating material designed to support a conductor physically and to electrically separate it from another conductor or object.

Leakage current: a component of the measured current that flows along the surface of the tool or equipment, due to the properties of the tool or equipment surface, including any surface deposit, when the device is connected as intended to the energized power system at rated voltage.

Leakage distance: the shortest distance, or the sum of the shortest distances, along the insulating parts of the insulator between those parts that normally have the operating voltage between them.

Maximum withstand voltage (V_{WS}): is established using constant contamination exposure. The tests are complete when three withstands in four tests are observed at one voltage level, and two flashovers are observed at 5% higher voltage level. The V_{WS} is the test level that gives three withstands out of four tests.

Minimum flashover voltage (V_{MF}): corresponds to a voltage level that is one step (5%) higher than V_{WS} and gives two flashovers out of a maximum of three tests.

Monitoring cylinder: a cylinder for measuring reference ice accretion, typically 25 – 30 mm in diameter, either rotating at 1 rpm or fixed.

Partial discharge: a discharge that does not completely bridge the insulation between electrodes.

Total air gap length ($L_{AG\text{-}tot}$): the sum of the lengths of air gaps.

Total Ice-Free Leakage Distance ($IFLD_{tot}$): the total of the shortest distances along the insulating surface between the high voltage and ground electrodes that are free of ice.

Uncertainty: an estimated limit based on an evaluation of the various sources of error.

Wet-grown ice (wet ice): is characterised by the presence of a water film of low resistivity at the surface of ice and icicles during their growth.

CHAPTER 1

INTRODUCTION

CHAPTER 1

INTRODUCTION

1.1 Overview and description of the problem

Electrical insulation and improving the flashover performance of HV insulators are challenging problems for many utilities in cold climate regions. In addition, the electrical problems of station insulators, such as high fault currents and equipment stresses, are more severe than for faults on line insulators. Actually, more than fifty percent of electrical icing flashover problems in North America are related to station insulators [1]–[5]. Thus, this project concentrates principally on the icing problems on station post insulators.

Several investigations and methods have been used to improve the performance of insulators in ice, snow, and pollution conditions [6]–[8]. One of the effective methods is using accessories such as booster sheds (BSs) and creepage extenders to break up icing patterns and to increase the threshold of ice accretion necessary for insulator bridging. BSs are flexible c-shape devices (Figure 1.1) which were invented in England to improve the flashover performance of insulators under heavy rain and high-pressure washing under energized conditions [9]–[13]. Some designs of booster shed (BS) have hemispherical "nubs" (Figure 1.1-a) to set a space between BSs the insulator surface. This space allows natural rain washing [2]. Figure 1.2 shows typical BSs applied to transformer bushings.

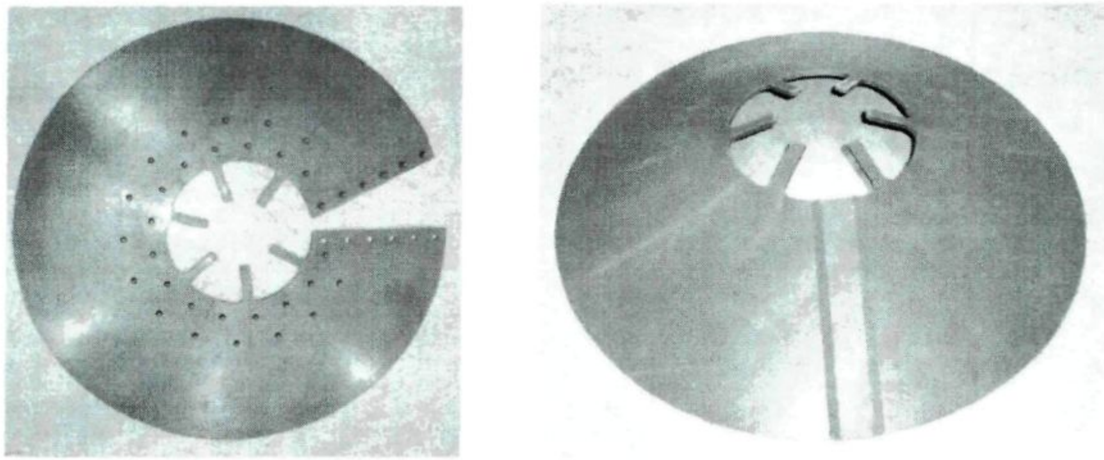

(a) (b)

Figure 1.1- Booster Shed (CIGELE Lab.)
a) underside and opened status b) upper side and closed status

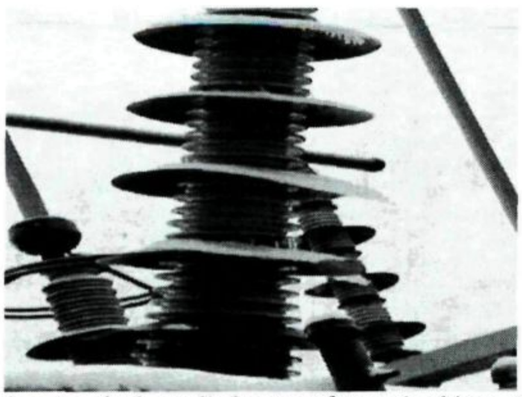

Figure 1.2- Typical booster sheds applied to transformer bushings. (Courtesy of Tyco.)

The effectiveness of BSs in heavy rain conditions is due mainly to a combination of features such as water shedding, discharge inhibition, and arc suppression [9], [11]. BSs can be used in cold regions with heavy ice and snow conditions as well [14]–[20].

The key parameters and/or properties that can be considered in BS optimized design and BS applications are:

1. Electrical properties (e.g. dielectric strength, volume, and surface resistance, permittivity or dielectric constant, tracking and erosion resistance).

2. Mechanical properties (e.g. tensile strength, ultimate elongation, low temperature flexibility).
3. Chemical properties (e.g. ultra violet resistance, hydrophobicity).
4. Aging properties i.e. the variations of above mentioned properties over time.
5. Geometrical parameters (e.g. diameters, inclination angle, thickness).
6. Installation parameters (e.g. number of BSs, positions, and speed in installation procedure).

Commercial BSs are generally made of ethylene vinyl acetate (EVA), a copolymer with suitable characteristics for industrial purposes under electrical, environmental, and mechanical stresses [11]. Hence, among the mentioned parameters, this PhD project contributes mainly to the optimization of some geometrical and installation parameters of BSs. It can close some major gaps in the present state of knowledge of BS applications under heavy icing conditions. For example, in the Tyco Company's manual for BSs, it is suggested to install BSs in equal distances. However, since the electrical field distribution along post insulators with BSs is not uniform, the ice accretion on BSs is not equal from top to bottom. In fact, the suggested method is not an optimum approach.

To solve the problems of the electrical performance of post insulators under heavy ice conditions, they can be substituted with new types of insulators. However, new insulators and their installation is much more expensive compared to the price of BSs. Thus, a more economical approach would be to add optimum BSs to the existing power network insulators.

1.2 Research objectives

The overall objective of this PhD project is to design booster shed parameters under heavy icing conditions through a generic approach in order to improve the electrical performance of EHV ceramic post insulators. The main BS parameters are as follows: number, diameter, inclination angle, position, and relative permittivity. Thus, a systematic study based on the combination of analytical analysis, simulations, and experimental tests should be performed. For this purpose, the specific objectives are as follows:

- To analyze different BS configurations by simulations of electrical field and potential distributions and parametric studies (water film effect, variation of BS parameters, flashover performance analyses, etc.);
- To establish an improved comprehensive hypothesis of BS effect under heavy icing conditions;
- To improve and develop effective geometric models in order to analyze the electrical performance of ice-covered post insulators equipped with BSs;
- To do optimality and post-optimality analyses of BS parameters using problem formulation process and modern techniques;
- To validate results by making proper BS prototypes and performing corresponding feasible experimental tests under heavy icing conditions.

1.3 General methodology

To achieve the main and specific objectives of the project, numerical modelling and calculations were done by Comsol Multiphysics™, Minitab and Matlab software, mainly based on previous BS tests in CIGELE. Finally, experimental validation tests were carried out. Figure 1.3 illustrates the general methodology by a flowchart. In the next chapters, the details of the methodology and the corresponding results are presented.

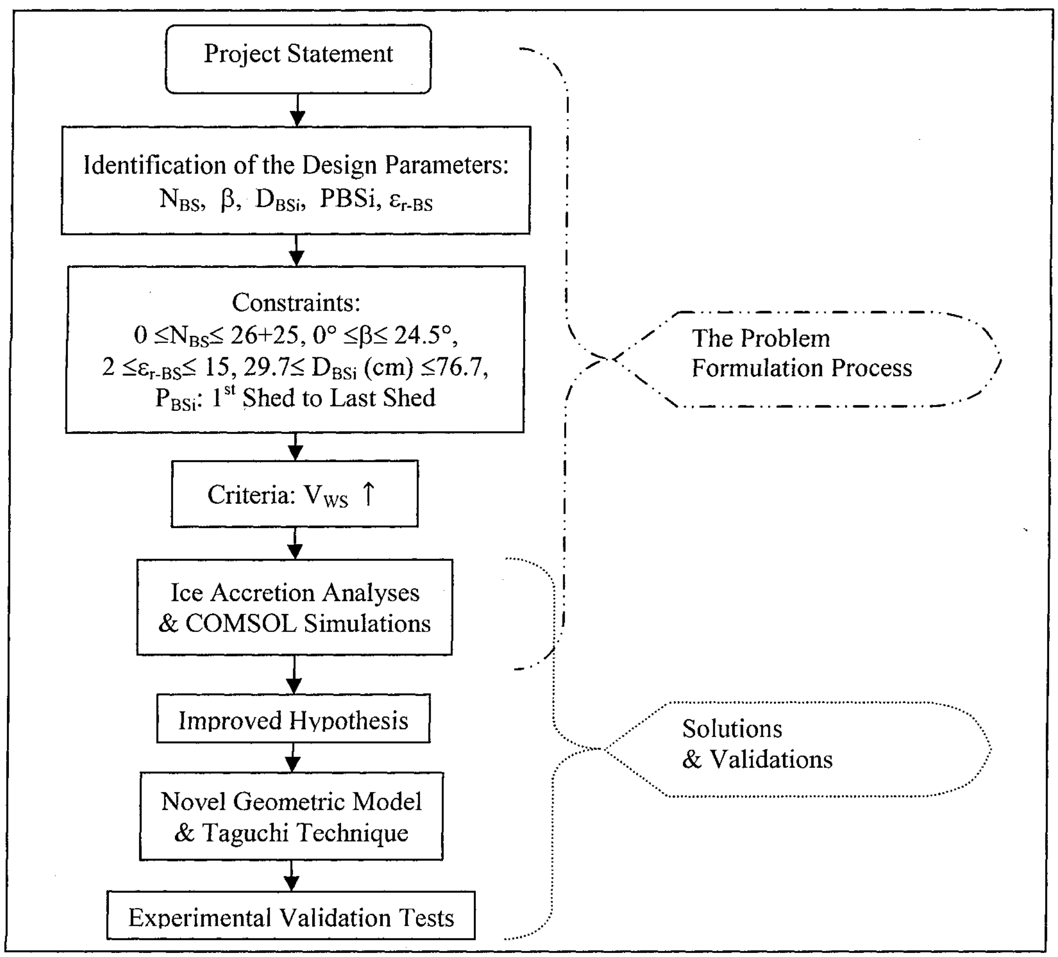

Figure 1.3- General Methodology

The main stages of the methodology can be summarized as:

1. Study of ice accretions on booster sheds
2. Computer simulations and parametric studies
3. Improved hypothesis concerning the effects of BSs under heavy icing conditions
4. Geometric modeling of the ice-covered post insulator equipped with BSs
5. Taguchi method application to design and optimize BS parameters
6. Experimental validation tests

1.4 Originality of the research and contribution to knowledge

Based on exhaustive study and consultation, only a few research results can be found on the effect of using BSs for insulators in cold climate environments and no systematic studies that analyze the major BS parameters installed on insulators in heavy icing conditions. Thus, the originality of this PhD project is summarized mainly as follows:

- the first extensive study to optimize BS parameters under icing conditions,
- the first simulations for various BS configurations, BS parameters and partial arcs on BS,
- upgraded model of BS dimensioning,
- improved hypothesis of the BS effects under heavy icing conditions,
- novel geometric modeling of ice-covered post insulators equipped with BSs, considering the precipitation angle,
- innovative indicator to quantify electrical performance of insulators with BSs,

- new design approach to use Taguchi method for optimality and post-optimality analyses,
- unique design method and fabrication of feasible BS prototypes for application on EHV ice-covered insulators that not only opened a locked door toward the final experimental tests in this research but also for the future studies in this domain,
- original optimized BS configuration to carry out the final experimental validation tests under heavy icing conditions.

1.5 Thesis outline

The structure of this dissertation is as follows:

Chapter 1 introduces general information about the problem, the necessity and motivation for the present research. Moreover, it presents the general and specific objectives, the general methodology, and the statement of the originality of the research.

Chapter 2 reviews the literature as it relates mainly to ice-covered insulators, booster sheds as well as design and optimization methods.

Chapter 3 proposes an upgraded model of booster shed dimensioning. It deals mainly with the diameter and position of booster sheds.

Chapter 4 describes the parametric simulation studies and the improved hypothesis of BS effects under heavy icing condition. Since the design approach is based on this improved hypothesis, this stage is as important as a foundation of a building.

Chapter 5 elucidates the geometric modeling of ice-covered post insulators equipped with BSs taking into account the precipitation angle. Then the geometric model is used to apply the Taguchi technique in the optimality and sensitivity analyses of various BS configurations under heavy icing conditions.

Chapter 6 deals with the fabrication of BS prototypes and the final experimental validation tests.

Finally, Chapter 7 concludes this study and it also presents the recommendations for future work.

CHAPTER 2

LITERATURE REVIEW

CHAPTER 2

LITERATURE REVIEW

2.1 Introduction

Outdoor insulators are widely used in power networks, but ice accretion may cause a drastic reduction in their electrical insulating performance in high altitudes and cold climate regions in many countries, such as Canada [21], [22], the USA [23], China [5], [24]–[27], Norway [28], Japan [29], and Iran [30]. In fact, in many cold regions of the world, atmospheric icing is a severe problem in electrical power systems. It can cause power outages and often incurs major costs by insulator flashover at service voltage [2], [31].

Two famous ice storms which clearly illustrate the disastrous consequences of the problem were firstly in Eastern Canada and US in 1998 and secondly in Southern China in 2008. The cost to the economy in the first one was estimated at nearly US$6 billion. Almost 1.6 million customers in Quebec and Ontario were left without power for periods of 3-30 days [32]. During the second ice disaster frozen rain and snow lasted for more than three weeks, caused a large-scale outage in several provinces of China, and led to an economic loss of US$7.9 billion [26], [33], [34]. These ice storms caused mainly mechanical damage, but fast restoration of service was affected by lack of reliability at critical substations.

Since BSs are known to be efficient and easy to use on already installed insulators, this option seems to be a very interesting solution to this problem [2], [15], [20]. Using BSs is a mitigation option generally in demand for heavy icing conditions. Hence, a review of competing mitigation options under heavy icing conditions is given in the next section.

2.2 Mitigation options under heavy icing conditions

Over the past decades, a large number of studies have been carried out by many research institutions and experts. This includes icing test methods, icing flashover performance, mitigation options. Several parameters and factors affect the dielectric strength of ice-covered insulators, such as the type and density of ice, length of icicles, freezing water conductivity, altitude, profile and type of insulator, and the position and length of ice-free zones (often called air gaps) [1], [21], [23], [24], [28], [29].

The presence of ice on insulators may initiate corona discharge, partial arcs resulting sometimes in flashover, if the required conditions are present. The flashover phenomenon is caused mainly by the presence of a highly conductive water film on the surface of the ice and the reduction in insulator leakage distance caused by ice bridging [35]–[37].

Based on field observations, EHV post station insulators are more susceptible to flashover than line insulators. This is mainly due to their higher electric field strength, smaller shed spacing, larger diameter, and their parallel application concentrated in small areas [1]. One of the main reasons causing significant decrease in flashover voltage of these insulators is the ice-bridging of their shed spacings. It has been shown that some approaches such as using BSs, creepage extenders, use of profiles with greater shed-to-shed distance, and semiconducting glaze insulators can reduce the probability of the bridging of the insulator sheds by icicles [15], [38], [39].

Reliability of insulators in icing conditions can be improved through several methods. The effectiveness of the solutions for improving their reliability and electrical performance varies in different ice severity. A rough distinction in icing severity for electrical performance includes very light (<1 mm), light (1-6 mm), moderate (6-10 mm) and heavy (>10-mm) ice accretion where the numbers represent radial ice accretion measured on a rotating reference cylinder. This classification is based on full bridging of station post insulators with uniform shed profile at 6 mm and full bridging of cap-and-pin insulator strings at 10 mm [2].

Insulators with close shed-to-shed spacing are more easily bridged by icicles. Once they are fully bridged, their electrical flashover performance will be compromised. For the heavy icing regime, countermeasures such as BSs and semiconducting glaze play roles that are somewhat different from the functions they perform in contaminated conditions [2]. The main mitigation options for heavy icing include:

- the increase in dry arc distance,
- semiconducting glaze,
- polymer insulators,
- the increase in leakage distance with the same dry arc distance,
- monitoring and washing,
- silicone coatings,
- accessories (e.g. corona rings, creepage extenders, and booster sheds).

One practical limit on increases in the dry arc distance of station post insulators relates to their cantilever strength requirements. A recommendation to increase dry arc distance by 25% may lead to an increase in post diameter by 33%, which, in turn, leads to additional ice accretion per unit length and a reduced leakage resistance [2]. This negative effect of increased diameter for the same strength requirements can negate the positive effect of additional dry arc distance.

The improved performance of semiconducting glaze insulators in heavy icing conditions is mainly a result of the improved voltage grading along the insulator surface. Moreover, in both laboratory tests and field exposure, these insulators develop larger ice-free zones than conventional glaze posts and develop these zones earlier in the melting phase [38], [40]. The larger the ice-free zones, the higher flashover strength.

Polymer insulators with typical 100 mm shed diameter perform better than IEEE standard disk insulators with 254 mm diameter. This improvement is essentially due to the effect of diameter, rather than any properties of the material [2]. Investigations on the effect of diameter on the electrical performance, supported by tests and modeling [41], also confirm that the flashover strength increases slowly with a reduction of insulator diameter.

One of the most important facets of electrical performance in icing conditions is associated with the partial or complete bridging of insulator leakage distance by icicle growth from shed to shed. The leakage distance of an insulator can be reduced nearly to its dry arcing distance in the worst conditions. More precisely, the effective leakage distance can be reduced to the dry arcing distance under fully bridged conditions. This extreme reduction in leakage distance (by a factor of about 2-3) can result in severe flashovers at numerous affected utilities [8], [21]. For 15-mm ice accumulation, uniform and alternating profiles gave identical performance per meter of post length [42]. In other words, the performances of the various profiles (standard uniform profile, the alternating profiles, etc.) are indistinguishable in the heavy icing condition.

The possibility of using leakage current activity as a predictor of the probability of icing flashover was studied in [43]. Based on the results, icing rate measurement and the severity of ice accumulation can be achieved by leakage current analysis, e.g. the time evolution of the third and fifth harmonic, the phase angle difference between leakage current and applied voltage. In the continuation of this study, artificial neural network (ANN) models were used to analyze leakage current evolution [44]. The obtained results verify that it is possible to use the proposed ANN model as part of a monitoring system for post insulators during icing events for early warning of potential flashover hazards.

Silicone rubbers have been used as housing material for transmission, distribution, and post insulators [45]. The Room Temperature Vulcanizing (RTV) type is cured in room temperature. The use of RTV silicone coating is generally not recommended on post insulators with shallow shed depth, especially in areas of heavy accumulation of ice, which would lead to full bridging. The loss of electrical strength is partly attributed to the longer duration of ice retention on the rougher RTV surface [2]. However, micro/nano fillers can be added to silicone rubber to improve its properties, such as the surface hydrophobicity, electrical conductivity, relative permittivity and thermal conductivity [46]. Therefore, the final product, e.g. semiconducting RTV coatings in [47], can provide promising results under icing conditions.

Corona rings are metal toroids; their main function is to prevent corona discharges by providing more uniform electric field distributions. They can be applied to any type of high voltage equipment, but they are often associated with nonceramic insulators to ensure a long-term reliability [2], [45]. "Grading rings" is generally used as a synonym for "corona rings", and their main function is to reduce the potential gradient along an insulator, thereby preventing premature electrical breakdown [2], [45]. Since grading rings produce a more uniform electric field, they affect the ionization of bipolar molecules of water and icicle growth. Hence, the result is more uniform shapes of ice accumulations (Figure 2.1) [48]. This phenomenon can especially be observed in the vicinity of the HV electrode, where the electric field is high. Even though uniform icing indicates satisfactory field grading, they can cause unsatisfactory electrical performance under icing conditions, because ice bridges the sheds of the insulator more quickly.

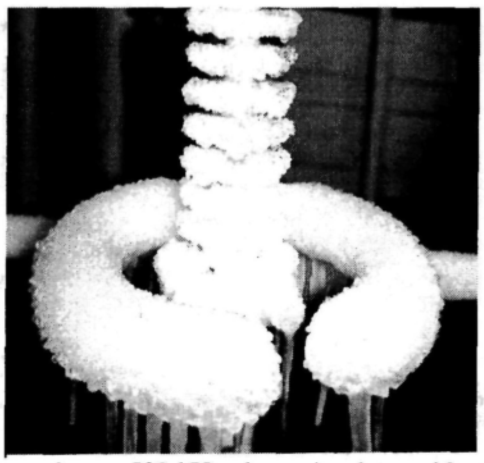

Figure 2.1- Ice accretion on 500-kV polymer insulator with grading ring [48]

A modified grading ring is proposed in [49] that also improves electrical performance under heavy icing conditions (Figure 2.2). It is a standard grading ring that includes a fine metallic mesh. The metallic mesh must be fine enough to prevent passing water drops through it under icing condition. This modification not only causes a better potential grading but it also creates a large air gap similar to the function of a BS.

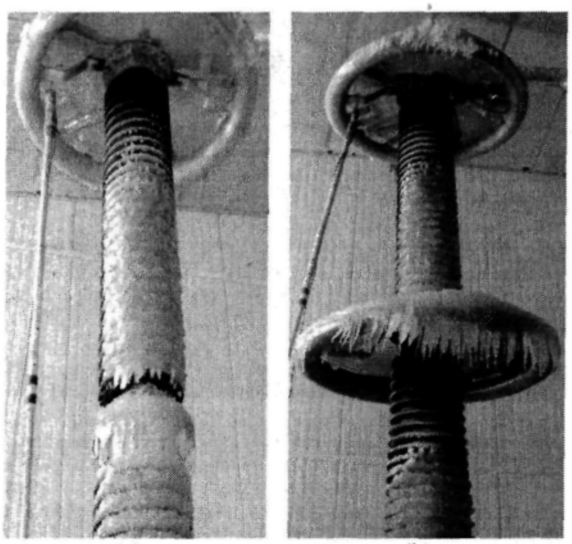

(a) (b)

Figure 2.2- Physical appearance of ice-covered insulators with modified grading rings after 15-mm/60 min ice accretion .a) one modified grading ring b) two modified grading rings [49]

Creepage extenders are applied to insulators to increase the creepage (or leakage) distance and shed diameter [2], [45]. They are bonded with an adhesive to the outside edge of the shed. The correct inner diameter of creepage extender must be selected to fit over the sheds. Figure 2.3 shows a common style of slip-on creepage extender with open small gaps. These open gaps face opposite directions in an alternating pattern. Hence, flashover arcs found their way through the open gaps rather than over the edges.

Figure 2.3- Slip-on creepage extender with open gap. (Courtesy of Tyco.)

2.3 Booster sheds under icing conditions

In a Cooperative Research and Development (CRD) collaboration between a utility, manufacturers and UQAC/CIGELE, the improvement in flashover performance of single station post insulators with 655-mm diameter booster sheds was evaluated [18]–[20]. The tests were performed using insulators with a total dry arc distance of 2.7 m and a stress of $105kV_{rms}$ per meter of dry arc distance. The post station insulators and stress levels correspond to those used on 735-kV substations in Quebec, Canada. The ice was formed with an applied water conductivity of 30μS/cm and an ice thickness of 15 or 30 mm on a rotating cylinder. The ice accretion, hardening, and melting sequences followed the IEEE Task Force recommendations defined in [50]. With a 30-mm ice accretion, as the number of BSs increased from four to six, the maximum withstand voltage increased by about 15kV per BS. When the BS positions were arranged to produce the largest air gaps and to prevent ice bridging, the best results for both icing thicknesses were obtained.

A multi-arc model for predicting flashover voltage of ice-covered insulators was introduced in [16]. This mathematical model is based on a previous model developed at

CIGELE [51] using Obenaus/Rizk model [52]. The number of air gaps depends mainly on the insulation profiles, voltage stress and insulator length. Overall results for the various insulators and configurations predicted with the model and experimentally determined are presented in Table 2.1 [16]. Two types of arc were defined– the arcs with one root and others with two roots on the ice surface. Their numbers are N' and N'', respectively, and the total number of arcs is N = N' + N''. Good agreement was achieved between the calculated and experimental results for the insulators without BSs. This result suggests that the multi-arc model can be applied to different types of insulators covered with ice, provided that the number and type of local arcs are properly considered.

Table 2.1- Experimental and calculated results [16]

Insulator type and configuration	Arcing distance (cm)	No. of arcs		Minimum flashover voltage (kV)		Error (%)
		N'	N"	Experimental results	From model	
IEEE standard	268	2	1	300	285	5.0
Post insulator	270	3	0	285	274	3.9
Post insulator with booster sheds	307	2	1	330	315	4.5
		2	2		360	-9.1
		2	4		432	-31

For the post insulator with BSs, the best results were obtained in the case of the 3-arc model (N'=2 and N"=1). This suggests that for the three tested types and configurations of insulator strings having an arcing distance longer than 2 m, normally there were three arcs: one at the top, one at the middle part and one at the bottom of insulator string, when the total arc length reaches its critical length.

In this investigation, adding six BSs to the two units of standard post insulators resulted in an increase in dry arcing distance from 2.70 m to 3.07 m, i.e., a 13.7 % increase. Correspondingly, the critical flashover voltage increased 15.7 % for the experimental results; it also corresponded to the critical flashover predictions using the 3-arc model. Then it was concluded that the increase in the critical flashover voltage of post insulators with BSs is mainly due to the increase in the dry arcing distance.

The multi-model can be used to predict the critical flashover voltage of ice-covered insulators provided that the number and type of local arcs are considered properly. On the other hand, in the case of 6 BSs, it seems hard to judge how many arcs formed at the critical point since the flashover process occurs very quickly. Thus, the multi-arc model is not suitable to attain a clear agreement between calculated and experimental results for the insulators with many BSs.

In [17] a method to determine the proper values only for two geometry parameters (i.e. positions and diameters) of three BSs along with one unit of a 735 kV standard ice-covered post insulator was presented. Figure 2.4 shows the considered BS set-up. "L" and "x" are considered as the length of the icicles and lengths of the air gaps, respectively. "e" is the ice thickness and "R_e" is clarified in Figure 2.4.

To calculate the diameter of BSs, D_{BS}, based on Figure 2.4 the following equation can be used:

$$D_{BS} \approx 2R_e / \cos 24.5°. \quad (1.1)$$

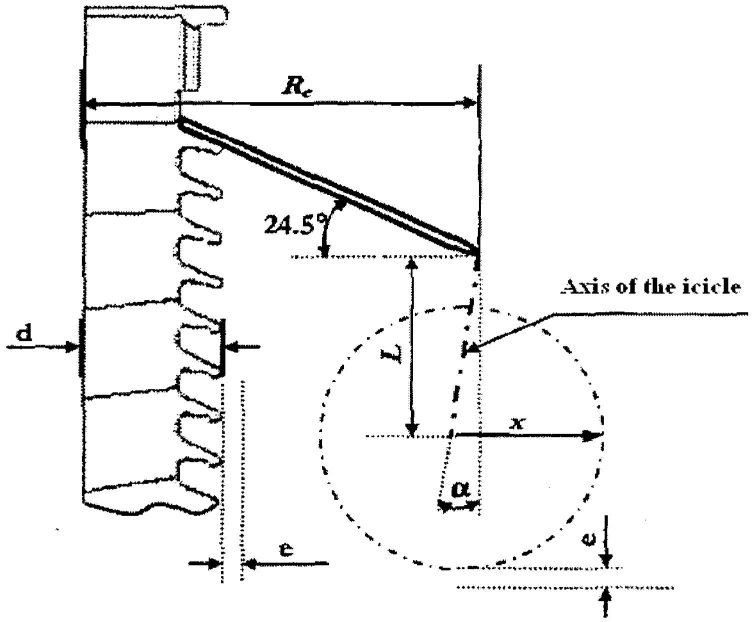

Figure 2.4- BS set up [17]

Then, to ease the evaluation of the proposed method, the final diameters are summarized in Table 2.2. Position (cm) means the distances between two consecutive BSs.

Table 2.2- Final dimensions of BSs considering the proposed method in [17]

BS No.	Diameter (cm)	Position (cm)
1	99.34	44.9
2	68.35	30.8
3	61.98	28.2

As it is clear form Table 2.2, the calculated diameter for the first BS is much bigger than what is commercially available. Moreover, the calculated positions are not suitable because they would lead to ice-bridging compared to the experimental test results in [2], [18]–[20]. The main problems of the proposed method are:

- using the simulation results of one unit of post insulator unequipped with BSs in the calculations,
- improper approximation of the length of the icicles along BSs,
- imprecise definitions regarding the radius of BS, diameter of insulator, etc.
- inaccurate estimation of the breakdown voltage as a function of the lengths of the air gaps.

Hence, the cited dimensioning method has been upgraded during this PhD project, and good agreements with the previous BS tests in [2] have been achieved. The upgraded model is presented in Chapter 3.

The flashover performance of 500kV porcelain post insulators with and without BSs was investigated in [53]. Test results showed the installation of BSs decelerated icicle growth, ice-bridging, and all of this led to a significant increase of 58% in the flashover voltage of the post insulator. Discharge path was mainly along the icicle and air gaps.

In [15] 0.6-m sections of a standard porcelain station post with 0, 1 or 2 BSs were tested. The maximum withstand voltage stress was reported to be 102 $kV/m_{dry\ arc}$ untreated, 113 $kV/m_{dry\ arc}$ with one and 147$kV/m_{dry\ arc}$ with two BSs in the icing regime tests.

In [14] strength improvements of 20% at 110 kV and 40% at 400 kV are stated. In addition, the tests in [39] show that the flashover voltage can increase about 50% for the post insulator after adding BSs. The differences in the reported improvements may be related to the test conditions and dimensions of the BSs and the insulators.

2.2.1 Problems of using BSs

One of the major problems of the application of BSs is the pollution issue. BSs can prevent natural washing of some parts of the insulators, and they may lead to glaze damage [1], [2], [21]. For example, under heavy icing conditions, there would be heavy ice on the top surfaces of BSs and none beneath. This situation could cause sufficient electrical stress so that the BSs would either puncture or confine flashover arcs between the neck of the BS and the insulator beneath, as shown in Figure 2.5 and Figure 2.6 [2]. This kind of damage is reported in the laboratory flashover tests, but should not occur in the field if there is no flashover under service voltage. However, if for any reason insulators face a flashover, the BSs should be checked for puncture and the insulators replaced if there is extensive damage beneath [2].

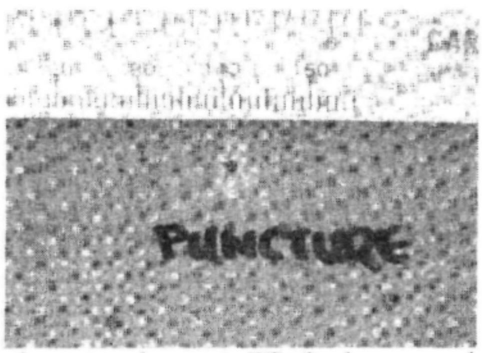

Figure 2.5- Typical puncture damage to BS after heavy, conductive ice test [2]

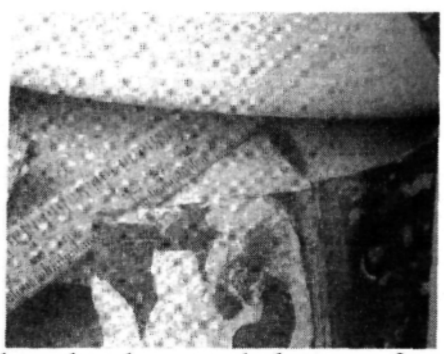

Figure 2.6- Insulator glaze damage under bottom surface of failed BS [2]

For good long-term performance more frequent cleaning or washing of insulators is required if they use BSs. Another proposed solution is to install the BSs during winter phase and remove them after winter [1]; however, that is an expensive approach. Moreover, some designs of BS have hemispherical "nubs" that set a small space between BSs and the insulator surface to allow for some natural rain washing (Figure 2.7).

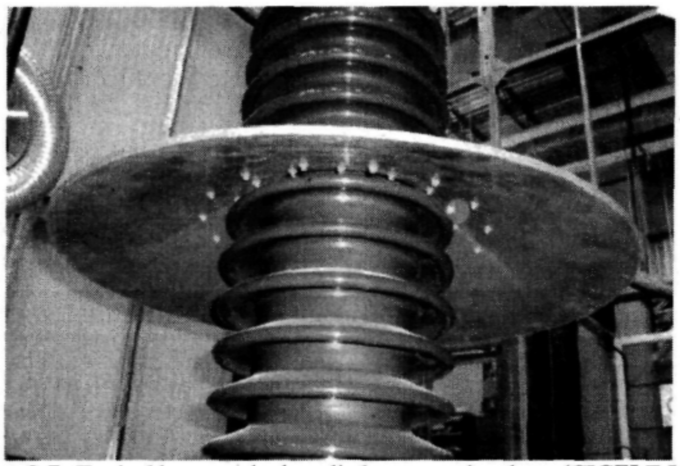

Figure 2.7- Typical booster shed applied to a post insulator (CIGELE Lab.)

2.4 Air gap effects on iced-covered insulators

Since using BSs can cause the formation of the long air gaps on a post insulator, it is necessary to study the role of these air gaps on the electrical performance of the ice-covered insulators. Several Finite Element and Boundary Element Methods (FEM and BEM) have been used for the investigation of ice-covered insulators. A coordination between simulations and experimental tests is often necessary [27], [40], [54]–[61].

Little research has been done on the influence of the number and position of air gaps on the electrical performance of insulators. A few papers have dealt with the influence of air gaps on the potential and electric field distribution along an EHV ceramic post insulator. The experimental and numerical results of voltage distributions of 1, 2, and 3 air gaps along one unit of an ice-covered post insulator show that [35-36]:

- An ice accretion with two air gaps seems to be more dangerous than one with three air gaps.
- During the melting period, around 96% of the applied voltage distributes along the air gaps, regardless of the number, position, and the length of the air gaps.
- It is the total length of air gaps, rather than their number, which is really significant in the process of partial arc formation.

All of the mentioned results were obtained during ice melting conditions, which are the most dangerous conditions for ice-covered insulators. These notes are used to propose an improved hypothesis of the effects of BSs under heavy icing conditions in Chapter 4. They were also used to conclude the minimum required number of BSs for installation on post insulator in order to apply the Taguchi method in the design approach of Chapter 5.

In [61] the influence of the number and position of air gaps on the 50% AC withstand voltage, V_{50}, of 5 IEEE standard insulator units covered with ice was experimentally investigated and numerically simulated. The results confirmed again that the number and position of air gaps have significant effects on the flashover voltage of ice-covered insulators. The results also showed that the presence of a partial arc along the air gap close to the high voltage (HV) electrode leads to a redistribution of the voltage along the ice-covered insulator.

It may be concluded that the effects of the air gaps on post and line insulators under heavy icing conditions are principally similar. Considering this similarity, the results of this PhD research on ice-covered post insulators with BSs could be extended for the applications on line insulators as well.

2.5 Design and optimization methods

Since the objective of this PhD project is the design and optimization of an expensive power system component (i.e. BS), a survey of classical and modern optimization and design methods is necessary.

In a design process, a trial design is analyzed to determine whether it satisfies prescribed requirements. If it is satisfactory, the design process is terminated. In the optimization process, the trial design is analyzed to determine if it is the optimum. Depending on the specifications, "optimum" can have different connotations for different systems. In general, it implies cost-effective, efficient, reliable, and durable systems. Based on the engineering optimization and design books [62], [63], for most engineering projects, the *formulation of a problem* consists of 5 steps:

- Step 1: Project/problem statement
- Step 2: Data and information collection
- Step 3: Identification/definition of design variables

- Step 4: Identification of a criterion to be optimized
- Step 5: Identification of constraints

However, the order of the steps can be changed. It is generally accepted that the *formulation of a problem* takes roughly 50 percent of the total effort needed to solve it. Therefore, it is critical to follow well-defined procedures for formulating design optimization problems. However, the design and/or optimization of a system is a creative process that can be quite complex.

Many analytical formulations of optimization and various algorithmic issues arise in the application of different methods in power electric equipment. In fact, electric power equipment optimization problems are difficult to solve because power equipment can be large and complex. Moreover, they are exposed by environment stresses and are influenced by many unexpected events. Therefore, it is necessary to employ most efficient optimization methods to take full advantage in simplifying the formulation and implementing the problem.

In [64], [65] the optimization of locations and dimensions of a corona ring is presented for EHV transmission line composite insulators. In order to set the optimal goal, the finite element method is employed to calculate the electrical field distribution along the composite insulator with corona ring that has various dimensions and locations. Moreover, the neural network model is built to map the location as well as the dimensions of the corona ring and the optimal goal. In these works the optimization is based on finding the maximum field along the insulator surface, such that this maximum field is well below the corona inception level. In design of corona rings, the design parameters are usually the ring diameter, the diameter of the ring tube, and the position of the ring in its vertical plane. Furthermore, the main criterion of the design is that the maximum field must not exceed the corona inception level.

Potential control inside a switch device using FEM and stochastic optimization algorithm is explained in [66], [67]. It describes the impact of selected insulation elements and the surrounding material, on the magnitude and distribution of electric potential in a switch device. The procedure is based on finite element method numerical analysis and stochastic optimization algorithm of differential evolution (DE). The optimal selection of mutually independent insulation materials has an impact on the control of potential and, consequently, on dielectric strengths, both inside the bushing and in other switchgear elements. The entire modeling procedure also includes optimization of the bushing's geometrical shape.

Optimization for high voltage composite insulators using experimental design theory is developed in [68]. This paper introduces a method for optimizing parameters of HV composite insulators. The optimal values of design parameters are determined by multivariable optimization procedure using theory of Design of Experiments (DOE). For repetitive calculation of the electric field strength the finite element method is used with domain decomposition. This method gives fast working software with accurate results to examine a very complex geometry without high computational effort.

2D and 3D simulations were used in [69] to analyze two stress grading options for 115 kV non-ceramic suspension insulators. The optimization criterion was to reduce the maximum electric field at the surface of the insulator. FEM was used to obtain the electric field distributions, and different functions of the MATLAB optimization toolbox were used to optimize the design parameters.

In [70] real coded genetic algorithm with simulated binary crossover were used for contour optimization of suspension insulators. The optimization criterion was to reach a desired uniform and minimal tangential field to increase the onset voltage of surface flashover. More precisely, the criterion was to minimize the tangential electric field and make the tangential electric field uniform, respecting the design constraints.

Taguchi method is a generally accepted methodology for modern design of experiments [71]–[73]. It can be used for virtual experiments (e.g. FEM simulations) as well [74]. The problem of using global optimization techniques (e.g. genetic algorithm and particle swarm optimization methods) is that the parameters of the algorithm are hard to determine. On the other hand, the Taguchi method uses orthogonal arrays to survey a large number of variables with a small number of experiments. So, it is used for optimal designs. An optimal design requires a smaller number of experiments to estimate the parameters with the same precision as a non-optimal design. The results are valid over the whole experimental region covered by the control factors and their settings. Hence, this method reduces costs. Moreover, after the problem formulation process in this PhD project, Taguchi method can provide effectively the required optimality and post-optimality results. Considering these advantages, Taguchi method is used in this project.

2.6 Conclusion

The reviewed literature mainly includes booster shed, ice-covered insulators and air gap effects, and optimization and design methods. It was observed that BSs improve the electrical performance of insulators under icing conditions. The reason for this improvement was attributed to the increase in dry arcing distance and creation of the air gaps. Then, the effects of these air gaps on ice-covered insulators were reviewed briefly, and three main points were emphasized. Finally, the five steps of the classical optimization approach as well as the modern techniques and the selected Taguchi method were introduced. Actually, to propose some feasible solutions to this challenging problem, not only a sufficient background about these three issues is required but also the interactions of all of them should be considered. Figure 2.8 illustrates this concept.

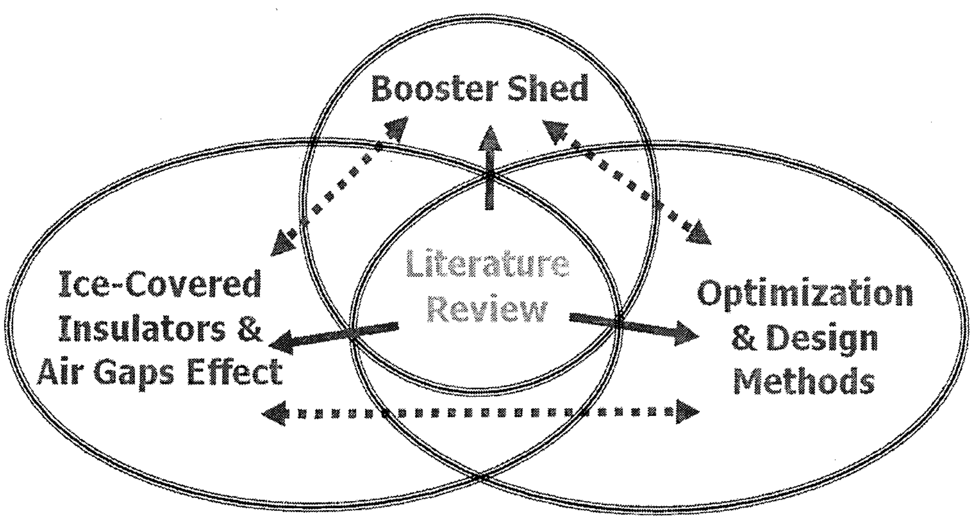

Figure 2.8- The main parts of the literature review and their interactions

CHAPTER 3

UPGRADED MODEL OF BS DIMENSIONING

CHAPTER 3

UPGRADED MODEL OF BS DIMENSIONING

3.1 Introduction

To advance the previous studies on BSs, this chapter presents an innovative approach of BS dimensioning under heavy ice conditions based on previous laboratory results in [2] and FEM 2D axisymmetric simulations by Comsol Multiphysics™. In fact, it is the upgraded model and approach of [17] which was reviewed and critiqued in Chapter 2. It deals with the two BS parameters (position and diameter) in the installation of 4, 5, and 6 BSs along 2 units of an ice-covered EHV ceramic post station insulator.

3.2 Description and observations of previous BS tests

Two units (bottom and middle) of a three-unit station post insulator were tested with a stress of 105 kV per meter of dry arcing distance which is equivalent to the stress on 735 kV substations in Quebec, Canada (Figure 3.1) [2], [18]–[20]. Heavy ice tests were carried out with an applied water conductivity of 30 μS/cm and ice accumulation of 30-mm on a rotating cylinder. The ice accumulation duration was 140 min, and the applied voltage was set at 285 kV. Each section has a 3500-mm leakage distance and a dry arcing distance of 1390 mm. The BSs that were used have an external diameter of 655 mm. Figure 3.1 shows

4-, 5- and 6-BS configuration tests after the heavy ice accretion in CIGELE climate room [2]. The ice accretion, hardening, and melting sequences followed the IEEE Task Force recommendations defined in [50]. The results of maximum withstand voltages (V_{WS}) and minimum flashover voltages (V_{MF}) are shown in Figure 3.1.

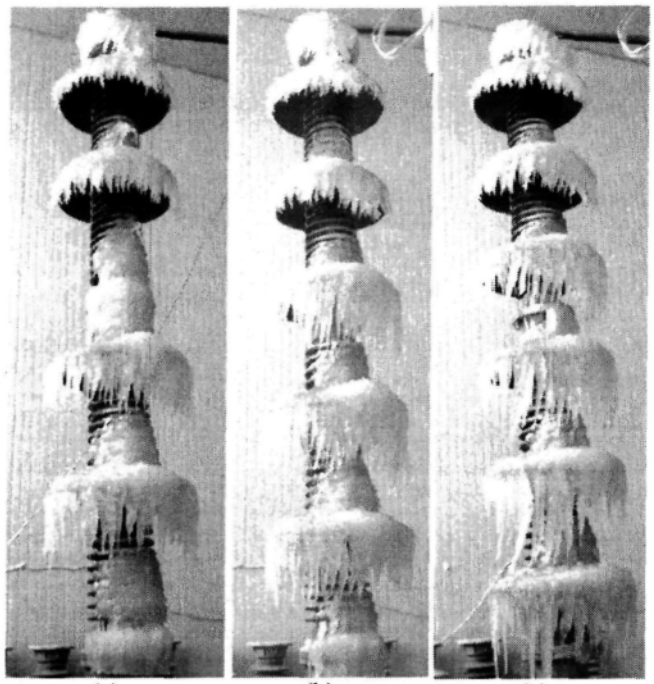

(a)	(b)	(c)
$V_{WS} = 285$ kV	$V_{WS} = 300$ kV	$V_{WS} = 315$ kV
($V_{MF} = 300$ kV)	($V_{MF} = 315$ kV)	($V_{MF} = 330$ kV)

Figure 3.1- Test results for standard post insulators in heavy icing conditions (30-mm ice accretion on rotating cylinder) with a) 4 BSs, b) 5 BSs and c) 6 BSs [2], [18]–[20]

BSs installed to a post insulator must have a satisfactory electrical performance under the most dangerous stresses. Based on the literature [35]–[37], a wet-grown ice is more dangerous than a dry-grown one. Thus, the ice formed under wet regime is selected to analyze the electrical performance of the insulator. A wet-grown ice is characterized by the presence of a water film with relatively low resistivity at the ice surface.

The test was repeated 5-6 times for the same configuration and test conditions [2], [50]. In the present study, the individual measured values of the corresponding 5-6 air gaps and icicle lengths of each BS from previous experimental results [2], [18]–[20] were averaged and summarized for those test conditions in Table 3.1 and Table 3.2.

Air gaps play an important role in the flashover process as they are where partial arcs appear and their formation directly depends on the electric field distribution [61]. The use of BSs allows the creation of "controlled" artificial air gaps along the ice-covered insulator.

Table 3.1- The average lengths of the air gaps (cm) during the BS tests

BS No.	4 BSs	5 BSs	6 BSs
1	23.2	23.2	21.8
2	16.2	16.2	13.8
3	9.6	9	8.4
4	11	9.6	7
5	-	11	2.6
6	-	-	9.2
Total	60.0	69.0	62.8

The length of icicles mainly depends on the accumulation time and the electrical field strength at the area of icicle growth. The average length of the icicles, L, between insulator sheds as a function of the accretion time in the space of insulator sheds is [75]:

$$L_t(cm) = 0.242t(min) \tag{3.1}$$

Using (3.1) as a primarily approximation for the icicle length on BSs (t=140 min) results in:

$$L_0(cm) = 33.9\ cm \tag{3.2}$$

Normalization of the lengths of the icicles based on L_0 (Normal), can also give us a good understanding of the effect of electric field on the icicle growth along BSs from top to bottom (Table 3.2). There is some tendency for longer icicle length on the BSs that are in regions of lower electrical stress, towards the bottom of the insulator.

Table 3.2- The average lengths of the icicles during the BS tests (per cm and per-normal (PN) as percent)

BS No.	4 BSs		5 BSs		6 BSs	
	L(cm)	L(PN)	L(cm)	L(PN)	L(cm)	L(PN)
1	17.4	51.3	17.4	51.3	19.8	58.4
2	20	59.0	20	59.0	24	70.8
3	30	88.5	32.2	95.0	29.8	87.9
4	37	109.1	29.6	87.3	33	97.3
5	-	-	26.8	79.1	37	109.1
6	-	-	-	-	44	129.8
Total	104.4	308	126	371.7	187.6	553.4
Average per BS	26.1	77.0	25.2	74.3	31.3	92.2

3.3 Numerical simulations

The simulations were done using the FEM commercial software COMSOL Multiphysics™. With this software surface conductivity and open boundary can be easily implemented. Moreover, to do the comparative calculations faster, 2D axisymmetric modeling was used instead of 3D modeling (Figure 3.2). The potential and the electric field distributions were calculated on the vertical and radial plane (zr-plane). The accuracy of this approach was verified in the previous studies [27], [76].

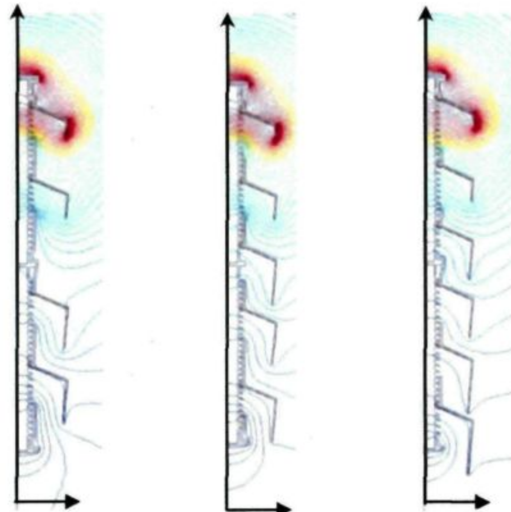

(a) (b) (c)

Figure 3.2- Equipotential line distributions of the post insulator with BSs under heavy wet-grown ice condition: a) 4 BSs b) 5 BSs c) 6 BSs in 2D axisymmetric view

The simulation parameters are summarized in Table 3.3.

Table 3.3-. Simulation parameters

	Porcelain	Air	Ice	Water film	Booster shed
Relative permittivity	6	1	75	81	2-15
Conductivity σ_s (μS/cm) at 20°C	0	0	0	30	0
Thickness (mm)	-	-	-	0.15	5

Next, Table 3.4 demonstrates the comparison of the voltage drops (ΔV (%)) for 4-, 5- and 6-BS tests. The voltage drops were computed by using reference lines located along the air gaps. More explanations about the modeling method and potential field distributions of all of the BS tests can be found in our previous papers i.e. [77], [78].

Table 3.4-. Comparison of the calculated voltage drops (ΔV (%)) for 4, 5 and 6 BS tests

Air gap no.	4 BSs	5 BSs	6 BSs
1	52.5	51.2	50.3
2	23.1	20.0	20.8
3	9.8	7.9	6.9
4	14.0	8.1	6.7
5	-	12.2	3.1
6	-	-	11.8
Total	99.4	99.4	99.4

3.4 Procedure for BS dimensioning

Figure 3.3 illustrates the geometric model for dimensioning two parameters of BSs (i.e. diameter and position). Based on the experimental test results, it is assumed that the tips of hanging icicles and ice surfaces are not contacted.

In Figure 3.3 and the coming equations and tables:

D_{BSi} (cm): is the diameter of BS_i.

R_{BSi} (cm): is the radius of BS_i.

$R_{ho\text{-}i}$ (cm): is the horizontal distance between the center axis of the insulator and the tip of the installed BS_i

BS_{ij}: signifies the zone between BS_i and BS_j.

e_{inij} (cm): is the thickness of ice on the insulator surface in BS_{ij}.

e_{bsj} (cm): is the thickness of ice accretion on the upper surface of BS_j ($e_{bsi} \approx 3$cm).

$d_{ext\text{-}i}$ (cm): is the average exterior diameter of the STD insulator shed under BS_i.

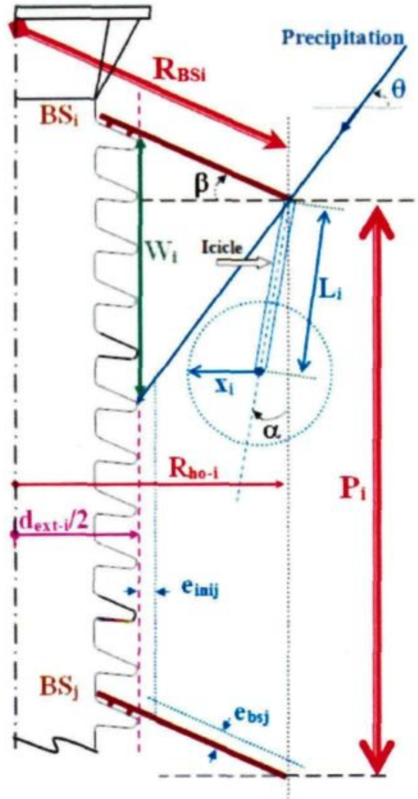

Figure 3.3- Geometric model for dimensioning two parameters of BSs
(i.e. diameter and position)

β (°): is the inclination angle of BS_i (in CIGELE Lab: $\beta = 24.5°$, upper shed angle of the insulator shed).

θ (°): is the incidence angle of precipitation ($0 \leq \theta$, and in CIGELE Lab: $\theta = 53 \pm 5°$).

α (°): is the slope angle of the icicles ($\alpha \approx 8°$, except $\alpha_{BS1} = -15°$).

L_i (cm): is the maximum length of the icicles on BS_i obtained from experimental results.

W_i (cm): is the total insulator length protected from precipitation by BS_i.

P_i (cm): is the distance between the extremities of two BSs that determine the position (P) of the BSs.

x_i (cm): is the minimum required length of each air gap to prevent electrical breakdown (between the tip of the icicles and the opposite surface of ice).

The AC breakdown voltage in the air gap of BS_{ij} ($V_{b\text{-}i}$) as a function of x_i (cm) can be stated as (3.3) or (3.4) [2], [60], [78]–[81]:

$$V_{b_i}(kV_{rms}) = ax_i + b \quad (3.3)$$

$$V_{b_i}(kV_{rms}) = cln(x_i) + d \quad (3.4)$$

Where,

"a", "b", "c", and "d": are real constant values.

If we obtain the values of $V_{b\text{-}i}$, "a", and "b", or $V_{b\text{-}i}$, "c", and "d", then we can calculate x_i as (3.5) or (3.6):

$$x_i = (V_{b_i} - b)/a \quad (3.5)$$

$$x_i = e^{(V_{bi}-d)/c} \quad (3.6)$$

According to the geometric model (Figure 3.3), the minimum required diameter of BS (D_{BSi_min}) to prevent electrical breakdown is:

$$D_{BSi\_min}(cm) = 2(R_{ho\_i})/\cos\beta \quad (3.7)$$

$$D_{BSi\_min}(cm) = 2\left(\frac{d_{ext\_i}}{2} + e_{inij} + x_i + L_i \sin\alpha\right)/\cos\beta \quad (3.8)$$

Moreover, the minimum required distance between the tips of two consecutive BSs (P_{i_min}) is (Figure 3.3):

$$P_{i\_min}(cm) = L_i \cos\alpha + e_{bsj} + x_i \quad (3.9)$$

To calculate $D_{bsi\text{-}min}$ and $P_{i\text{-}min}$, all of the parameters are known in (3.8) and (3.9) except x_i. In other words, the main challenge in this approach is the estimation of x_i. Thus, in this method, the estimation of the breakdown voltage equations in the BS air gaps is the key required point to calculate the proper diameters and positions of BSs. In the next section the estimation approaches are explained.

3.5 Estimation of the breakdown voltage equations in the BS air gaps

3.5.1 First approach

Air gaps formed during the ice accumulation in a wet regime can be assimilated to rod-plane configuration. The rod and the plane respectively represent the icicle on the booster shed and the ice surface on the upper surface of the next BS (Figure 3.4).

The high value of the freezing water conductivity (σ=340µS/cm) of the icicles used in the previous icicle-plane experimental tests were based on field experience [82]. In fact, during the freezing process impurities are rejected from the solid part toward the liquid portion of droplets [83]. Therefore, they increase the surface conductivity of ice and enable it to reach values as high as ten times those of the freezing water conductivity in the BS tests (σ = 30µS/cm). This is the reason that σ = 340µS/cm corresponds to the BS test conditions. In reality freezing water conductivity has a wide range of natural values but levels of 30 µS/cm are more typical in Quebec. Values in this high level are influenced by road salt [84].

By curve fitting of the obtained results in [80], we reach the AC breakdown voltage V_b as a function of minimal air gap length x (between the tip of icicle and the surface) for the corresponding temperature (temp) and σ = 340µS/cm and 1cm $\leq$ x $\leq$ 4cm:

$$V_b(kV_{rms}) = 6.3x(cm) + 8 \qquad \text{temp=0°C} \qquad (3.10)$$

$$V_b(kV_{rms}) = 7.3x(cm) + 12 \qquad \text{temp = -4°C} \qquad (3.11)$$

Moreover, the BS tests were performed at temperature (temp) of -1°C. Thus, using a linear estimation between (3.10) and (3.11), leads in:

$$V_b(kV_{rms}) = 6.55x(cm) + 9 \qquad \text{temp = -1°C} \qquad (3.12)$$

The presence of a water film on the tip of icicle can result in around 27% reduction in the breakdown voltage [75]. Thus, multiplying (3.12) by 73% results in the final required breakdown voltage (σ=340µS/cm and 1cm $\leq x \leq$ 4 cm):

$$V_b(kV_{rms}) = 4.78x(cm) + 6.57 \qquad \text{(temp=-1°C with water film effect)} \qquad (3.13)$$

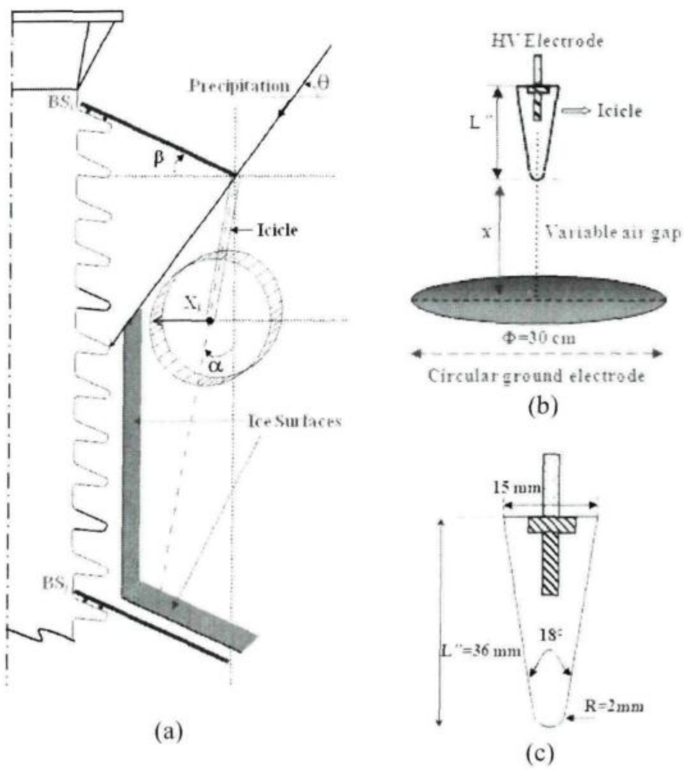

Figure 3.4- Schematic diagrams: a) the icicle on BS b) the icicle-plane configuration c) the icicle dimensions

3.5.2 Second approach

The breakdown voltage (V_b) obtained from (3.6) can be compared with the values of the voltage drop at the air gap no. i ($\Delta V_{ag\text{-}i}$) in two conditions. Firstly, when the applied voltage equals the flashover voltage (V_{MF}), and secondly, when it equals the withstand voltage (V_{WS}). In short, the following inequality must be satisfied:

$$\Delta V_{ag\_i\_WS} \ < \ V_{b\_agi} \ < \ \Delta V_{agi\_MF} \tag{3.14}$$

Where

$\Delta V_{ag\_i\_WS}$: is the voltage drop at the air gap no. i (ΔV_{agi}) when the applied voltage equals the flashover voltage.

$\Delta V_{ag\_i\_MF}$: is the voltage drop at the air gap no. i (ΔV_{agi}) when the applied voltage equals the withstand voltage.

$V_{b\text{-}agi}$: is the breakdown voltage of the air gap no. i.

Actually, the objective of this section is the estimation of the breakdown voltage equations in the BS air gaps considering their average air gap lengths and their variation (ΔL_{ag} (cm) $\neq 0$). To this end, it is sufficient to focus only on the first air gap (close to HV electrode), because:

1) It was shown that following the addition of 4, 5 or 6 BSs, the majority of the applied voltage (more than 50%) was dropped along the air gap closest to the HV electrode (Table 3.5).
2) In addition, based on the previous BS tests, partial arcs usually appear first in the first air gap closest to HV electrode.

In other words, the air gap no. 1 has the most determinant role in the electrical performance of the ice-covered insulator.

Table 3.5 shows the voltage drops along the first air gaps (obtained from simulations) for 4-, 5- & 6-BS tests when the applied voltage is equal to V_{MF} or V_{WS} during melting period (30-mm ice accretion on rotating cylinder). In addition, $L_{ag1\text{-}ave}$ is the average length of the air gap no. 1 during the previous BS tests.

Table 3.5-.Analysis of the voltage drops along the first air gaps for 4-, 5- & 6-BS tests when the applied voltage equals to V_{MF} or V_{WS}

	4 BSs	5 BSs	6 BSs
V_{WS}	285	300	315
V_{MF}	300	315	330
$\Delta V_{ag1\text{-}WV}$	149.62	153.6	158.44
$\Delta V_{ag1\text{-}MF}$	157.50	161.28	165.99
$\Delta V_{ag1\text{-}MF} - \Delta V_{ag1\text{-}WV}$	7.88	7.68	7.55
$L_{ag1\text{-}ave}$ (cm)	23.2	23.2	21.8

The breakdown voltage equations for icicle-plane configurations in [2], [60], [78], [80], [81] suggest that the typical values for a and b can be in the ranges below:

$$3.5 < a < 8 \quad and \quad 6 < b < 13 \tag{3.15}$$

To begin, consider 6-BS tests.

Note (1): *Inequality (3.14) must not only be satisfied for the average length of the air gap1 ($L_{ag1\text{-}ave}$) but it must also be satisfied for minimum and maximum length of the air gap no. 1 ($L_{ag1\text{-}min} \leq x \leq L_{ag1\text{-}max}$) measured during the BS tests.*

So the following relations can be obtained:

$$V_b(x = L_{ag1\_min}) = a \times L_{ag1\_min} + b \tag{3.16}$$

$$V_b(x = L_{ag1\_max}) = a \times L_{ag1\_max} + b \tag{3.17}$$

Suppose:

$$L_{ag1\_max} - L_{ag1\_min} = \Delta L_{ag1} \tag{3.18}$$

$$V_b\ (x = L_{ag1\_min}) = V_{b1} \tag{3.19}$$

$$V_b\ (x = L_{ag1\_max}) = V_{b2} \tag{3.20}$$

From (3.16)-(3.20), we obtain:

$$V_{b2} - V_{b1} = a \times \Delta L_{ag1} \tag{3.21}$$

Then, from (3.14) and note (1), we calculate:

$$V_{b2} - V_{b1} < \Delta V_{ag1\_MF} - \Delta V_{ag1\_WV} \tag{3.22}$$

So, from (3.21) and (3.22), we compute:

$$a < (\Delta V_{ag1\_MF} - \Delta V_{ag1\_WV}) / \Delta L_{ag1} \tag{3.23}$$

Furthermore, the following relations can be written by using (3.14) and Table 3.5:

$$149.62 < 23.2a + b < 157.5 \qquad \text{(4 BS tests)} \tag{3.24}$$

$$153.6 < 23.2a + b < 161.28 \qquad \text{(5 BS tests)} \tag{3.25}$$

$$158.44 < 21.8a + b < 165.99 \qquad \text{(6 BS tests)} \tag{3.26}$$

To isolate values of a and b, equations (3.24), (3.25), and (3.26) can be rewritten as:

$$6.62 - b/23.2 < a < 6.79 - b/23.2 \qquad \text{(4 \& 5 BS tests)} \tag{3.27}$$

$$7.26 - b/21.8 < a < 7.61 - b/21.8 \qquad \text{(6 BS tests)} \tag{3.28}$$

From (3.15), suppose b = 9, then (3.27) and (3.28) result in:

$$6.23 < a < 6.40 \qquad \text{(4 \& 5 BS tests)} \tag{3.29}$$

$$6.84 < a < 7.20 \qquad \text{(6 BS tests)} \qquad (3.30)$$

Suppose $\Delta L_{ag1} \leq 1$ cm, then, from (3.23) and Table 3.5, we acquire:

$$a < 7.88 \qquad (4 \text{ BS tests}, \Delta L_{ag1} \leq 1 \text{ cm}) \qquad (3.31)$$

$$a < 7.71 \qquad (5 \text{ BS tests}, \Delta L_{ag1} \leq 1 \text{ cm}) \qquad (3.32)$$

$$a < 7.55 \qquad (6 \text{ BS tests}, \Delta L_{ag1} \leq 1 \text{ cm}) \qquad (3.33)$$

Therefore, considering $\Delta L_{ag1} \leq 1$ cm, the following breakdown voltage equations can be proposed:

$$V_b = 6.3x + 9 \qquad (4\&5\text{-BS-tests}, b=9, \Delta L_{ag1} \leq 1 \text{ cm}) \qquad (3.34)$$

$$V_b = 7.0x + 9 \qquad (6 \text{ BS test}, b=9, \Delta L_{ag1} \leq 1 \text{ cm}) \qquad (3.35)$$

3.5.3 Comparison of the approaches

The first approach, (3.13) can be used only as a primarily estimation to predict the breakdown voltage on the air gaps of ice-covered post insulator equipped with BSs; because:

1) The air gap lengths in the BS tests were around 0 to 27 cm. However, (3.13) is actually valid for 1cm $\leq x \leq$4cm. Thus, if (3.13) be used for the air gaps more than 4 cm, the error of the prediction can be high and unacceptable.
2) The slope of the icicles can affect the breakdown voltage as well. As stated in the previous study [78], based on the BS tests, the direction of the icicles on BS_1 is directed away from the ice surface on the upper surface of BS_2. This phenomenon is because of the effect of the direction of the high electric field (close to the HV

electrode) on bipolar water molecules during the freezing process. Thus, the maximum error for the V_b estimations by (3.13) will be in the first air gap, which it is the most important air gap as stated before.

The first approach is similar to the approach that was used in [17]. Application of (3.13) results in unsuitable dimensioning of BSs. In contrast, as it is shown in the next section, (3.34) and (3.35) lead to their suitable dimensioning.

3.6 The application of the geometric model to the BS configurations

This section presents the application of the geometric model to calculate the proper diameters and positions of the BSs for the mentioned 4-, 5-, and 6-BS configurations under 30-mm ice accretion.

From (3.34) and (3.35), x_i can be expressed as:

$$x_i = (V_{bsi} - 9)/6.3 \qquad \text{(4 \&5-BS tests)} \qquad (3.36)$$

$$x_i = (V_{bsi} - 9)/7 \qquad \text{(6-BS test)} \qquad (3.37)$$

The $D_{BSi\text{-}min}$ and $P_{BSi\text{-}min}$ were calculated in Table 3.6, to Table 3.8 considering (3.14) i.e. the possible range of the breakdown voltage (V_b (kV_{rms})) and using the results of the BS tests and the voltage drops obtained in the simulations. $\Delta D_{BSi\text{-}min}$ and $\Delta P_{i\text{-}min}$ signify respectively the variation range of $D_{BSi\text{-}min}$ and $P_{i\text{-}min}$ taking into account the possible range of V_b in the calculations already mentioned.

The diameters and positions of the BSs must satisfy the extreme possible states in the BS tests. Thus, the extreme states must be considered in the dimensioning of the BSs.

As stated before, the previous BS tests were repeated 5-6 times for each configuration and test condition. Hence, regarding to *note (1)*, the maximum icicle lengths among the 5-6 measured values of the BS tests should be used in the calculations.

The minimum required diameter of BS_i ($D_{BSi\text{-}min}$) and the minimum required distance between the extremities of BS_i and BS_j that determine the positions ($P_{i\text{-}min}$) of BSs are (Figure 3.3):

$$D_{BSi\_min} \approx 2(d_{ext\_i}/2 + e_{inij} + x_i + L_{i\_max} \sin\alpha)/\cos\beta \tag{3.38}$$

$$P_{i\_min}(cm) \approx L_{i\_max} \cos\alpha + e_{bsj} + x_i \tag{3.39}$$

The measured values in the BS tests [i.e. $L_{i\text{-}max}$ (cm), e_{bs} (cm), e_{inij} (cm), $d_{ext\text{-}i}/2$ (cm), α (°)], the simulation results [ΔV (%)], and BS dimensioning equations [(3.36) to (3.39) and (3.14)] were used in MATLAB m-files to calculate the required values [V_b (kV_{rms}), x_i (cm), $D_{BSi\text{-}min}$ (cm), $\Delta D_{BSi\text{-}min}$ (cm), $P_{i\text{-}min}$ (cm), $\Delta P_{i\text{-}min}$ (cm)] in Table 3.6, Table 3.7, and Table 3.8. Furthermore, Table 3.9 displays the distances between the installed BSs in the tests.

Table 3.6-. Calculation of the positions and diameters of 4 BSs for the standard post insulator (V_{WS} = 285 kV, V_{MF} = 300 kV)

BS_{ij}	BS_{12}	BS_{23}	BS_{34}	BS_{4G}
$L_{i\text{-}max}$ (cm)	19	22	37	38
e_{bs} (cm)	3	3	3	0
e_{inij} (cm)	0	0	3	3
$d_{ext\text{-}i}/2$ (cm)	12.5	12.8	13.8	14.2
α (°)	-15	8	8	8
ΔV (%)	52.5	23.1	9.8	14.0
V_b (kV_{rms})	149.6-157.5	65.8-69.3	27.9-29.4	39.9-42.0
x_{min} (cm)	22.32-23.57	9.02-9.57	3.0-3.24	4.90-5.24
$D_{BSi\text{-}min}$ (cm)	65.73-68.47	54.69-55.90	54.85-55.36	60.21-60.94
$\Delta D_{BSi\text{-}min}$ (cm)	2.75	1.21	0.51	0.73
$P_{i\text{-}min}$ (cm)	43.67-44.92	33.81-34.36	42.64-42.88	42.53-42.87
$\Delta P_{i\text{-}min}$ (cm)	1.25	0.55	0.23	0.33

Table 3.7-. Calculation of the positions and diameters of 5 BSs for the standard post insulator (V_{WS} = 300 kV, V_{MF} = 315 kV)

BS_{ij}	BS_{12}	BS_{23}	BS_{34}	BS_{45}	BS_{5G}
$L_{i\text{-}max}$ (cm)	19	22	38	38	38
e_{bs} (cm)	3	3	3	3	0
e_{inij} (cm)	0	0	3	3	3
$d_{ext\text{-}i}/2$ (cm)	12.5	12.8	13.1	13.9	14.4
α (°)	-15	8	8	8	8
ΔV (%)	51.2	20.0	7.9	8.1	12.2
V_b (kV_{rms})	153.6- 161.3	60.0-63.0	23.7-24.9	24.3-25.5	36.6-38.4
x_{min} (cm)	22.95-24.17	8.10-8.57	2.52-2.71	2.62-2.81	4.38-4.67
$D_{BSi\text{-}min}$ (cm)	67.11-69.79	52.65-53.70	52.55-52.97	54.53-54.95	59.50-60.13
$\Delta D_{BSi\text{-}min}$ (cm)	2.68	1.05	0.41	0.43	0.63
$P_{i\text{-}min}$ (cm)	44.31-45.52	32.88-33.36	43.15-43.34	43.25-43.44	42.01-42.30
$\Delta P_{i\text{-}min}$ (cm)	1.21	0.52	0.19	0.19	0.29

Table 3.8-. Calculation of the positions and diameters of 6 BSs for the standard post insulator (V_{WS} = 315 kV, V_{MF} = 330 kV)

BS_{ij}	BS_{12}	BS_{23}	BS_{34}	BS_{45}	BS_{56}	BS_{6G}
$L_{i\text{-}max}$ (cm)	20	27	32	35	40	50
e_{bs} (cm)	3	3	3	3	3	0
e_{inij} (cm)	0	0	3	3	3	0
$d_{ext\text{-}i}/2$ (cm)	12.4	12.8	13.1	13.8	14.2	14.7
α (°)	-15	8	8	8	8	8
ΔV (%)	50.32	20.77	6.88	6.66	3.09	11.79
V_b (kV_{rms})	158.5-166.1	65.4-68.5	21.7-22.7	20.8-21.8	9.7-10.2	37.1-38.9
x_i (cm)	21.36-22.44	8.06-8.51	1.81-1.96	1.71-1.85	0.10-0.17	4.02-4.27
$D_{BSi\text{-}min}$ (cm)	62.82-65.19	54.11-55.09	49.15-49.48	51.39-51.71	50.27-50.42	56.44-56.99
$\Delta D_{BSi\text{-}min}$ (cm)	2.37	0.98	0.32	0.31	0.15	0.56
$P_{i\text{-}min}$ (cm)	43.68-44.76	37.80-38.24	36.50-36.65	39.37-39.51	42.72-42.78	53.53-53.79
$\Delta P_{i\text{-}min}$ (cm)	1.08	0.45	0.15	0.14	0.07	0.25

Table 3.9-.Distances (cm) between the installed BSs in the tests

	BS_{12}	BS_{23}	BS_{34}	BS_{45}	BS_{56}
4 BS test	60.5	96	57.5	-	-
5 BS test	60.5	54	56	62.5	-
6 BS test	56.5	48.5	51	52	50.5

Comparison of the calculated values ($P_{i\text{-}min}$) of Table 3.6, Table 3.7, and Table 3.8 with Table 3.9 demonstrates that the values are in a good agreement with BS positions in the previous BS tests. Moreover, the obtained values of the diameters are in good agreement with the diameter used (D_{BS}=65.5 cm) in the BS tests. As a result, the fitting BSs can be selected among the available commercial BSs, considering the minimum required diameter of BS_i ($D_{BSi\text{-}min}$). As well, the minimum required distance between the BSs ($P_{i\text{-}min}$) must be respected during the installation.

3.7 Discussion

The relation of the AC breakdown voltage as a function of air gap length is the key required equation [i.e. equation (3.3)] in the proposed method. This equation depends on several factors such as the length of the air gaps, the radius or sharpness of the tip of icicles, and the presence of a water drop and conductivity at the tip of wet icicles.

The calculated values in Table 3.6 to Table 3.7, demonstrate that the breakdown equation [(3.36) and/or (3.37)] mainly affects the diameter of BS_1 and the distance between BS_1 and BS_2. For example, in Table 3.6 to Table 3.7 the variation range of x_i for the first and second air gaps are 21.36-24.27 cm and 8.06-9.57 cm, respectively. Similarly, the variation ranges of voltage drops [ΔV (%)] for the first and second air gaps are 50.3-52.5% and 20.2-23.1%, respectively. In other words, it can be concluded from (3.36) and (3.37) and Table 3.6 to Table 3.7 that variations of x_i are directly proportional to the variation of the breakdown voltages and/or the voltage drops along the air gaps. In addition, the

ΔD_{BSimin} (cm) and ΔP_{i-min} (cm) values in Table 3.6 to Table 3.7 might be considered as the sensitivity of the D_{BSi} and P_{BSi} calculations to the voltage drops from top to bottom.

In fact, in (3.38) and (3.39) the variations of the maximum icicle length (L_{i-max}) and the minimum required air gap length (x_i) chiefly influence the calculated values of D_{BSi} and P_{BSi}. In the area close to HV electrode, electric field strength is high and consequently a large air gap length (x) is required to resist against the electrical breakdown. On the other hand, for the BSs close to ground, icicle length and/or ice bridging is the main factor that determines the proper position and diameter of the BSs. It is due to the lower electric field and the larger icicle length in this lower region.

Actually, the accurate estimation of the equation is essential only for the first air gap. Hence, to calculate the proper BS dimensions, a rough estimation of the equation is sufficient for all the air gaps except the first one. This is the reason that in the proposed method, the estimated breakdown equations of the first air gaps were used for the dimensioning of the other BSs as well.

As mentioned before, the BSs used in the previous BS tests have an outer diameter of 65.5 cm. Thus, in the proposed dimensioning method, the calculated values of the D_{BSi} should be less than or equal to 65.5 cm in order to have complete agreement with the previous BS tests. Regarding Table 3.6 to Table 3.8, the complete agreement was achieved for all of D_{BSi} values except D_{BS1} in 4- and 5-BS configurations. In these two cases, the obtained values are close to 65.5 cm and they are still in a rather good agreement compared to the previous experimental BS test results. This agreement is achieved in spite of the simplifications and estimations in the simulations and the proposed equations. In any case, more investigations are required to attain complete agreement and industrial applications.

Diameters and positions of the BSs must resist against the most extreme possible states in the BS tests. Hence, the extreme states must be considered in the dimensioning of the BSs. Since the direction of the icicles on BS_1 is away from the insulator ($\alpha < 0°$, Figure 3.3); based on (3.8), $D_{BS1\text{-}min}$ is a decreasing function of L_I. Thus, actually, the shortest L_I on BS_1 corresponds to the extreme case and should be considered in the calculations indeed. The use of the shortest L_I leads to a greater discrepancy. Therefore, again, the necessity of more research in this issue comes in mind. To this end, a suggestion for future work is presented in Chapter 7. Since the key equation to calculate D_{BS1} is the breakdown voltage as a function of the air gap length, some experimental tests should be performed to achieve better estimations of the breakdown equation [i.e. equation (3.3)]. From the previous studies [2], [85], [86] it can be concluded that main parameters for the determination of breakdown voltage are as follows:

1) the length of the air gap
2) ambient and ice temperature
3) water and surface conductivity
4) appearance of water drops
5) the radius of the tip of the icicles
6) pressure
7) humidity

Hence, a systematic study should be undertaken, which is explained in the recommendation for future work in Chapter 7.

There is a hidden hypothesis concerning the BS effects in the presented model of BS dimensioning. Based on this hypothesis, the useful effects of BS under icing conditions are the prevention of the electrical breakdown and ice-bridging along the created air gaps. Moreover, it states that the length of the air gaps plays the main role in the prevention of flashover and/or the electrical performance of the BS configurations. In the upgraded model of BS dimensioning, it was supposed that this hypothesis is acceptable. Then, in order to achieve a good agreement with the previous experimental tests, several simplifications and assumptions were considered. However, in spite of the achieved agreement, some realities demonstrate that the mentioned hypothesis should be improved. Most importantly:

- In order to find a way for proposing suitable equations of the electrical breakdown [i.e. (3.34) and (3.35)], it was supposed that $\Delta L_{ag1} \leq 1$ cm. However, based on the previous experimental test (see Table A. 6 in Appendix.), we have $\Delta L_{ag1} \approx$ 3-5 cm.
- Inequality (3.14) [i.e. $\Delta V_{ag\_i\_WS} < V_{b\_agi} < \Delta V_{agi\_MF}$] is only true if all of the experimental uncertainty is a result of the variability in the air gap size.
- In order to achieve a good agreement with the previous experimental tests, two separate breakdown equations [i.e. (3.34) and (3.35)] were proposed for the BS configurations. In other words, in spite of the similarity of the first air gap in 4-, 5-, and 6-BS configurations, it was not possible to propose only one breakdown equation for obtaining a good agreement.

Moreover, the following presented assumptions can be changed or improved. However, these changes/improvements will lead again to similar conclusions (i.e. separate breakdown equations and/or the reality that the mentioned hypothesis should be improved.).

- In view of physical interpretation of a and b in inequality (3.40) (i.e. $3.5 < a < 8$ and $6 < b < 13$); a is breakdown stress (usually 5 kV_{peak} per cm for large dimension) and b is a threshold voltage. It is possible to consider a wider range for a and b, for example: $3.1 < a < 8$ and $-5 < b < 22$.
- To achieve the breakdown equation at -1°C [equation (3.12)], a linear estimation was used. However, the change is abrupt at -0.5 °C and nonlinear indeed [87]. Thus, it would be better to simply use the breakdown equation at 0 °C and then evaluate the error of the estimation.
- In addition to the two described approaches for estimation of the electrical breakdown equations [i.e. equations (3.34) and (3.35)], it is also possible to use rod-to-plane flashover strength in standard test (metal rod to ground plane).

Hence, in the next chapter an improved hypothesis regarding the BS effects under heavy icing conditions will be presented.

3.8 Conclusion

This chapter presents an original method of BS dimensioning, based on previous experimental results, new numerical simulations, and analytical calculations. The method was applied for two units of a post station insulator under heavy icing conditions (30-mm ice accretion on a monitoring rotating cylinder) during the melting period. The stress levels equal those used at 735-kV Hydro-Quebec substations.

The FEM 2D axisymmetric simulation results are in good agreement with those of laboratory experiments in spite of the complexity of the insulator geometry and the simplifications made with the numerical model. Thus, the numerical simulation can be a good alternative to experimental measurements, which are time consuming and difficult to perform, especially for a full-scale station post insulator. However, practical care must be taken if the results presented here are to be carried out over a three-section post insulator due to the non-uniformity of the potential distribution along it. The presented dimensioning method also can be generalized to other types of insulators such as bushings and suspension insulators.

Moreover, the effects of the electric field and ice bridging in the dimensioning of the BSs were quantified from top to bottom along the post insulator. The analysis showed that to determine the proper diameters and positions of the BSs, the intensity of the electric field is the main factor for the BSs close to HV electrode. In contrast, ice bridging (icicle length) is the main factor for those close to the ground electrode.

It was assumed that the useful effects of BS on ice-covered insulators are the prevention of ice-bridging and electrical breakdown along the created air gaps. Also, the length of the air gaps have the main function in the prevention of flashover However, some realities demonstrate that this assumption/hypothesis should be improved.

CHAPTER 4

PARAMETRIC SIMULATIONS AND IMPROVED HYPOTHESIS

CHAPTER 4

PARAMETRIC SIMULATIONS AND IMPROVED HYPOTHESIS

4.1 Introduction

BSs can increase the reliability of insulators in ice or snow conditions by the prevention of icicle or snow bridging and by protecting the leakage distance from ice accretion [1]. That is to say, BSs can make alternating diameters of sheds (as a kind of new shed profiles) on insulators by boosting some of the insulator-shed surfaces.

Chapters 4, 5, and 6 present an original approach to analyze systematically the effect of BSs on ice-covered post insulators. This process leads to the optimization of the BS parameters (i.e. diameter, inclination angle, number, permittivity, and position), thereby making it more beneficial for electrical industries in high voltage insulators.

Chapter 4, herein, explains the parametric studies and the improved hypothesis of the effect of BSs under heavy icing conditions. It is demonstrated that FEM 2D axisymmetric simulation is a valuable option as opposed to expensive experimental tests and time consuming 3D simulations in order to analyze the influence of BS in improving the electrical performance of post insulators under heavy icing conditions.

4.2 Study of ice accretions on BS tests

In Section 3.2, a brief description and some observations of the previous BS tests were presented. In the current section ice accretions on the mentioned BS tests are studied in more detail. Then some parametric simulation studies will be explained in the next section. The main objective of these studies is to propose an improved hypothesis of the effect of BSs that leads to an improvement in the electrical performance of the post insulators under heavy ice conditions. Figure 4.1 depicts 4-, 5- and 6-BS configuration tests in CIGELE climate room after heavy ice accumulation. As the number of BSs increases from 4 to 5 and/or 5 to 6, there was an increase in V_{WS} of about 15 kV.

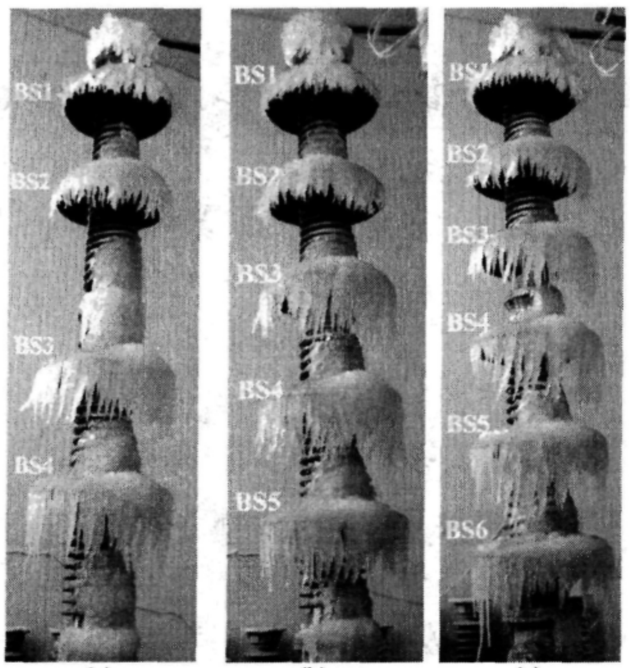

(a) V_{WS} = 285 kV Improvement over untreated: 5.6%

(b) V_{WS} = 300 kV Improvement over untreated: 11.1%

(c) V_{WS} = 315 kV Improvement over untreated: 16.7%

Figure 4.1- Test results for standard post insulators in heavy icing conditions (30 -mm ice accretion on rotating cylinder) with a) 4 BSs, b) 5 BSs and c) 6 BSs [2], [18]–[20]

BS positions were selected to produce air gaps without ice bridging. The applied voltage was set at 285 kV. The levels of the withstand voltages (V_{WS}) were compared to the value of 270 kV, usually considered for the post insulators without BSs under heavy ice accretion of 15-30 mm.

The middle and bottom units have 26 and 25 sheds, respectively. Table 4.1 presents the installation positions of the BSs based on the shed numbers of the units from HV to ground electrodes.

Table 4.1- The installation positions of the BSs based on the shed numbers of the post insulator units

BS No.	4 BSs	5 BSs	6 BSs
1	3	3	2
2	15	15	13
3	3	26	23
4	14	6	2
5	-	18	12
6	-	-	22

Next, Table 4.2 shows the average lengths of the air gaps (AGs) and icicles of the BS tests. Air gaps play an important role in the flashover process as it is where partial arcs appear, and their formation depends directly on the electric field distribution [61].

The icicle lengths of the BSs strongly depend on the position of the BS along the two insulator units. As the BS comes closer to the ground, the average icicle length becomes larger. This is due to the fact that the potential distribution along the insulators is not uniform. In fact, the icicles along the BSs closer to HV electrode are growing in a stronger electric field. The appearance of corona discharges at the tip of icicles in a strong electric field leads to the reduction of icicle growing rate. As BS approaches the ground electrode, electric field strength decreases and consequently icicles grow with lower level restrictions.

Table 4.2-. Average lengths (cm) of the air gaps and icicles in BS tests

BS No.	4 BSs		5 BSs		6 BSs	
	AG	Icicle	AG	Icicle	AG	Icicle
1	23.2	17.4	23.2	17.4	21.8	19.8
2	16.2	20	16.2	20	13.8	24
3	9.6	30	9	32.2	8.4	29.8
4	11	37	9.6	29.6	7	33
5	-	-	11	26.8	2.6	37
6	-	-	-	-	9.2	44
Total	60.0	104.4	69.0	126	62.8	187.6

However, it was a general observation that the icicles in a lower BS have longer lengths; in some cases it was observed that a lower BS has a shorter icicle length. This occurred for the icicles of installed BSs on the bottom unit of the standard insulator close to the ground electrode. Since the electric field is not strong in this area and the potential differences are lower, the electric field has a minor role in the icicle growth of the BSs on the bottom unit. Thus, a lower BS can have a shorter icicle length due to the random manner of the formation of the icicles.

Finally, Table 4.3 shows the *Ice-Free Leakage Distances (IFLD)* during the mentioned BS tests in Figure 4.1.

Table 4.3-.Equivalent total ice-free sheds and ice-free leakage distances (IFLD) (cm), during the BS tests

	4 BSs	5 BSs	6 BSs
Equivalent total ice-free sheds	22.5	27	32
$IFLD_{1\text{-}t}$ (along shed surfaces (cm))	283.3	339.9	402.9
$IFLD_2$ (beneath of BSs (cm))	92	115	138
$IFLD_{tot}$ (total ice-free leakage distance of the BS test (cm))	375,3	454,9	540,9

In Table 4.3, to calculate the equivalent total ice-free sheds, the relations (4.1) to (4.4) are used:

$$N_{\text{equivalent total ice-free sheds}} = N_{\text{total ice-free sheds}} + 0.5 \times N_{\text{partially ice-bridged sheds}} \quad (4.1)$$

It means the number of equivalent total ice-free sheds equals the number of total ice-free sheds plus 50% of the number of partially ice-bridged sheds.

$$IFLD_{1\_t}(\text{cm}) \approx K \times N_{\text{equivalent total ice-free sheds}} \times d_{sh\_sh}(\text{cm}) \quad (4.2)$$

Where,

$IFLD_{1\_t}$: is the sum of the equivalent IFLD on surfaces of insulator-sheds in the BS tests.

K: is the ratio of total leakage distance to the dry arcing distance of one section of the post insulator: 2.52 (3.5 meter / 1.39 meter).

d_{shsh}: is the shed-to-shed distance of the post insulator: ≈ 5 cm.

$$IFLD_2(\text{cm}) \approx IFLD_{b\_BSi} \times N_{BS} \quad (4.3)$$

Where,

N_{BS}: is the number of installed BSs.

$IFLD_{b\_BSi}$: is the IFLD of bottom surface of BS_i (cm) ≈ 23 cm.

$IFLD_2$: is the sum of the IFLD of bottom surfaces of BSs (cm).

At the end, we obtain the total IFLD ($IFLD_{tot}$) as follows:

$$\mathrm{IFLD}_{tot}(\mathrm{cm}) = \mathrm{IFLD}_{1\_t}(\mathrm{cm}) + \mathrm{IFLD}_2(\mathrm{cm}) \tag{4.4}$$

Figure 4.2 clarifies schematically the definitions of $\mathrm{IFLD}_{b\text{-}BSi}$, ice-free sheds and partially ice-free sheds used in the above equations.

The correlations of IFLD_{tot}, total dry arcing distance and total length of the air gaps with the maximum withstand voltage will be discussed in Section 4.4.

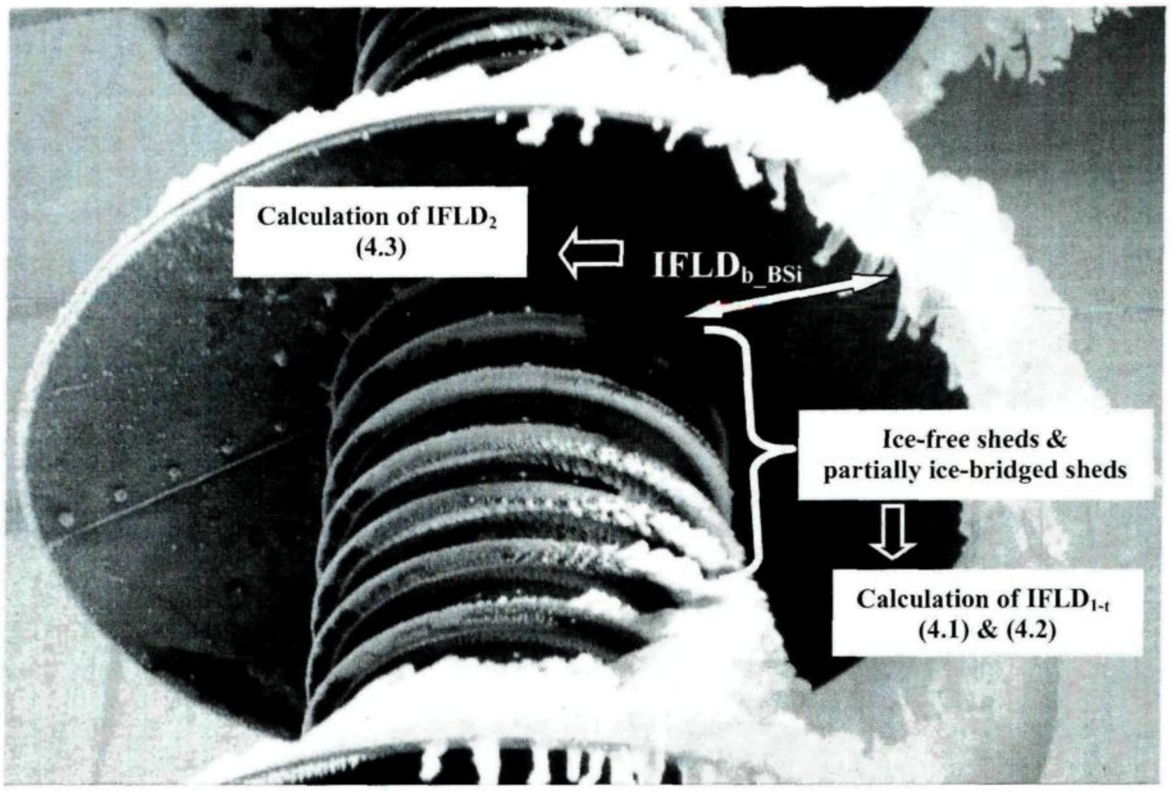

Figure 4.2- Clarification of IFLD_{b_BSi}, ice-free sheds and partially ice-bridged sheds

4.3 Parametric simulations

As stated in Section 3.3, the numerical simulations were done using the FEM commercial software COMSOL Multiphysics™. The current section presents comparative studies of various BS configurations and situations. The 2D axisymmetric simulations are used here mainly to determine voltage drops along air gaps and to detect partial discharges.

4.3.1 The effect of water film

Figure 4.3 depicts the effect of water film on equipotential line distributions of an ice-covered post insulator equipped with 6 BS. Wet grown ice is characterized by the presence of a water film on the surface of ice.

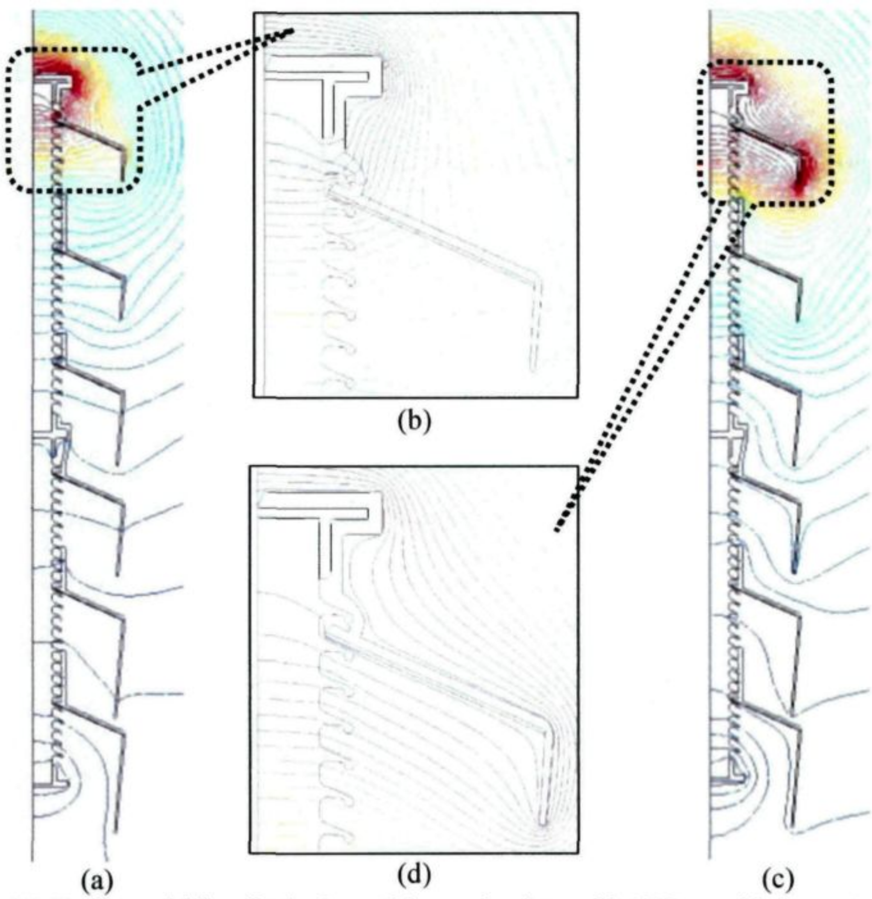

Figure 4.3- Equipotential line distributions of the post insulator with 6 BSs considering water film effect under heavy icing conditions a) and b) without water film (dry ice); c) and d) with water film (thickness = 0.15 mm, conductivity = 30 μS/cm)

Table 4.4 shows the effect of water film on the voltage drops along the air gaps in the 6 BS configuration. The total voltage drops (ΔV) along the air gaps are 43.3% and 99.4% for the dry-ice and wet-ice conditions, respectively. The higher ΔV leads to a higher probability of electric breakdown and appearance of flashover. It confirms the literature's statement that wet-grown ice is more dangerous than a dry-grown one [35]–[37].

Table 4.4-.Comparison of voltage drops in the sample 6-BS configuration considering the effect of water film (thickness = 0.15 mm, conductivity = 30 μS/cm)

Air gap no.	ΔV (%) without water film	ΔV (%) with water film
1	22.2	50.3
2	7.6	20.8
3	2.9	6.9
4	2.7	6.7
5	1.2	3.1
6	6.7	11.8
Total	43.3	99.4

A post insulator equipped with BSs must assure a proper electrical performance under the most severe conditions. Thus, in this research the wet-grown ice is commonly selected for following parametric studies.

4.3.2 The effect of number of BSs

In section 3.3, the numerical simulations of 4-, 5-, and 6-BS tests under heavy ice accretion were explained. The comparison of their calculated voltage drops (Table 4.5 and Figure 4.4) demonstrates that in all of the configurations:

1. The total voltage drops (ΔV_{tot}) on the air gaps is around 99.4 %. It indicates that the air gaps have the main role in resisting the applied voltage and, consequently, to increase the flashover voltage.
2. The voltage drop distribution is non-uniform and the longest air gap close to the HV electrode has the highest voltage drop (more than 50% of the applied voltage).
3. There is a slight decrease ($\approx$1%) in the voltage drop of air gap 1 (ΔV_{AG1}) as the number of BSs increase from 4 to 5 and 5 to 6.

Table 4.5-.Comparison of the calculated voltage drops (ΔV (%)) for 4, 5 and 6 BS tests

Air gap no.	4 BSs	5 BSs	6 BSs
1	52.5	51.2	50.3
2	23.1	20.0	20.8
3	9.8	7.9	6.9
4	14.0	8.1	6.7
5	-	12.2	3.1
6	-	-	11.8
ΔV_{tot}	99.4	99.4	99.4

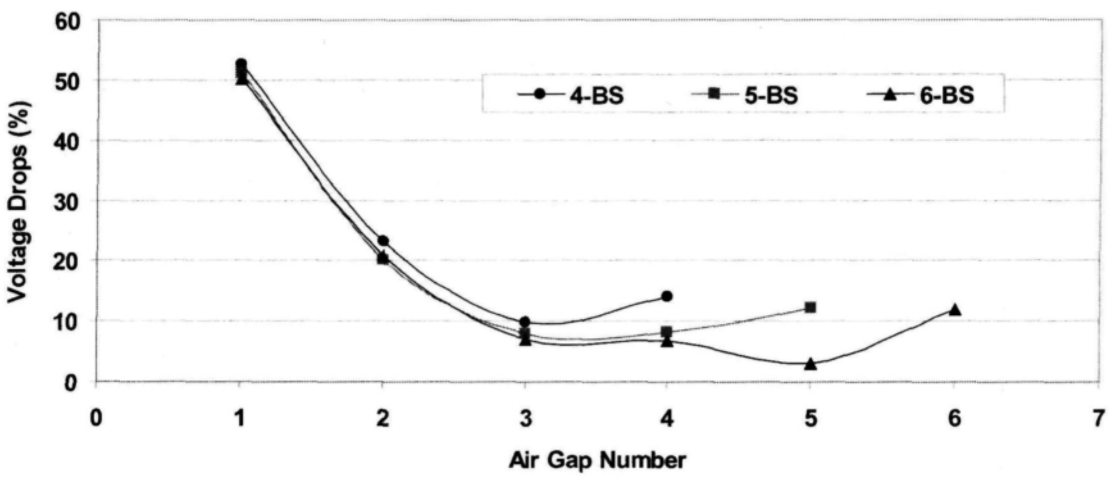

Figure 4.4- Potential distribution of the post insulator with 4, 5 and 6 BSs under heavy wet-grown ice condition

4.3.3 The effect of variations in the permittivity of ice and BS

The variation of ice relative permittivity in the range of ($\varepsilon_{r\text{-}ice}$= 75-110) has no major effect on the calculated potential and electric-field distributions along the EHV insulator in the wet-grown ice regime. The mentioned variation range was selected based on [2], [60]. The practical variation of relative permittivity of BSs ($\varepsilon_{r\text{-}BS}$= 2-15) [88] has no significant effect on the calculated electrical field distributions as well. Actually, the increase in $\varepsilon_{r\text{-}BS}$ may increase the portability of tracking and puncturing on BSs in practical applications.

In fact, melting period simulations show that the presence of a conductive water film at the ice surface has the most important role in the distribution of the potential along the insulator. It increases the voltage drop along the different air gaps and consequently enhances the electric field strength along them drastically.

4.3.4 The effect of air gap length variation on the voltage drops

The effect of the variation of air gap length on the voltage drops (ΔV) of the air gaps was investigated in a sample simulation of 6 BSs configuration test. To this end, only the icicle length on BS_3 (L_{ice3}) was reduced by 50% (Figure 4.5). More precisely, it was changed from 26.8 cm to 13.4 cm in the simulation model. Therefore, the length of the air gap no. 3 (L_{ag3}) was approximately increased twice. It changed from 13.2 cm to 25.6 cm.

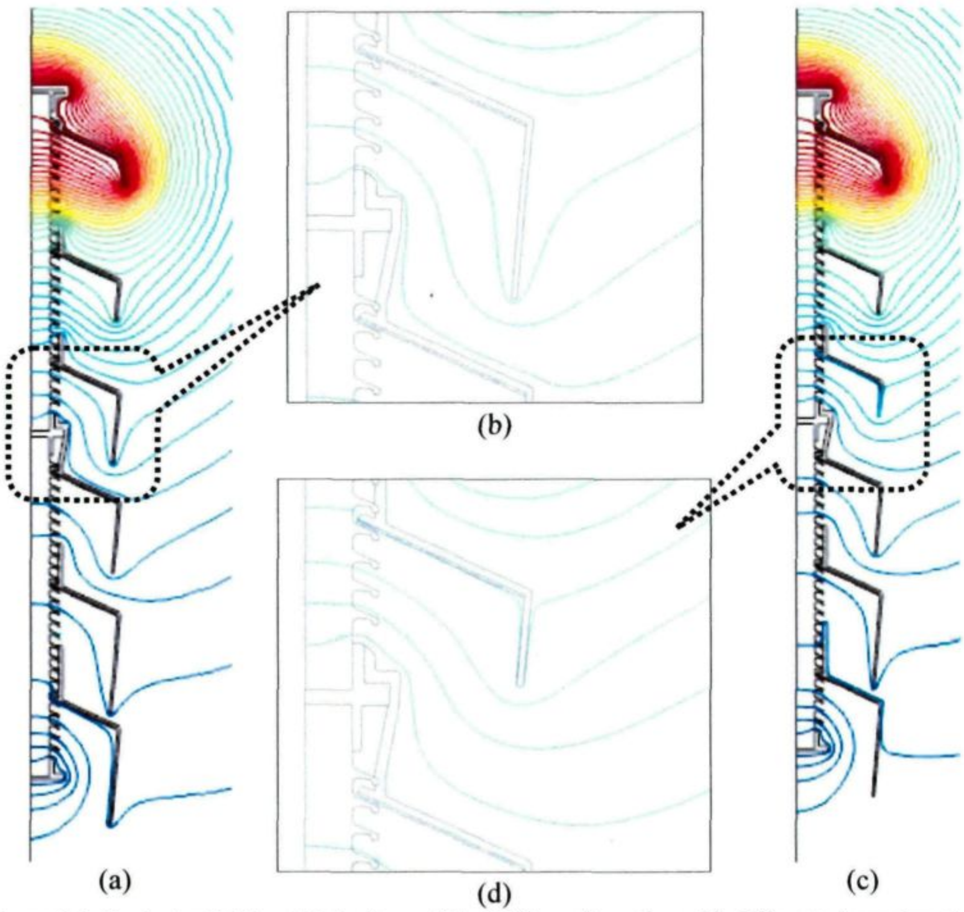

Figure 4.5- Equipotential line distributions of the 6-BS configuration with different air gap lengths: a) and b) before the change in air gap no. 3; c) and d) after the change in air gap no. 3

Table 4.6-.Comparison of voltage drops in the 6-BS configuration by changing the air-gap length no. 3

Air gap no.	Air gap length(cm) **before** the change	Air gap length(cm) **after** the change	ΔV (%) **before** the change	ΔV (%) **after** the change	ΔV (%) Variation
1	32.8	32.8	53.65	52.8	-0.85
2	24.5	24.5	18.60	17.41	-1.19
3	**13.4**	**25.6**	**6.42**	**8.8**	**2.35**
4	14.6	14.6	6.28	5.9	-0.38
5	3.2	3.2	2.98	2.9	-0.08
6	22.3	22.3	11.51	11.2	-0.29
Total	110.6	122.8	99.44	99.01	-0.43

The results depicted in Table 4.6 shows that by 93% increase in the L_{ag3} (i.e. 100% decrease in L_{ice3}):

1) The maximum of voltage drop variations occurs in air gap no. 3 (AG_3) and it is an increase less than 2.5%.

2) Total voltage drop (ΔV_{tot}) along AGs decreases less than 0.5 %.

4.3.5 The effect of icicle direction of the first BS on the voltage drops

The inclination of icicles (α, Figure 4.6) on the first BS is different from those on the other BSs because of the high electric-field strength in this area. Thus, the effect of the variation of the first icicle-direction on the voltage drops of the air gaps were investigated for 2 states in the simulation of 6 BSs configuration test (Figure 4.7 and Table 4.7).

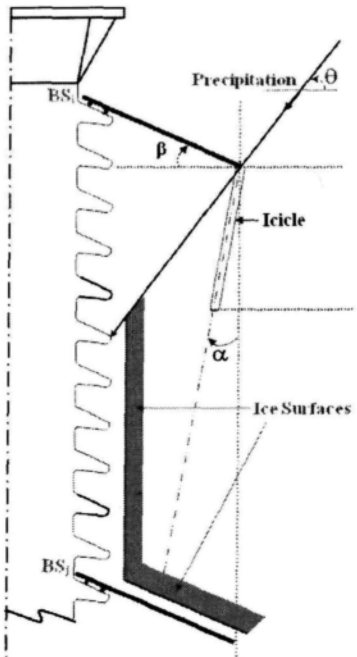

Figure 4.6- Schematic diagram of the icicles on BSs and the ice surfaces to estimate breakdown voltage equations

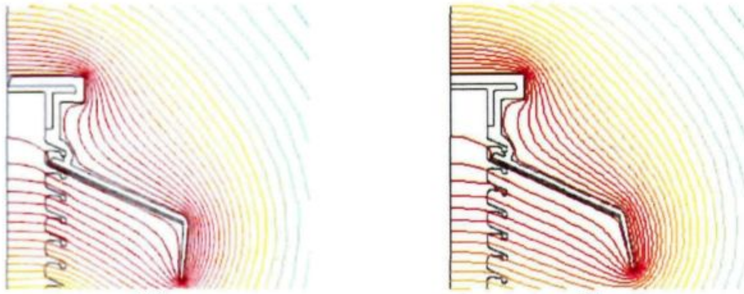

(a) (b)

Figure 4.7- Equipotential line distributions around BS_1 with different angles of icicles: a) state 1: $\alpha_{BS1} \approx 8°$, b) state 2: $\alpha_{BS1} \approx -15°$

Table 4.7-.Comparison of voltage drops in the 6 BS configuration by changing the icicle slope on BS_1

Air gap no.	Air gap length (cm) **before** the change	ΔV (%) **before** the change (state 1: $\alpha_{BS1} \approx 8°$)	ΔV (%) **after** the change (state 2: $\alpha_{BS1} \approx -15°$)	ΔV (%) variation (state2-state1)
1	32.8	50.3	49.9	-0.4
2	24.5	20.8	20.8	0
3	13.4	6.9	6.9	0
4	14.6	6.6	6.7	0.1
5	3.2	3.1	3.2	0.1
6	22.3	11.8	12.0	0.2
Total	110.6	99.5	99.5	0

The results show that by changing the slope angle of the icicles (α, Figure 4.6) on the first BS from 8° to -15°:

1) The maximum variation of ΔV occurs along the first air gap (AG_1) and it is a decrease around of 0.4%.
2) Total voltage drop (ΔV_{tot}) along the air gaps does not vary.

4.3.6 The effect of the diameter variation of the BSs

Figure 4.8 shows the equipotential line distributions of the 6-BS configuration with different diameters.

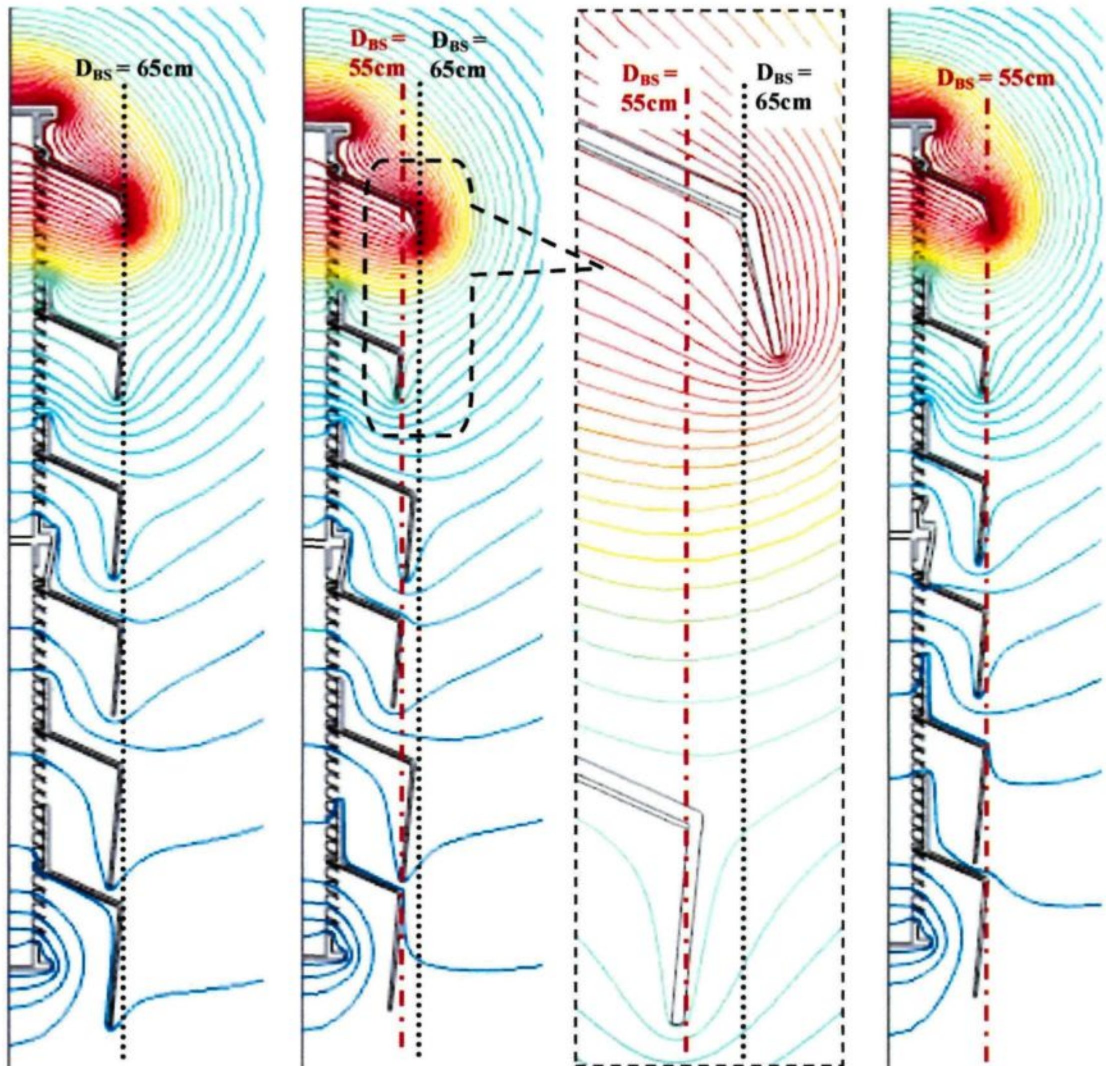

(a) (b) (c) (d)

Figure 4.8- Equipotential line distributions of the 6-BS configuration with different diameters: a) state 1: D_{BS} = 65cm, b) and c) state 2: alternative diameters (D_{BS} = 65cm & 55cm) d) state 3: 55cm

The comparison of voltage drops in the 6-BS configuration by changing the BS diameters is shown in Table 4.8. The results show that by changing the BS diameters from 65 cm to 55 cm in the three different states in Table 4.8:

1) The maximum of ΔV variations occurs in AG_1 or AG_2 and it is less than 1.5%.

2) The maximum of the total voltage-drop (ΔV_{tot}) variations is less than 0.1%.

Table 4.8-.Comparison of voltage drops in a sample 6-BS configuration by changing the BS diameters

Air gap no.	Air gap length (cm) **before** the change	ΔV (%) All BSs =65 cm (state 1)	ΔV (%) Alternative BSs BS_{135}=65cm BS_{246}=55 cm, (state 2)	ΔV (%) All BSs =55 cm (state 3)	ΔV (%) Variation (state2-state1)	ΔV (%) Variation (state3-state1)
1	32.8	53.40	52.04	54.14	-1.36	0.74
2	24.5	18.53	19.86	18.32	1.33	-0.21
3	13.4	6.42	6.32	6.67	-0.10	0.25
4	14.6	6.25	6.49	6.39	0.24	0.14
5	3.2	2.98	3.19	2.98	0.21	0.00
6	22.3	11.47	11.16	10.63	-0.31	-0.84
Total	110.6	99.05	99.05	99.12	0.00	0.07

4.3.7 The effect of the inclination angle variation of the BSs

Figure 4.9 shows the equipotential line distributions of the 6-BS configuration with different inclination angles (β in Figure 4.6) of BSs. Table 4.9 shows the comparison of voltage drops in the 6-BS configuration by changing the BS inclinations.

Table 4.9-.Comparison of voltage drops in the 6-BS configuration by changing the inclination angles of BSs

Air gap no.	Air gap length (cm) **before** the change (state 1)	ΔV (%) All β=24.5° (state 1)	ΔV (%) All β=9.5° (state 2)	ΔV (%) Variation (state 2-state 1)
1	32.8	53.40	52.56	-0.84
2	24.5	18.53	18.60	0.07
3	13.4	6.42	6.49	0.07
4	14.6	6.25	6.32	0.07
5	3.2	2.98	3.23	0.25
6	22.3	11.47	11.82	0.35
Total	110.6	99.05	99.02	-0.03

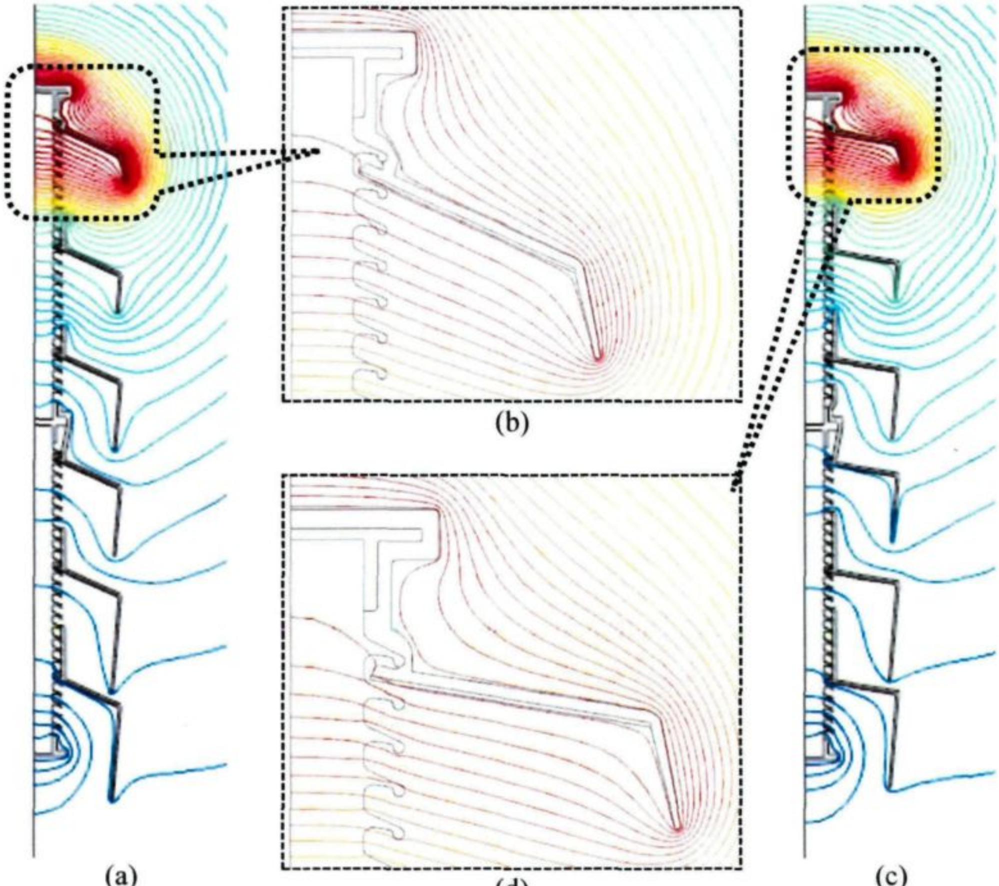

Figure 4.9- Equipotential line distributions of the 6-BS configuration with different inclination angles of BSs: a) and b) $\beta = 24.5°$; c) and d) $\beta = 9.5°$

The results show that by 15° variation of the BS inclinations (β, Figure 4.6) from 24.5° cm to 9.5° in the different states:

1) The maximum of ΔV variations occurs in AG_1 or AG_2 and it is less than 1%.
2) The maximum of the total voltage drop (ΔV_{tot}) variations is 0.1%.

4.3.8 The effect of the metal ring at the top of the insulator

As mentioned in Chapter 2 corona rings improve field grading, and they tend to promote accumulation of a uniform ice layer. Moreover, they reduce the production of ozone from the corona discharge activity. In the previous BS tests, a small metal ring was used at the top of HV electrode (Figure 4.1). According to the images, the metal ring was not much bigger than the metal hardware of the post insulator end fitting and would had a limited effect in the testing shown. Figure 4.10 shows the equipotential line distributions around the first BS with and without the small corona ring. The calculated voltage drops were approximately the same.

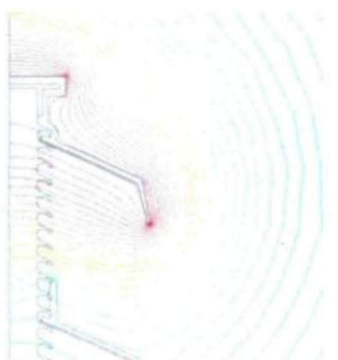
(a)

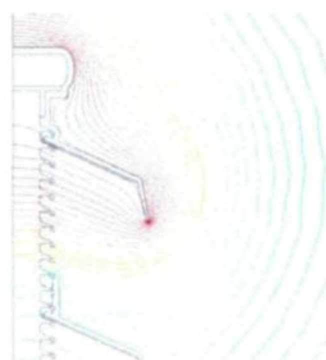
(b)

Figure 4.10- Equipotential line distributions around BS_1 and small corona ring effect
a) without corona ring b) with corona ring

4.3.9 Comparison of the results for HVAC (f=50 or 60 Hz) and HVDC

The simulation results of potential and electric-field distributions along the EHV insulator for the wet-grown ice condition show that the values of voltage drops in the air gaps for HVAC (f=50 or 60 Hz) and HVDC are the same, ignoring space charge effects.

This is due to the size of an EHV post insulator (height ≈ 4.5 m) which is much smaller than the wavelength of the AC voltage (wavelength = wave velocity/frequency = 5×10^7 m). In other words, the system is in a quasi-static condition for both AC and DC. However, in order to attain a more accurate comparison regarding the frequency effect, the presence of the displacement (capacitive) currents in HVAC systems should be considered as well. There is no capacitive current in HVDC systems and this is due to frequency = 0 [89].

4.3.10 The effect of partial arc appearance on the voltage drops

The partial arc modeling method presented in [59] was used in this study. The model considers voltage drop along the partial arc during its propagation at the ice surface. To calculate the voltage drop, the equation for the voltage gradient along the partial arc can be expressed as:

$$E_{arc} = 0.3464 I_m^{-0.3555} \qquad x < 7 \text{ cm} \tag{4.5}$$

$$E_{arc} = 0.2047 I_m^{-0.6607} \qquad x > 7 \text{ cm} \tag{4.6}$$

where E_{arc} is in kV_{rms}/cm and I_m in A represents the leakage current flowing on the ice surface. The voltage drop is obtained by multiplying (4.5) or (4.6) by the air gap length (cm):

$$V_{arc} = E_{arc} x \tag{4.7}$$

According to the previous BS tests, the transition between a breakdown streamer to a white arc corresponds to a leakage current of about 18-mA on the ice surface. By substituting this value in (4.1) and (4.2), we obtain the voltage drop (kV_{rms}):

$$V_{arc} = 1.44x \qquad x < 7 \text{ cm} \tag{4.8}$$

$$V_{arc} = 2.91x \qquad x > 7 \text{ cm} \tag{4.9}$$

Firstly, as stated in our paper [77], since the voltage drops for the small air gaps (i.e. $x < 7$ cm) are less than 4%, it might be concluded that the small air gaps have no significant effect on the total voltage drop. That is, in the vicinity of the HV electrode, a sufficiently large air gap in the ice layer is helpful, but a small air gap is not.

Secondly, according to the laboratory tests, partial arcs are mostly observed on the first BS closed to the HV electrode. When the applied voltage is increased to flashover voltage, it appears that the voltage drop (ΔV) value of air gap 1 becomes higher than its breakdown voltage (V_b) value. It indicates that a partial arc can be initiated along this one. If this occurs, a redistribution of potential along the ice-covered insulator should occur, similar to the process explained in [59]. Redistribution can lead to appearance of partial arcs across the other air gaps that may develop to flashover. Whenever the number of remaining air gaps is higher, they can better resist the redistribution of the voltage drops after the formation of the partial arc. This may be a reason for the increase in V_{WS} as the number of BSs increase from 4 to 5 and 5 to 6.

Figure 4.11 shows the appearance of partial arcs along air gaps during the evaluation period in a 6-BS test at CIGELE. Moreover, Figure 4.12 shows the simulation results of 4-, 5-, and 6-BS configurations with and without partial arc (PA).

Table 4.10, Table 4.11, Table 4.12 and their corresponding figures, i.e. Figure 4.13, Figure 4.14 and, Figure 4.15 compare the voltage drops (ΔV) in the 4-, 5- and 6-BS configurations before and after partial arc appearance at the first air gap.

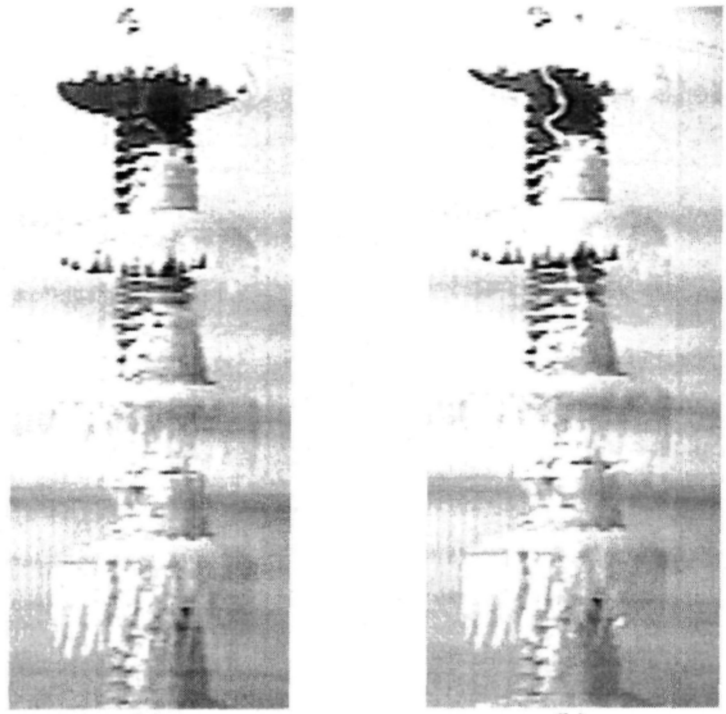

(a) (b)

Figure 4.11- Appearance of partial arcs along air gaps in a 6-BS trial test at CIGELE during application of 330 kV, a) after ≈1min b) after ≈6 min

Based on the simulation results, around 58.5-64.6% of ΔV_{ba-1} (variation of the voltage drop along air gap 1 before and after the formation of the partial arc) shifts to air gap 2. This means that air gap 2 acts as a potential barrier, and it prevents the re-equilibrium of the potential distribution along air gaps 2 and the other air gaps.

These 2D axisymmetric simulation results are in good agreement with previous validated 3D simulations in [59] which indicate that for three air gap configuration on a post insulator, 77% of ΔV_{ba-1} shifts to air gap 2 (Table 4.13 and Figure 4.16).

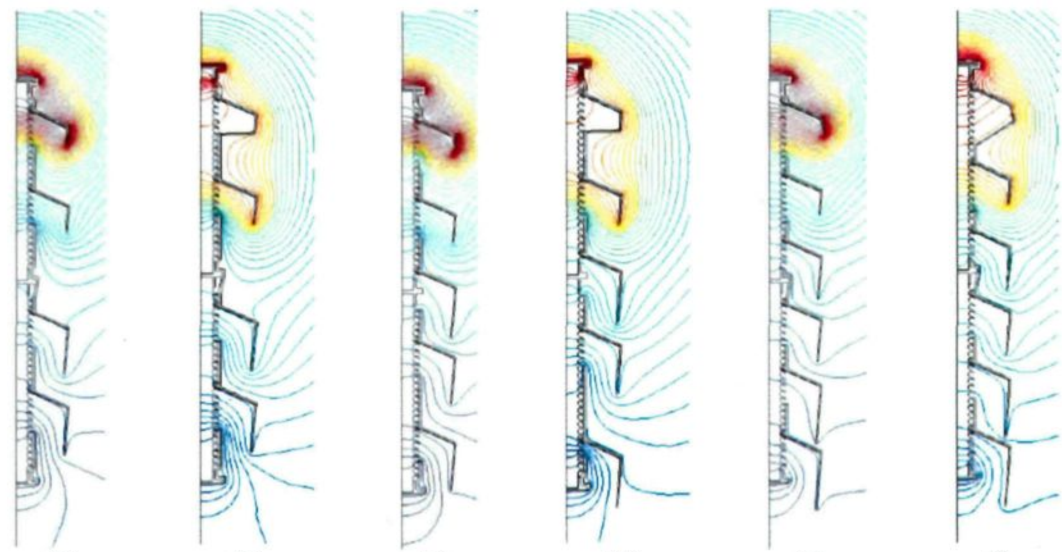

Figure 4.12- Equipotential line distributions for different BS configurations with and without partial arc (PA) a) 4BS, b)4BS with :PA, c) 5BS, d)5BS with :PA, e) 6BS, f)6BS with :PA,

Table 4.10-. Comparison of voltage drops (ΔV (%)) along the air gaps of 4-BS tests, before and after the formation of a partial arc along air gap1

Air gap no.	Before PA (ΔV_b)	After PA (ΔV_a)	Variation (ΔV_{ba})	Normalized Variation (ΔV_{ba-n})
1	52.5	23.7	-28.8	-100
2	23.1	41.7	18.6	**64.6**
3	9.8	14.9	5.1	17.7
4	14.0	19.1	5.1	17.7
Total	99.4	99.4	0	0

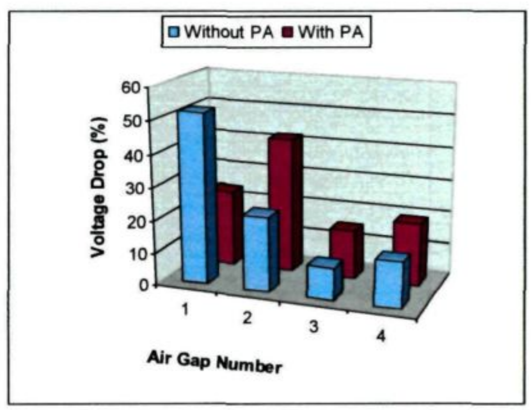

Figure 4.13- Comparison of voltage drops (ΔV (%)) along the air gaps of 4-BS tests, before and after the formation of a partial arc along air gap1

Table 4.11-.Comparison of voltage drops (ΔV (%)) along the air gaps of 5-BS tests, before and after the formation of a partial arc along air gap1

Air gap no.	Before PA (ΔV_b)	After PA (ΔV_a)	Variation (ΔV_{ba})	Normalized Variation ($\Delta V_{ba\text{-}n}$)
1	51.4	23.7	-27.7	-100
2	20.2	36.4	16.2	**58.5**
3	8.1	12.6	4.5	16.2
4	9.2	13.0	3.8	13.7
5	10.5	13.6	3.1	11.2
Total	99.4	99.3	-0.1	-0.4

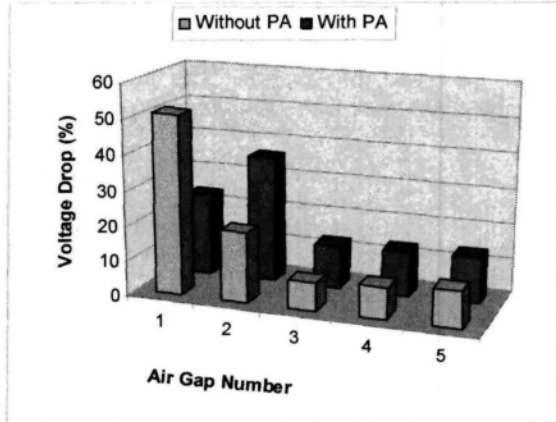

Figure 4.14- Comparison of voltage drops (ΔV (%)) along the air gaps of 5-BS tests, before and after the formation of a partial arc along air gap1

Table 4.12-.Comparison of voltage drops (ΔV (%)) along the air gaps of 6-BS tests, before and after the formation of a partial arc along air gap1

Air gap no.	Before PA (ΔV_b)	After PA (ΔV_a)	Variation (ΔV_{ba})	Normalized Variation ($\Delta V_{ba\text{-}n}$)
1	50.3	22.3	-28	-100
2	20.8	37.5	16.7	**59.6**
3	6.9	10.7	3.8	13.6
4	6.7	9.5	2.8	10.0
5	3.1	4.3	1.2	4.3
6	11.8	15.0	3.2	11.4
Total	99.4	99.3	-0.1	-1.1

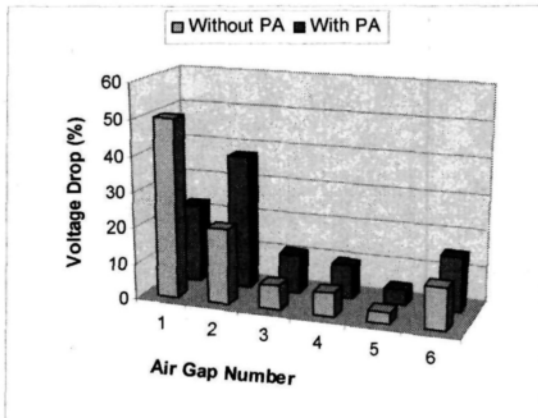

Figure 4.15- Comparison of voltage drops (ΔV (%)) along the air gaps of 6-BS tests, before and after the formation of a partial arc along air gap1

Table 4.13-.Comparison of voltage drops (ΔV (%)) along the 3 air gaps for 1 unit post insulator, before and after the formation of a partial arc along air gap1 (obtained data from [59])

Air gap no.	Before PA (ΔV_b)	After PA (ΔV_a)	Variation (ΔV_{ba})	Normalized Variation ($\Delta V_{ba\text{-}n}$)
1	54.8	34.3	-20.5	-100
2	18.0	33.9	15.9	77.6
3	23.4	29.1	5.7	27.8
Total	96.2	97.3	1.1	5.4

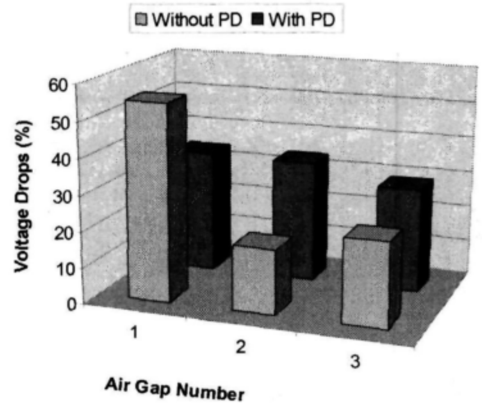

Figure 4.16- Comparison of voltage drops (ΔV (%)) along the 3 air gaps for 1 unit post insulator, before and after the formation of a partial arc along air gap1 (obtained data from [59]))

4.4 Improved hypothesis of BS effects

One of the acceptable approaches to rank electrical performance of insulators under icing conditions is determination of maximum withstand voltage (V_{WS}) [50], [48]. The approach requires a minimum of five tests to determine the V_{WS} for each insulator configuration, and it can give adequate data for design. The tests are complete when three withstands in four tests are observed at one voltage level, and two flashovers are observed at 5% higher voltage level. The V_{WS} is the test level that gives three withstands out of four tests. Test severity must be held constant in a series of the five trials. This method was used in the previous test of 4-, 5- and 6- BS configurations to rank their electrical performance.

As stated in section 4.2, it was found out, as the number of BSs increases from 4 to 5 and/or 5 to 6, there was an increase in V_{WS} of about 15 kV (Figure 4.1). Now, the key point of the optimization is responding to the following challenging question:

What are the effects of BSs on the ice-covered post insulator that lead to the increase in the maximum withstand voltage and/or a better electrical performance ranking?

It is generally stated in the literature that this improvement is due to the increase in dry arcing distance and to the delaying of ice bridging [2], [15], [16]. However, sometimes the emphasis is on the increase of dry arcing distance and sometimes on the creation of the air gaps (ice-free zones).

To continue replying precisely this key question, it is beneficial to review some important definitions which are:

1. Dry Arcing Distance (DAD): is the shortest distance in air between the high voltage and the ground electrodes.
2. Total air gap length ($L_{AG\text{-}tot}$): is the sum of the lengths of the air gaps which are created by BSs.
3. Total Ice-Free Leakage Distance ($IFLD_{tot}$): is the total of the shortest distances along the insulating surface between the high voltage and ground electrodes that are free of ice.

Actually, the above parameters can help us to quantify the created ice-free zones by BSs and to discover more precisely their effect in the heavy ice conditions. Thus, the average values of DAD, $L_{AG\text{-}tot}$ and $IFLD_{tot}$ which were measured or estimated in this study from the previous BS test results [2], [18]–[20] are shown in Table 4.14. In addition, Figure 4.17 is a graphical illustration of Table 4.14 for the four normalized parameters (V_{WS}, DAD, $L_{AG\text{-}tot}$ and $IFLD_{tot}$). As can be understood from Table 4.14, the four mentioned parameters have been normalized based on their corresponding values in the 4-BS configuration.

There is a slight increase in the DAD as the number of BSs increases from four to five and five to six (Table 4.14, Table 4.15, and Figure 4.17). However, the following analyses in this study demonstrate that in spite of their positive effect in DAD, this effect cannot be their principal effect that leads to the increase in the V_{WS}.

1. In fact, DAD depends only on the position of extreme (the top and bottom) BSs. In consequence, since the other BSs have no role in the increase of DAD, it can be concluded that they have no role in the increase of V_{WS} as well. However, it is undeniable that the other BSs have an important role in V_{WS} by creating some air gaps.

2. The level of V_{WS} increased by about 15 kV (5.3%) per BS as the number of BSs increased from four to six. On the contrary, based on the measurement of DAD (Table 4.14), the levels of DAD increase only 0.7% and 1.3% as the number of BSs increased from four to five and five to six, respectively. Thus, when we compare the BS test results, there is not a firm correlation between the increase in the DAD and the V_{WS}.

When comparing the figures of the BS tests (Figure 4.1), perhaps a focus on the remaining total unbridged zones rather than increased DAD would be helpful. In addition, the numerical results showed that when there is a conductive water film on the ice surface, about 99% of the applied voltage distributes along the different air gaps, regardless of the number, length, position, or inclination angle of the BSs. Thus, these ice-free zones have the principal role to determine the V_{WS}.

Table 4.14-.Comparative test results for post insulators with 4, 5 and 6 BSs under 30-mm ice accretion

BS Config.	4	5	6
V_{WS} (kV)	285	300	315
DAD (m)	3,01	3,03	3,07
$L_{AG\text{-}tot}$ (cm)	60,0	69,0	62,8
$IFLD_{tot}$ (m)	3,75	4,55	5,41
V_{WS} (%)	100	105,3	110,5
DAD (%)	100	100,7	102,0
$L_{AG\text{-}tot}$ (%)	100	115,0	104,7
$IFLD_{tot}$ (%)	100	121,3	144,3

Table 4.15-.Variation of the parameters for post insulators with 4, 5 and 6 BSs under 30-mm ice accretion

	4 to 5 BS	5 to 6 BS
V_{WS} (kV)	15 kV	15 kV
DAD (m)	0.02	0.04
$L_{AG\text{-}tot}$ (cm)	9.0	- 6.2
$IFLD_{tot}$ (m)	80	86
V_{WS} (%)	5.3	5.3
DAD (%)	0.7	1.3
$L_{AG\text{-}tot}$ (%)	15.0	-10.3
$IFLD_{tot}$ (%)	21.3	23

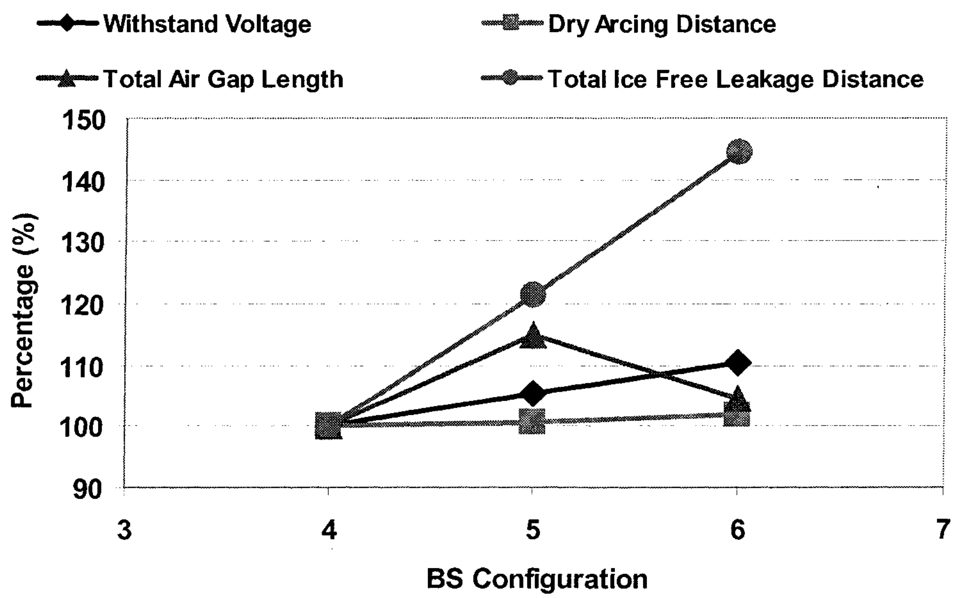

Figure 4.17- Comparative test results for post insulators with 4, 5, and 6 BSs under 30mm ice accretion

The levels of $IFLD_{tot}$ increase 21.3% (121,3-100) and 23.0% (144,3-121,3) as the number of BSs increases from 4 to 5 and 5 to 6, respectively (Table 4.14 and Figure 4.17). On the other hand, for the same transitions, the variations of $L_{AG\text{-}tot}$ are +15% (115-100) and -10.3 % (104.7-115), respectively. Therefore, among these three parameters (DAD, $L_{AG\text{-}tot}$ and $IFLD_{tot}$), $IFLD_{tot}$ has the best correlation with V_{WS}.

Moreover, by increasing the number of BSs from 5 to 6, not only $L_{AG\text{-}tot}$ does not increase but also it decreases around 10.3 %. In fact, the total length of the air gaps ($L_{AG\text{-}tot}$) depends mainly on the following parameters:

1. the number of BSs (N_{BS})
2. the average distance between the BSs ($D_{BSij\text{-}ave}$).

In the previous tests, to increase N_{BS} from 5 to 6, $D_{BSij\text{-}ave}$ decreases from 58.25 cm to 51.7 cm. Thus, however the number of AGs is increased, the mentioned decrease in the $D_{BSij\text{-}ave}$ is more determinant in the final variation of $L_{AG\text{-}tot}$.

In the previous 6-BS tests, it has been observed if two BSs (BS_5 and BS_6, Figure 4.1-c) are fully bridged, the V_{WS} =315 kV cannot be achieved. Table 4.16, Table 4.17, and Figure 4.18 compare the parameters for ice-bridging during the 6 BS-test under 30-mm ice accretion.

As Table 4.17 shows the variations of the parameters in the ice-bridged and no-ice-bridged states, there is a large difference ≈ 23% between their $IFLD_{tot}$ but no difference in their DADs and only a slight difference (≈ 3%) between their $L_{AG\text{-}tot}$. Hence, the effect of ice-bridging on the V_{WS} can be distinguished clearly by comparing the $IFLD_{tot}$ of the ice-bridged and unbridged states. However, it cannot be distinguished and explained by the other indicators (i.e. DAD and $L_{AG\text{-}tot}$).

According to the above analyses, the following "*improved hypothesis about the effects of BSs on standard post insulators under heavy icing conditions*" is proposed:

- *Qualification of BS effects:*

  A) The major effect is the creation of ice-free zones (unbridged ice zones).

B) The minor effect is the increase in dry arcing distance (DAD).

- *Quantification of BS effects:*

Among DAD, $L_{AG\text{-}tot}$, and $IFLD_{tot}$, the best indicator to quantify the electrical performance ranking (variation of V_{WS}) is the total ice-free leakage distance ($IFLD_{tot}$).

Table 4.16-.Comparison of the parameters in ice-bridging during the 6 BS-test under 30-mm ice accretion

BS Config.	6-BS-ice-bridged	6-BS
V_{WS} (kV)	300	315
DAD (m)	3,07	3,07
$L_{AG\text{-}tot}$ (cm)	60,8	62,8
$IFLD_{tot}$ (m)	4,55	5,41
V_{WS} (%)	105,3	110,5
DAD (%)	100,7	102
$L_{AG\text{-}tot}$ (%)	101,3	104,7
$IFLD_{tot}$ (%)	121,3	144,3

Table 4.17-.Variation of the parameters in ice-bridging during the 6 BS-test under 30-mm ice accretion

	"6-BS-ice-bridged" to 6-BS
V_{WS} (kV)	15
DAD (m)	0
$L_{AG\text{-}tot}$ (cm)	2
$IFLD_{tot}$ (m)	80
V_{WS} (%)	5.3
DAD (%)	0
$L_{AG\text{-}tot}$ (%)	3.4
$IFLD_{tot}$ (%)	23

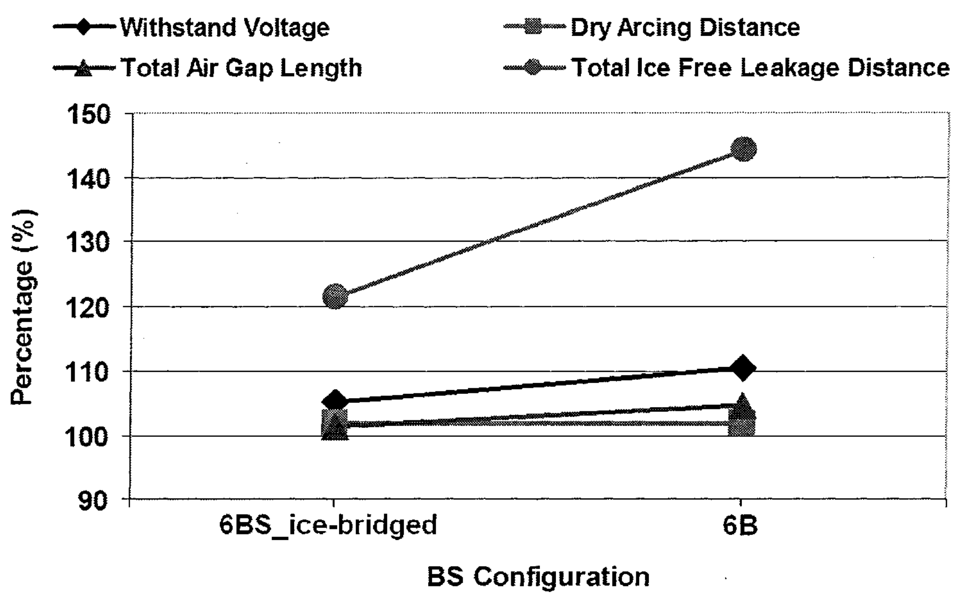

Figure 4.18- Comparison of the parameters in ice-bridging during the 6 BS-test under 30-mm ice accretion

4.5 Conclusions

The following conclusions and recommendations can serve to optimize the BS parameters and configurations:

1) Since the main objective of the BS installation is the improvement of the electrical performance under heaviest icing conditions, it is necessary to optimize BS parameters mainly under the heaviest anticipated icing situations. For example:

   A. Radial ice accretion of 30-mm on a rotating cylinder, corresponding to 60 mm on the ground or a fixed cylinder,

   B. Melting conditions,

   C. Horizontal incidence angle of precipitation (i.e. winter storm with strong winds).

2) The simulation results show that, the variation on the relative permittivity of BSs ($\varepsilon_{r\text{-}BS}$= 2-15), actually has no considerable effect on the electrical field distributions of the ice-covered insulator during the melting period. Therefore, from the viewpoint of the electrical field distributions or voltage drops along the air gaps, the optimized value of $\varepsilon_{r\text{-}BS}$ is an arbitrary value in the mentioned range.

3) The numerical results of the EHV ceramic ice-covered insulator equipped with BSs showed that when there is a conductive water film at the ice surface, the total voltage drops distributed along the air gaps (ΔV_{tot}) is about 99% of the applied voltage. This reality ($\Delta V_{tot} \approx$ 99%) is regardless of the number, lengths, or positions of the air gaps. This value (99%) is also constant in spite of the variations in inclination angles, diameters of the BSs, and the inclination angle of the icicles on BSs. ΔV_{tot} does not vary during the transition from HVAC to HVDC and frequency variation from 60 Hz to 50 Hz as well. These 2D

axisymmetric simulation results are in good agreement with previous validated 3D simulations in [59], [60] which, indicate that the total voltage drop across the air gaps in a melting period is around 96% regardless of the number, length or position of the air gaps. In addition, the results of the 2D simulations were verified during the analysis of the effect of partial discharge appearance on the voltage drops.

4) The improved hypothesis concerning the positive effects of BSs on standard post insulators under heavy icing conditions is:

   - Qualification of BS effects:

     A) The major effect is the creation of ice-free zones (unbridged ice zones).

     B) The minor effect is the increase in dry arcing distance (DAD).

   - Quantification of BS effects:

     Among DAD, $L_{AG\text{-}tot}$, and $IFLD_{tot}$, the best indicator to quantify the electrical performance ranking (variation of V_{WS}) is the total ice-free leakage distance ($IFLD_{tot}$).

5) It was shown that following the addition of 4, 5 or 6 BSs, more that 50% of the applied voltage distributes along the closet air gap to the HV electrode, which was also the longest one. Hence, the air gap 1 (or ice-free zone 1) and consequently the BS_1 has the most determinant role in the electrical performance of the ice-covered insulator. Thus, it is recommended to select the largest possible diameter for BS_1 to create the largest ice-free zone. Also, the experimental test observations validated that the most electrical field stresses are on BS_1. Therefore, to prevent any damages (puncture, etc.) under the high electric field stresses close to HV electrode, using a modified grading ring or a creepage extender instead of a BS might be recommended. Another solution is the

installation of BS_1 on 2nd or 3rd insulator shed instead of 1st shed, which is closest to HV electrode. However, this latter solution has a negative side – a slight decrease in DAD.

CHAPTER 5

GEOMETRIC MODELING AND DESIGN

CHAPTER 5

GEOMETRIC MODELING AND DESIGN APPROACH

5.1 Introduction

In the previous chapter, parametric studies and an improved hypothesis of the effect of BSs under heavy icing conditions were presented. The current chapter describes the geometric modeling of the post insulator equipped with BSs considering the precipitation angle. Then, optimality and post-optimality analyses of BS parameters using Taguchi Method is explained.

5.2 Geometric modeling of the precipitation on the insulator with BSs

Figure 5.1-a and Figure 5.1-b show two-unit post station insulator after heavy ice accretion for two situations; i.e. without BS and equipped with 6 BSs, respectively [16]. Figure 5.2-a and Figure 5.2-b illustrate the dimensions of these standard post insulator units and the geometric model of the ice-covered post insulator outfitted with BSs taking into account precipitation direction.

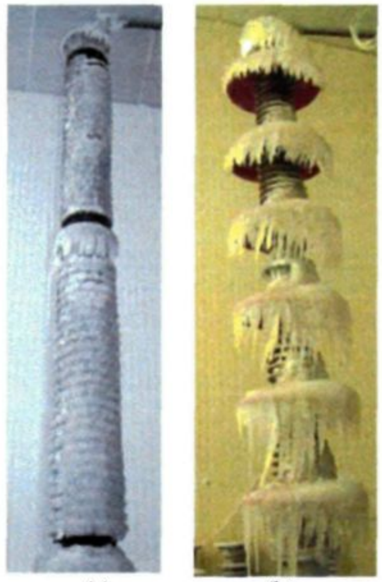

(a) (b)

Figure 5.1- Two-unit post station insulator after ice accretion:
(a) untreated state (b) equipped with 6 BSs [2], [18]–[20]

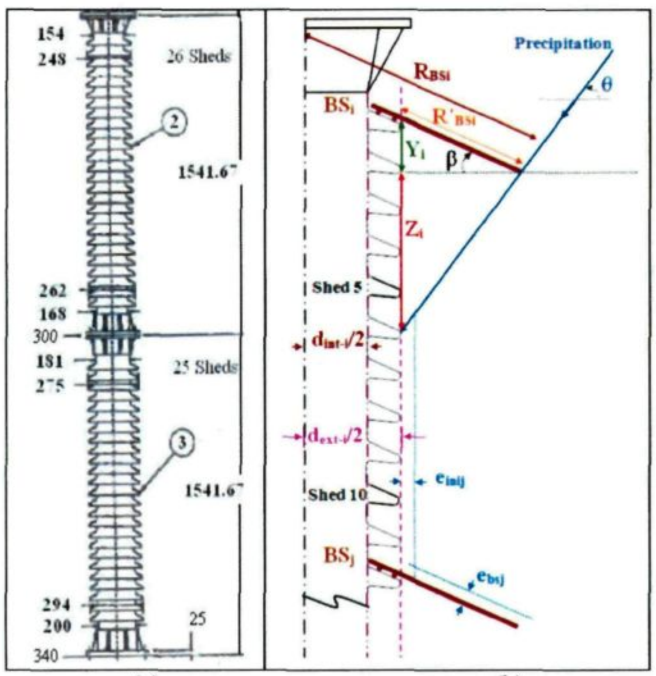

(a) (b)

Figure 5.2- Illustration of the standard post insulator and the geometric model
(a) Standard post insulator dimensions (mm) (b) Geometric model of the ice-covered post insulator with BSs considering precipitation direction

In the geometric model (Figure 5.2-b) and the consequent equations:

D_{BSi} (cm): is the outer diameter of BS_i.

R_{BSi} (cm): is the radius of BS_i.

R'_{BSi} (cm): is the portion of BS_i that exceeds the insulator-shed length.

BS_{ij}: signifies the zone between BS_i and BS_j.

e_{inij} (cm): is the ice thickness on the insulator surface in BS_{ij}.

e_{bsj} (cm): is the ice thickness on the upper surface of BS_j.

d_{ext-i} (cm): is the average exterior diameter of the standard insulator shed under BS_i.

d_{int-i} (cm): is the average interior diameter of the standard insulator shed under BS_i.

β (°): is the inclination angle of BS_i ($0 \leq \beta \leq 24.5°$; 24.5° is the upper angle of the insulator shed.).

θ (°): is the incidence angle of precipitation ($\theta \geq 0$).

Y_i (cm): is the insulator length protected from precipitation by BS_i and it is independent to θ.

Z_i (cm): is the insulator length protected from precipitation by BS_i and it dependent to θ.

According to the geometric model (Figure 5.2-b) the following relations can be written:

$$R'_{BS_i} = 0.5D_{BS_i} - \frac{0.5d_{ext\_i}}{\cos\beta} \tag{5.1}$$

$$Y_i = R'_{BS_i} \sin\beta \tag{5.2}$$

$$Z_i = (R'_{BS_i} \cos\beta)\tan\theta \tag{5.3}$$

The sum of Y_i and Z_i is the total protected length (W_i) of insulator under BS_i. Therefore:

$$W_i = Y_i + Z_i \qquad (5.4)$$

$$W_i = R'_{BS_i}(\sin\beta + \cos\beta \times \tan\theta) \qquad (5.5)$$

$$W_i = 0.5(D_{BS_i} - \frac{d_{ext\_i}}{\cos\beta})(\sin\beta + \cos\beta \times \tan\theta) \qquad (5.6)$$

The incidence angle of precipitation (θ) in the CIGELE Laboratory condition is 53° (±5°) [90], [91].

The previous BS tests were carried out on the middle and bottom units (unit 2 and 3 in Figure 5.2-a) of a three-unit station post insulator, typically used on 735 kV Hydro-Quebec network [36]. Thus, the average values in the equations should be calculated for these 2 units as well. Figure 5.2-a indicates that "d_i" is in the range of 24.8-29.4 cm. To ease the calculation of W_i, the average of d_i (d_{ave}=27.1 cm) can be used. Hence,

$$R'_{BS_i} \approx 0.5(D_{BS_i} - \frac{d_{ave}}{\cos\beta}) \qquad (5.7)$$

$$W_i \approx 0.5(D_{BS_i} - \frac{d_{ave}}{\cos\beta})(\sin\beta + \cos\beta \times \tan\theta) \qquad (5.8)$$

To have a better sense of W_i, it can be stated based on the total number of protected sheds (N_{wi}). So:

$$N_{W_i} = \frac{W_i}{d_{shsh}} \qquad (5.9)$$

Where, d_{shsh} is the average shed-to-shed distance of the post insulator ($d_{shsh} \approx 5cm$).

Finally, using (5.8) and (5.9), we obtain:

$$N_{wi}(D_{BSi},\beta,\theta) \approx 0.1(D_{BS_i} - \frac{d_{ave}}{\cos\beta})(\sin\beta + \cos\beta \times \tan\theta) \tag{5.10}$$

The above equations were implemented in a MATLAB m-file. Table 5.1 and Figure 5.3 show the calculated values of N_{wi} based on the variations of θ for D_{BS}= *65.5 cm* and β=*24.5°*.

Table 5.1-.The effect of incidence angle of precipitation (θ) on the N_{wi} for D_{BS}= *65.5 cm* and β =*24.5°*

State no.	1	2	3	4	**5**	**6**	**7**	8
θ	0	20	40	45	**48**	**53**	**58**	60
N_{wi}	1.49	2.67	4.22	4.75	**5.11**	**5.82**	**6.71**	7.14

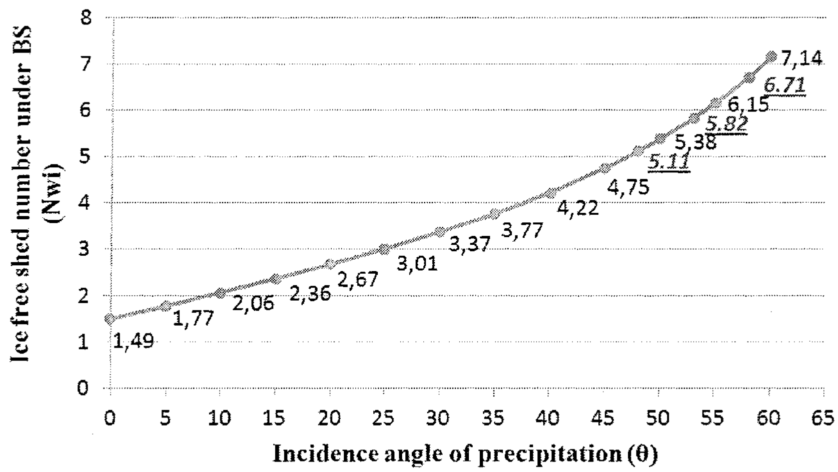

Figure 5.3- The effect of incidence angle of precipitation (θ) on the N_{wi} for D_{BS}= *65.5 cm* and β=*24.5°*

The values (D_{BS}= *65.5 cm* and β=*24.5°*) were selected based on the previous BS test conditions. The comparison of the states no. 5, 6, and 7 in Table 5.1 with the previous BS test results in [2] shows good agreement. Because in the BS tests, the total number of completely or partially ice-free sheds under each BS were between 5 to 7.

Figure 5.4 and Figure 5.5 show the effect of β (BS angle) and D_{BSi} (Diameter of BS) variations on N_{wi}, respectively, for the 4 different incidence angles of precipitation. In fact, "$\theta = 53\pm5°$" represents the CIGELE Laboratory condition and "$\theta = 0°$" represents the worst possible state of θ (winter storms with strong winds). To better understand the BS configurations, much valuable information can be concluded from Figure 5.3 to Figure 5.5. For example:

Firstly, these three figures quantify the effect of wind or precipitation direction on the total number of protected sheds (N_{wi}). The following relation obtained from Figure 5.5 compares the effect of precipitation direction under laboratory ($\theta = 53°$) and winter storm ($\theta = 0°$) conditions.

$$N_{wi}(\theta=0°) \approx \tfrac{1}{4} N_{wi}(\theta=53°) \qquad (\beta=24.5°,\ D_{BS}= 65.5\ cm) \qquad (5.11)$$

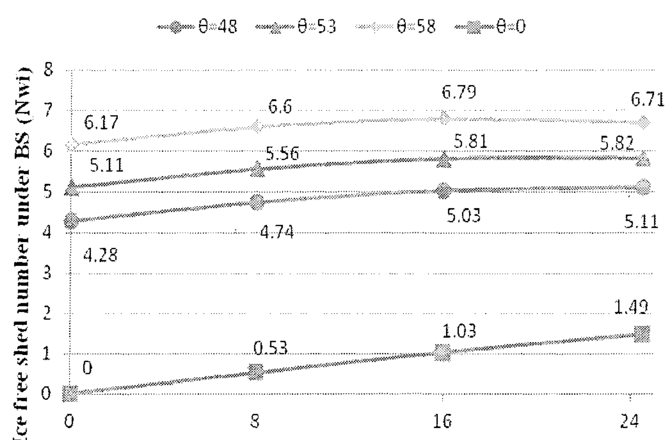

Figure 5.4- The effect of β (BS angle) variation on N_{wi} ($D_{BS}= 65.5\ cm$) for $\theta = 53\pm5°$ and $\theta = 0°$

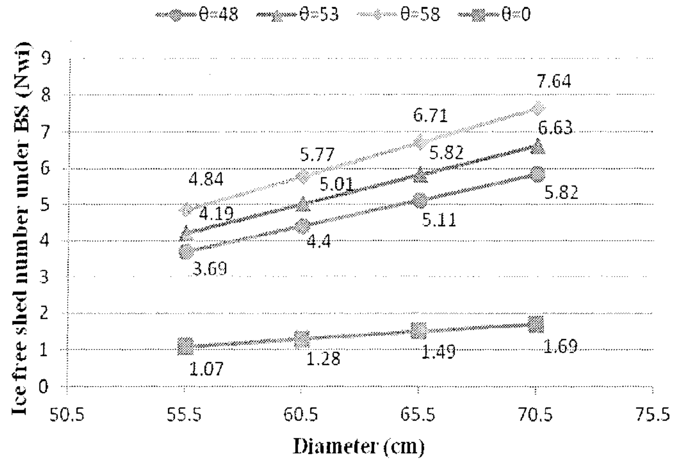

Figure 5.5- The effect of D_{BSi} (Diameter of BS) variation on N_{wi} ($\beta = 24.5°$) for $\theta = 53\pm5°$ and $\theta = 0°$

Secondly, comparing the graphs that correspond to "$\theta = 0°$" in Figure 5.4 and Figure 5.5, the graph slope in Figure 5.4 [$slope \approx 1.49 / 3 = 0.50$] is about 2.4 times more than the slope graph in Figure 5.5 [$slope \approx (1.69\text{-}1.07) / 3 = 0.21$]. That is:

$$Slope\ of\ N_{wi}\ (D_{BSi}{=}65.5cm,\ \beta,\ \theta{=}0°) \approx 2.4 \times Slope\ of\ N_{wi}\ (D_{BSi},\ \beta{=}24.5°,\ \theta{=}0°) \qquad (5.12)$$

This indicates that in the selected steps of variation for the diameter and the inclination angle of BSs, the angle has a more determinant role in the creation of the ice-free zones. This point is confirmed in the Taguchi Method and the importance ranking of the BS parameters as well (Figure 5.6 and Figure 5.7).

5.3 Calculation of the total ice-free leakage distance ($IFLD_{tot}$)

To calculate the ice-free leakage distance along the surface of insulator using the model ($IFLD_{1\text{-}m}$), we can write:

$$IFLD_{1\text{-}m}\ (cm) \approx N_{BS} \times K \times N_{wi} \times d_{sh\text{-}sh}\ (cm) \qquad (5.13)$$

Where,

N_{BS}: is the number of installed BSs.

K: is the ratio of total leakage distance (3.5 m) on the total dry arcing distance (1.39 m) of the post insulator unit: 2.52.

d_{shsh}: is the shed-to-shed distance of the post insulator: ≈ 5 cm.

Also, the ice-free leakage distance of the bottom surface of BS_i ($IFLD_{b\_BSi}$) can be calculated by:

$$IFLD_{bBS_i} = 0.5(D_{BS_i} - d_{BS_i}) \tag{5.14}$$

Where, D_{BSi} and d_{BSi} are outer and inner diameter of BS_i, respectively. In the previous BS tests (Figure 5.1-b), we have: $IFLD_{bBSi} = 23.0\ cm$.

Then, we can obtain the total Ice-Free Leakage Distance of bottom surfaces of BSs ($IFLD_2$) as:

$$IFLD_2\ (cm) \approx IFLD_{b\text{-}BSi} \times N_{BS} \tag{5.15}$$

A special attention is required for the calculation of IFLD under the last BS near the ground electrode to prevent over estimation. In fact, the calculated number of ice-free sheds under the last BS (N_{wi}) must not be more than the number of sheds located between the last BS and the ground electrode (N_G). Thus, $IFLD_{G\text{-}m}$ is defined by equations (5.16) and (5.17):

$$IFLD_{G\text{-}m} = 0 \qquad (if\ N_{wi} \leq N_G) \tag{5.16}$$

$$IFLD_{G\text{-}m} = (N_{wi} - N_G) \times K \qquad (if\ N_G \leq N_{wi}) \tag{5.17}$$

At the end, we achieve the total ice-free leakage distance as follows:

$$IFLD_{tot\text{-}model} \approx IFLD_{1\text{-}m} + IFLD_{2\text{-}m} - IFLD_{G\text{-}m}. \tag{5.18}$$

The above equations were implemented in a Matlab m-file to calculate the $IFLD_{tot\text{-}model}$ (total ice-free leakage distance obtained from the model). Table 5.2 shows the verification of the geometric model by comparing its results for the calculation of $IFLD_{tot}$ with the results of the previous BS test in [2]. The maximum error is 1.6% which is for 5-BS configuration. More precisely, taking into account the effective precipitation angle equals to 51° ($\theta = 51°$) the model has its best agreement (i.e. minimum errors) to calculate the $IFLD_{tot}$ of the previous BS tests.

Table 5.2-.Comparison of $IFLD_{tot}$ of the geometric model results and the experimental test results, 30 mm ice accretion on rotating cylinder

	4 BSs	5 BSs	6 BSs
$IFLD_{tot}$ (test)	375.3	454.9	540.9
$IFLD_{tot}$ (model)	369.8	462.2	535.6
Error (%)	-1.5	1.6	-1.0

5.4 Design approach using Taguchi method

Taguchi method was introduced in Chapter 2 at the end of Section 2.5. This method is used for the optimization of a single performance characteristic. Moreover, signal-to-noise (S/N) ratio is used to represent a response or quality characteristic. In other words, S/N ratio represents the magnitude of the mean of a process compared to its variation and the largest S/N is required. Calculation of the S/N ratio depends on the objective of real or virtual experiments [71]–[74]. Three types of quality characteristics for the Taguchi Method are introduced in Minitab software, i.e., larger-the-better, nominal-the-best, and smaller-the-better. They are defined as follows:

a) larger-the-better

$$\frac{S}{N} = -10\log\left(\frac{1}{n}\sum_{i=1}^{n}\frac{1}{y_i^2}\right) \tag{5.19}$$

b) nominal-the-best

$$\frac{S}{N} = -10\log\left(\frac{1}{nS}\sum_{i=1}^{n} y_i^2\right) \tag{5.20}$$

c) smaller-the-better

$$\frac{S}{N} = -10\log\left(\frac{1}{n}\sum_{i=1}^{n} y_i^2\right) \tag{5.21}$$

where

S: is the standard deviation.

y_i: is the calculated index.

n: is the number of the real or virtual experiments.

S/N ratio of smaller-the-better is used in the current study. This S/N ratio is usually chosen for the characteristics that need the smallest possible ideal value.

In the following, it is clarified how to define a proper single index to compare the electrical performance of the various BS configurations. As stated in Chapters 3 and 4:

1. Air gaps have an important role in the electrical performance of ice-covered insulators. The numerical results of the EHV ceramic ice-covered insulator equipped with BSs show that when there is a conductive water film at the ice surface, about 99% (ΔV_{tot} = 99%) of the applied voltage distributes along the air gaps, regardless of the number, length, position, inclination angle, or diameter of the BSs. Also, ΔV_{tot} is independent of the inclination angle of the icicles.

2. In the previous BS tests, among DAD, $L_{AG\text{-}tot}$, and $IFLD_{tot}$, the best indicator to quantify their electrical performance ranking (variation of V_{WS}) is the total ice-free leakage distance.

Thus, the following index (y_i) was proposed to use Taguchi design approach for the BS configurations:

$$y_i = \Delta V_{tot\_i} / IFLD_{tot\_i} \tag{5.22}$$

Minitab software was used to implement the Taguchi Method. Three controlling parameters of BS were selected, namely: the number, inclination angle, and diameter of BSs (Table 5.3). It aims to study the effect of these BS parameters in the improvement of the electrical performance of the two units of the standard post insulator.

Table 5.3-. The parameters of BSs and the corresponding levels in the Taguchi method

Parameter	Notation	Level 1	Level 2	Level 3	Level 4
Number of BSs	N_{BS}	3	4	5	6
Angle (degree)	$Angle_{BS}$	0	8	16	24.5
Diameter (cm)	D_{BS}	55.5	60.5	65.5	70.5

Regarding the selected values for BS parameters in Table 5.3:

1. the range of the number of BSs was selected from 3 to 6. Because, firstly the literature recommends the creation of at least three air gaps [59]. In fact, the in-between air gap function as a potential barrier and it impedes the formation of partial arcs and flashover development. Secondly, based on the previous BS tests under 30-mm ice accretion, the maximum number of BSs to prevent ice bridging is six.
2. The selected inclination angles of BSs were 0, 8, 16, and 24.5 degree. They cover the 0-24.5 degree range in equal steps approximately. Moreover, " 0° " and " 24.5° "

were considered, respectively, as the minimum and maximum degrees which are feasible for the installation of BSs on the post insulator (Figure 5.2-b).

3. Next, the range of the diameter variations was selected between 55.5 and 70.5 cm by equal steps of 5 cm. The "65.5 cm" corresponds to the previous BS tests in CIGELE [2].
4. Finally, it was supposed that the different configurations have equal DADs roughly. So, the effect of the variation of DADs on the electrical performance of the BS configurations was neglected. Moreover, it was supposed that the distances between BSs are enough to prevent ice-bridging and electrical breakdown along the air gaps.

Taguchi method was used to analyze the virtual experiments (i.e. the configurations defined by the geometric model) under two incidence angles of precipitation i.e. $\theta = 51°$ and $0°$ (Figure 5.2-b). In fact:

1. $\theta = 51°$ is the effective incidence angle which matches the conditions of the previous BS test in CIGELE Lab.
2. $\theta = 0°$ represents the worst possible state of θ that is winter storms with strong winds.

Table 5.4 shows the selected design matrix based on Taguchi L16 orthogonal array consisting of 16 states of the virtual experiments. In addition, it depicts the results of the normalized $IFLD_{tot\ i}$ and the corresponding index values. $IFLD_{tot\ i}$ was calculated by a MATLAB programming for each virtual experiment using the geometric modeling and consequential mathematical equations of the insulator equipped with BSs (Figure 5.2-b).

In order to prevent being faced with very small values in Table 5.4, the index values were normalized based on the bolded sate (i.e. state 8 of " $\theta = 51°$ "). Moreover, among the 32 virtual experiments in Table 5.4, the 8th is the only one with available experimental results. So, normalizing based on state 8 can provide a good benchmark for a general comparison of all virtual experiments. "Empty" in Table 5.4 means this column represents no design parameter in the calculations. This trick can be used in Taguchi method without occurring any problem in the analysis [72], [92].

Table 5.4-. Matrix of the virtual experiments (orthogonal array L16) and the consequent results

	BS N	Inclination Angle (°)	Diameter (cm)	Empty	$IFLD_{tot\ i}$ (θ=51) (cm)	$IFLD_{tot\ i}$ (θ=0) (cm)	Normalized Index (θ=51)	Normalized Index (θ=0)
1	3	0	55.5	1	202.0	69.0	183.0	535.9
2	3	8	60.5	2	240.1	86.5	154.0	427.6
3	3	16	65.5	3	275.8	108.0	134.1	342.5
4	3	24.5	70.5	4	306.4	133.0	120.7	278.1
5	4	0	60.5	3	300.5	92.0	123.1	401.9
6	4	8	55.5	4	285.8	111.8	129.4	330.7
7	4	16	70.5	1	404.6	150.9	91.4	245.0
8	**4**	**24.5**	**65.5**	2	369.8	166.9	**100.0**	221.6
9	5	0	65.5	4	414.5	115.0	89.2	321.6
10	5	8	70.5	3	485.9	152.9	76.1	241.9
11	5	16	55.5	2	367.6	162.6	100.6	227.4
12	5	24.5	60.5	1	413.8	195.5	89.4	189.1
13	6	0	70.5	2	526.7	138.0	70.2	268.0
14	6	8	65.5	1	516.4	178.2	71.6	207.5
15	6	16	60.5	4	487.0	205.5	75.9	179.9
16	6	24.5	55.5	3	438.5	219.0	84.3	168.9

To determine which BS parameters significantly affect the electrical performance of the insulator, the S/N ratio based on smaller-the-better criterion for " $\theta = 51°$ " and " $\theta = 0°$ " were calculated in Table 5.5 and Table 5.6, respectively.

Table 5.5-. The response of the S/N ratios and their rank (in CIGELE Lab. condition, θ= 51°)

Parameters	Level 1	Level 2	Level 3	Level 4	Max-Min	Rank
Numbers of BSs	-43.30	-40.81	-38.93	-37.54	5.76	1
Angle	-40.75	-40.18	-39.86	-39.79	0.95	3
Diameter	-41.51	-40.55	-39.66	-38.85	2.66	2

Table 5.6-. The response of the S/N ratios and their rank (winter storm condition, θ= 0°)

Parameters	Level 1	Level 2	Level 3	Level 4	Max-Min	Rank
Numbers of BSs	-51.69	-49.29	-47.62	-46.14	5.56	1
Angle	-51.34	-49.26	-47.68	-46.47	4.87	2
Diameter	-49.16	-48.83	-48.52	-48.22	0.94	3

The concept of the Max-Min values in Table 5.5 and Table 5.6 can be interpreted as the *impact factor* of the each BS parameter (Figure 5.6). For example, the impact factor of the inclination angle of BSs can be compared under laboratory and winter storm conditions (0.95 versus 4.87 in Figure 5.6). Moreover, in winter storm condition ($\theta = 0°$), the inclination angle of BS has a much more important role in the formation of larger ice-free zones and increasing V_{WS} than the BS diameter (4.87 versus 0.94 in Figure 5.6). Figure 5.6 concludes the importance order (rank) of the three BS parameters for the laboratory condition and the winter storm condition as follows:

$$1.\ N_{BS},\quad 2.D_{BS},\quad 3.Angle_{BS} \qquad \text{(in the laboratory condition, } \theta = 51°) \tag{5.23}$$

$$1.\ N_{BS},\quad 2.Angle_{BS},\quad 3.D_{BS}. \qquad \text{(in winter storm condition, } \theta = 0°) \tag{5.24}$$

These orders or rankings of the parameters (sensitivity analysis) have been achieved based on the specific selected variation of the parameters. In other words, sensitivity analysis is completely dependent on the selected variation ranges of the inputs. Reasonable variations should be selected in order to obtain acceptable post-optimality (sensitivity) results.

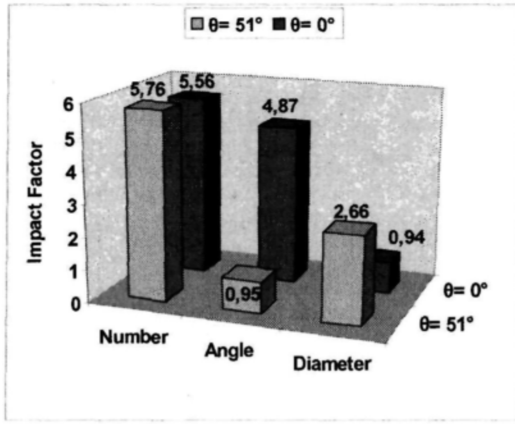

Figure 5.6- Impact factor of the BS parameters

Figure 5.7 shows graphically the S/N ratios of Table 5.5 and Table 5.6. The middle line represents the value of the total mean of the S/N ratios. Regardless of the category of the four controlling parameters, the larger S/N ratio corresponds to the better performance. Therefore, according to the S/N results (Figure 5.7), the optimal condition for the BS configurations is:

$N_{BS} = 6,\ Angle_{BS} = 24.5°,\ and\ D_{BS} = 70.5\ cm.$ (5.25)

This conclusion is obtained for both the incidence angles of precipitation ($\theta = 51°$ and $0°$) and the defined ranges of the BS parameters.

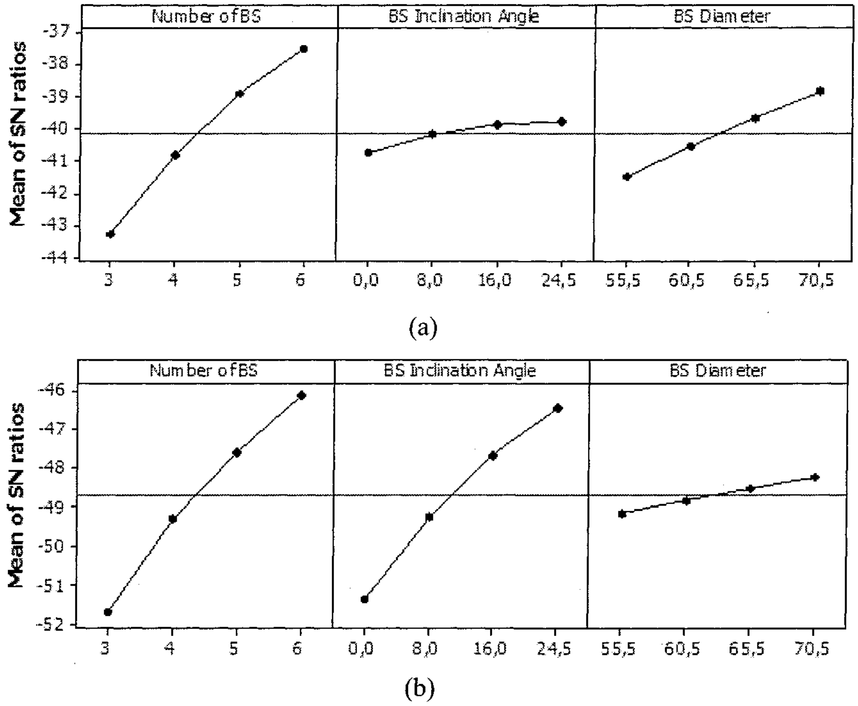

Figure 5.7- Variation of average S/N ratios (smaller is better) with factor levels a) CIGELE Lab. Condition ($\theta = 51°$) b) winter storm condition ($\theta = 0°$)

5.5 Optimization of BS positions

According to the improved hypothesis, the optimum positions (P_{BSi}) are those which:

1) Maximize $IFLD_{tot}$ (i.e. creation of the largest ice-free zones) as the first priority.

2) Maximize dry arcing distance as the second priority.

Maximizing the $IFLD_{tot}$ can be achieved using the described geometric model (Figure 5.2-b) for various possibilities. If only one case results in a maximum $IFLD_{tot}$, then that case includes the optimum positions. However, it is also possible that several cases provide a same maximum $IFLD_{tot}$. Then, it is recommended to select the case which includes the highest dry arcing distance. Figure 5.8 depicts a geometric model in order to evaluate the variation of dry arcing distance for different BS positions. It graphically confirms that DAD depends only on the first and last BS. Table 5.7 shows the three cases to compare their DAD. According to Figure 5.8, we conclude:

$$\overline{HCBG} < \overline{HABG} \tag{5.26}$$

$$\overline{HADG} < \overline{HABG} \tag{5.27}$$

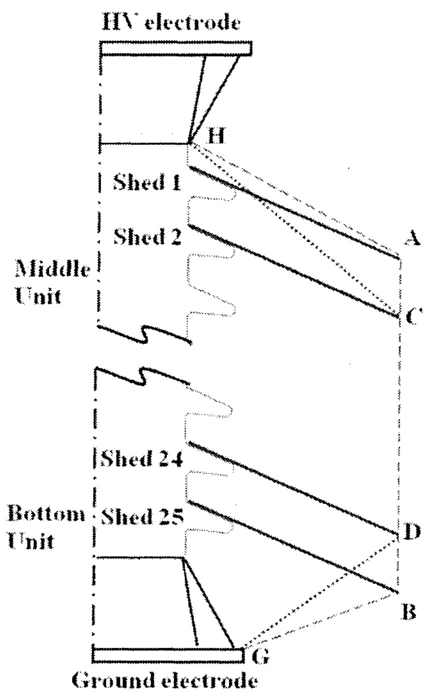

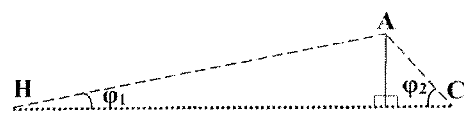

$$\overline{HC} = \overline{HA}\cos\varphi_1 + \overline{AC}\cos\varphi_2$$

$$\cos\varphi_1 \ \& \ \cos\varphi_2 < 1$$

Hence:

$$\overline{HC} < \overline{HA} + \overline{AC}$$

Similarly, we can conclude:

$$\overline{GD} < \overline{GB} + \overline{BD}$$

Figure 5.8- Geometric model of dry arcing distance

Table 5.7-. Comparison of dry arcing distance for different cases

	First BS	Last BS	Dry Arcing Distance
Case I	on shed 1	on shed 25	HABG
Case II	on shed 2	on shed 25	HCBG
Case III	on shed 1	on shed 24	HADG

It means that case I (Table 5.7) has the highest DAD. In fact, to achieve the maximum DAD, the first and the last BS should be installed on the first and the last shed of the insulator, respectively. Moreover, based on the geometric model of DAD (Figure 5.8), a closer BS position to the ends (i.e. HV or ground), leads to a higher DAD. However, the installation of the last BS on closer sheds to the ground electrode may reduce the $IFLD_{tot}$. On the other hand, a closer BS to the HV electrode may damage sooner due to the higher electric field stress and partial arcs. In brief, for the 3 to 6-BS configurations with 30 mm radial ice accretion, it is advised to:

- Consider at least 48-50 cm (i.e. 9-11 shed-to-shed distance) between consecutive BSs.
- Install the first BS on the 1^{st} or 2^{nd} shed of the insulator-unit close to HV (middle unit) and the last BS on 19^{th} up to 22^{nd} shed of the unit close to the ground (bottom unit).

Figure 5.8 illustrates the flowchart of the described optimization procedure.

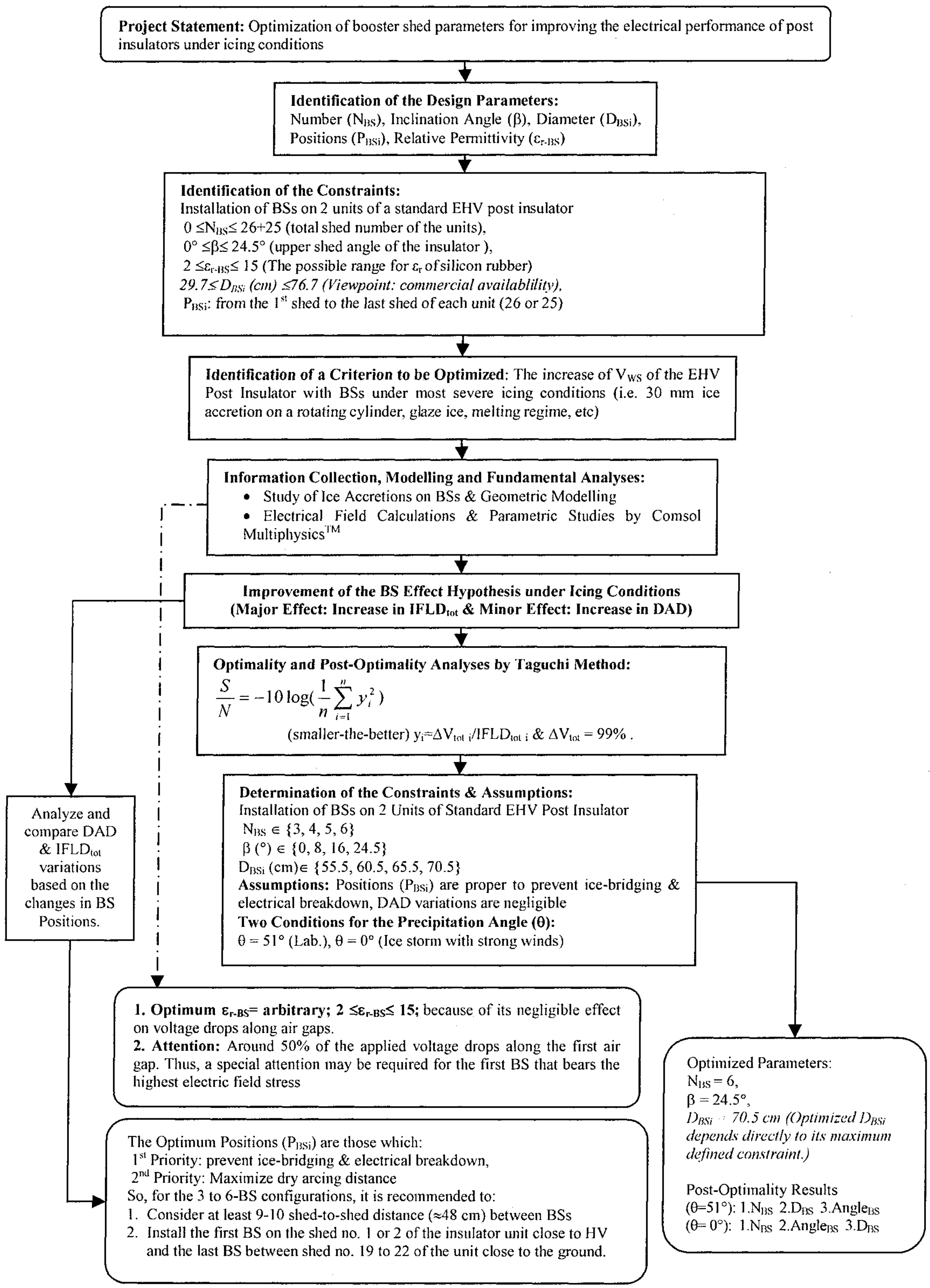

Figure 5.9- Optimization flowchart 1 (analytical and simulation analyses)

5.6 Response surface analyses

Response surface methodology (RSM) is a set of mathematical and statistical procedures. Following the Taguchi method analyses, RSM is frequently used to achieve a deeper analysis. It investigates the relations between some explanatory variables and one or more response variables. It tracks a target response, which helps researchers to improve products and services. A low-order polynomial in some area of the explanatory variables is usually used. Almost all RSM use the first-, second-order, or both models. In RSM problems, generally the correlation between the independent variables and the response(s) can not be formulated, consequently it is approximated. In order to approximate the parameters in the polynomials, the least squares method is used. Then, based on the fitted surface, the response surface analysis can be achieved [72], [93].

Figure 5.10 shows The 3D response surface plot of the $IFLD_{tot}$ as a function of inclination angle and diameter of BSs. As we can see, there is no local maximum in the response surfaces of $IFLD_{tot}$. Moreover, Figure 5.11 shows the 2D response surface plots of the $IFLD_{tot}$ for some specific values. These graphs provide various selections of BS parameters to reach a specific $IFLD_{tot}$. Therefore, it can be used as an effective tool to provide a more reliable design of BSs under heavy icing conditions.

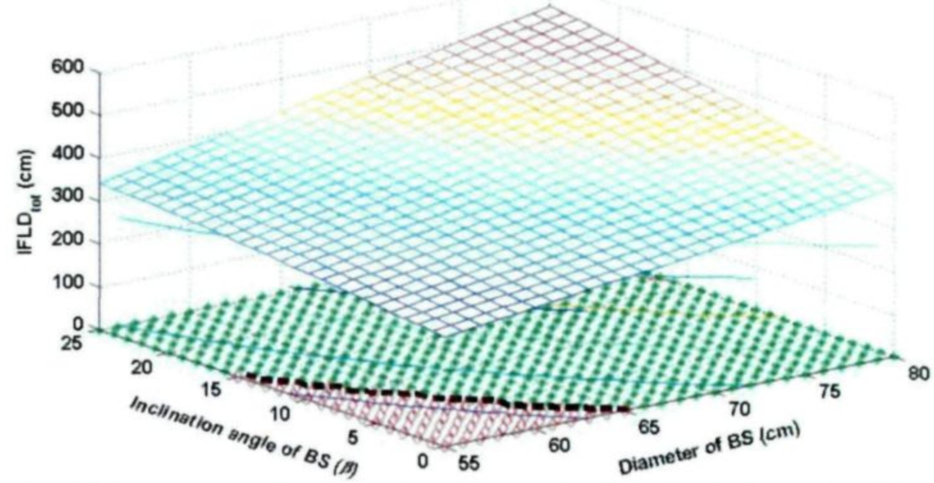

Figure 5.10- The 3D response surface plot of the $IFLD_{tot}$ as a function of inclination angle and diameter of BSs

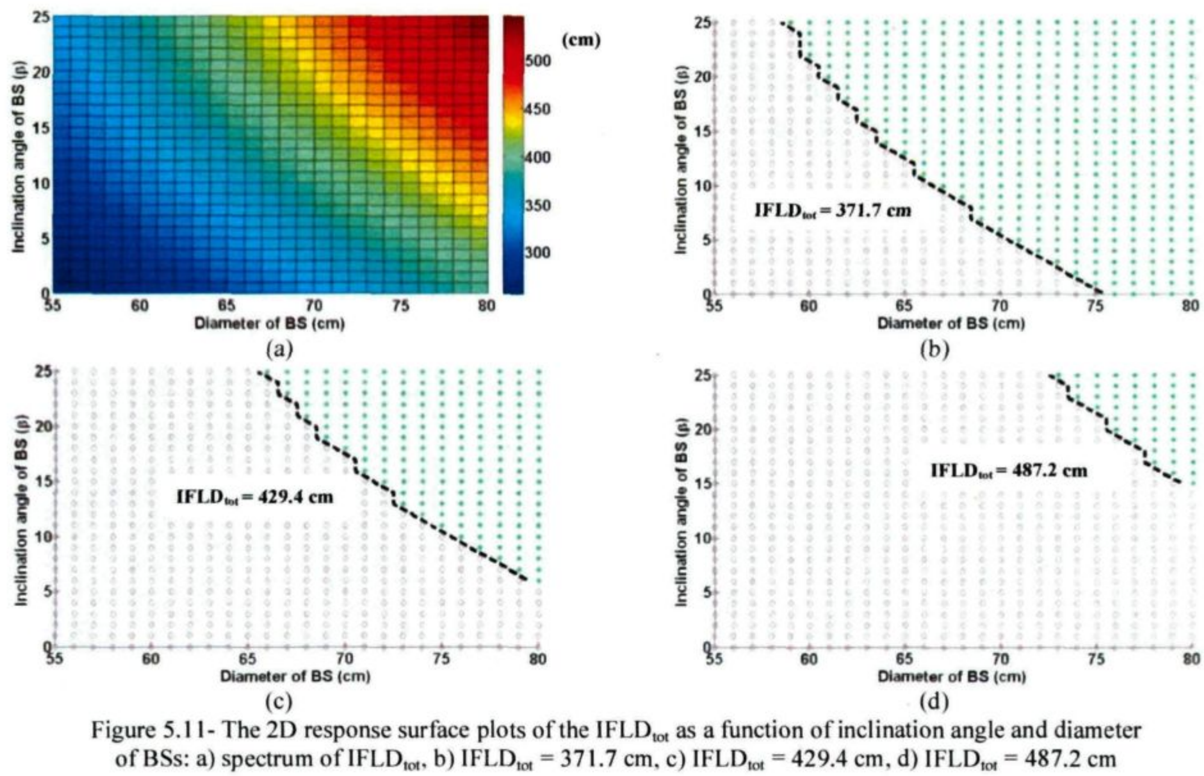

Figure 5.11- The 2D response surface plots of the $IFLD_{tot}$ as a function of inclination angle and diameter of BSs: a) spectrum of $IFLD_{tot}$, b) $IFLD_{tot}$ = 371.7 cm, c) $IFLD_{tot}$ = 429.4 cm, d) $IFLD_{tot}$ = 487.2 cm

5.7 Conclusions

This chapter investigated numerically various BS configurations on two units of an EHV standard post insulator under heavy icing conditions. The following conclusions and recommendations may be drawn:

1) A geometric model was proposed for a standard post insulator equipped with BSs considering the angle of precipitation. Its results were in a good agreement with previous BS tests in spite of the complexity of the insulator geometry and the simplifications made with the geometric model.

2) To analyze various BS configurations by Taguchi Method, 128 virtual experiments were considered by the geometric model. Moreover, a novel index ($y_i = \Delta V_{tot\ i} / IFLD_{tot\ i}$) was proposed to quantify the electrical performance of the virtual experiments as well as to apply Taguchi model for optimality and post-optimality analyses.

3) Based on the analyses by the Taguchi method (see the flowchart in Figure 5.8.), the optimal values of the BS parameters are:

   $N_{BS}=6$, $Angle_{BS}=24.5°$, and $D_{BS}= 70.5\ cm$.

   These results were based on the analyses of two units of an EHV standard post insulator equipped with BSs under heavy icing conditions. Moreover, two angles of precipitation were considered; i.e. $\theta = 51°$ and $0°$ correspond to normal laboratory and severe winter storm conditions, respectively.

4) Logical constraints for BS parameters and equal step variations in the parameters were considered in the Taguchi method. Then, the importance ranking of the controlling parameters in two different precipitation angles were concluded as:

1. N_{BS}, 2. D_{BS}, 3. $Angle_{BS}$; (in the laboratory condition, θ= 51°)

1. N_{BS}, 2. $Angle_{BS}$, 3. D_{BS}. (in winter storm condition, θ= 0°)

5) To optimize the positions of BSs different possibilities should be considered. Then, the $IFLD_{tot}$ and dry arcing distance as the major and minor concern, respectively, should be compared. For analysis in this procedure, the presented geometric model of dry arcing distance can used.

6) Response surface methodology is often used to obtain a deeper analysis after Taguchi method studies. There was no local maximum in the response surfaces of $IFLD_{tot}$. Moreover, in the design of BS parameters to reach a specific $IFLD_{tot}$, RMS provides various selections of BS parameters. The relationship between the BS parameters and the response(s) of $IFLD_{tot}$ can be approximated by standard approaches such as least squares.

CHAPTER 6

VALIDATION TEST RESULTS

CHAPTER 6

VALIDATION TEST RESULTS

6.1 Introduction

In the previous chapters computer aided analyses (parametric simulations, geometric modeling, Taguchi method, etc.) were presented. The present chapter mainly explains an experimental validation of those computer aided analyses by a series of tests. The experimental tests includes two trial tests (i.e. flashover tests with the first fabricated BS prototype and previous 6-BS configuration), the main validation design test, and finally experimental study of the effect of electric field on icicle growth of BSs.

6.2 Validations based on previous researches

The simulation results are validated by comparing with the previous validated simulations in the literature and the results of the previous BS tests; most importantly:

1) The voltage drops along the air gaps should have a realistic trend from the HV electrode to the ground electrode resembling the calculated results of voltage drops in the previous studies [59], [60], [75]. For example, the voltage drops should have a U-shaped curve (Figure 4.4). Also, it was shown that following the addition of 4, 5, and 6 BSs, more that 50% of the applied voltage drops along the closest air gap to the HV

electrode. It parallels the results of the previous validated 3D simulations of one unit of an EHV ice-covered post insulator in [59], [60]. They indicate that the voltage drop along the first air gap (close to HV) is around 50% of the applied voltage. These similarities in the voltage drops along the first air gap are reasonable theoretically.

2) The numerical results showed that when there is a conductive water film on the ice surface, about 99% of the applied voltage distributes along the different air gaps, independent of the number, lengths, positions, or inclination angle of BSs. These results are in good agreement with the previous validated simulations in [59], [60]. They demonstrate that the total voltage drop along the air gaps during a melting period is around 96% of the applied voltage, independent of the number, lengths, or positions of the air gaps. Furthermore, the effect of partial discharge on the redistribution of voltage drops obtained by 2D-axisymetric simulations. The results were logically similar to redistributions of voltage drops with the corresponding results in [59] (Table 4.13 and Figure 4.16).

3) The accuracy of 2D-axisymmetric simulation has been verified in the previous studies [27], [76].

4) As it was explained in Chapter 3, the simulation results had a good agreement with the previous BS test results [2] when comparing the voltage drops of the air gaps with the corresponding breakdown voltages.

Following the above verifications, the validation of the simulation results and the improved hypothesis were also finalized by the establishment of a series of experiments. The maximum withstand voltage (V_{WS}) was determined for an optimized BS configuration on an EHV standard post insulator under heavy ice conditions of 30-mm/140min. The subsequent sections explain the trial tests, the classifications and calculations for BS parameters, and finally the results of the experimental validation tests.

6.3 Trial tests

Before the validation tests, two series of trial tests were carried out:

- the tests with the first prototype of BS,
- the tests with the previous 6-BS test configuration in [2], [18]–[20].

6.3.1 Trial tests with the first prototype of BS

To build BS prototypes, a material with specific electrical and mechanical characteristics is required. As mentioned in section 4.3.3, the relative permittivity of BS should be in the range of "2-15". The material must be fire retardant to resist against partial arcs and flashover as well. For example, wood is not a proper material for this purpose. Moreover, it should be an electrical insulating material that is rather flexible. In addition, it should be readily available commercially and bear the weight of heavy ice accretion. After a comprehensive search and receiving various material samples from different companies, PVC ($\varepsilon_{r\text{-}PVC} = 2.7\text{-}5$) [2], [94]–[96] was selected for this purpose. Figure 6.1 shows the stages of preparing the first prototype of BS.

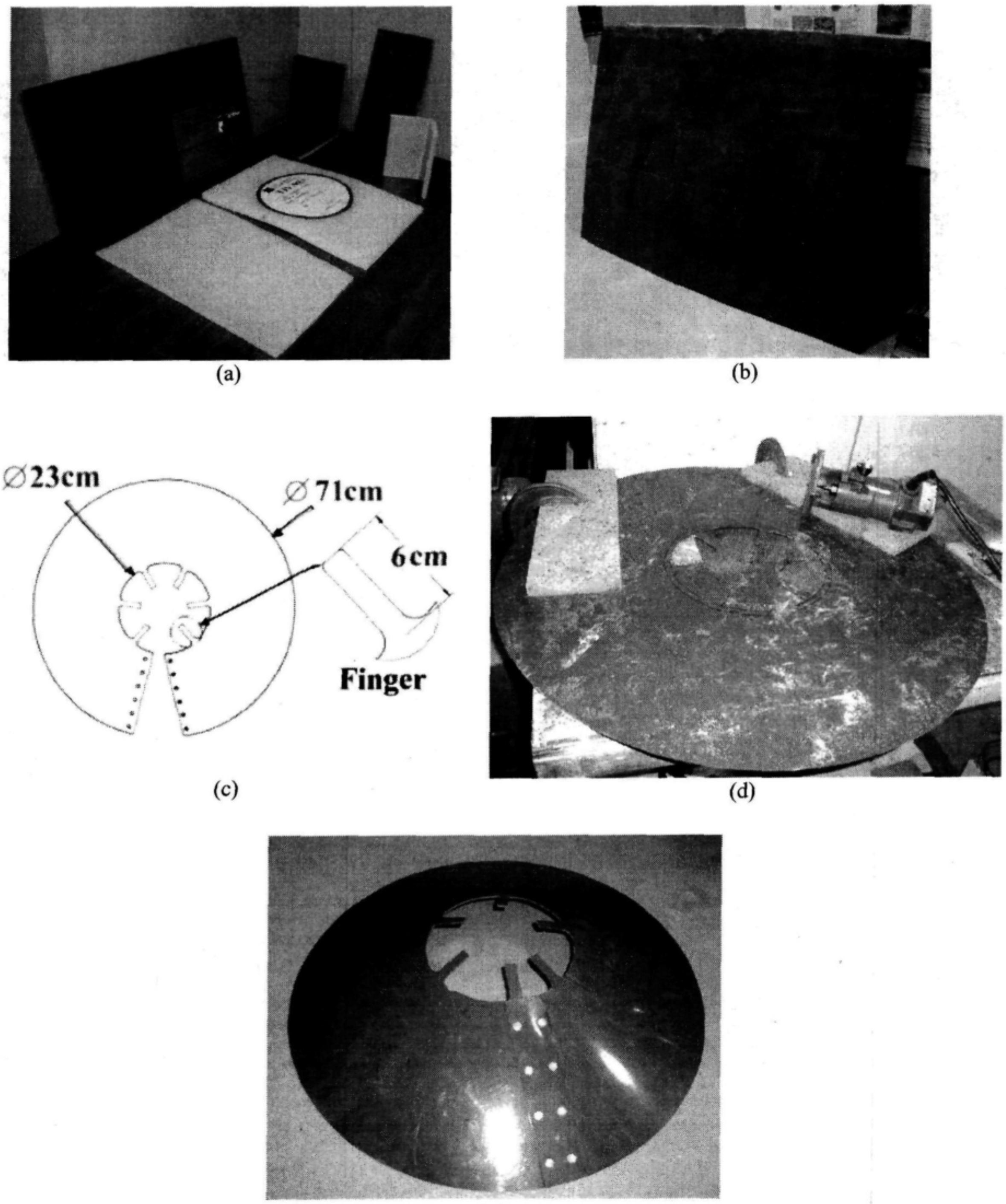

Figure 6.1- The stages of preparing the first prototype of BS
a) material search, b) the selection of PVC sheet c) scheme and dimensions of the BS,
d) fabrication of the BS in CIGELE Lab. e) Final fabricated BS

Since some PVC characteristics (insulating strength, discharge inhibition and arc suppression) are not as good as the characteristics of commercial BS material (i.e. silicone rubber or EVA: Ethylene Vinyl Acetate), some problems (puncture, etc) may occur. Thus, before performing the main validation test, a trial flashover test under heavy icing condition was required. The results were rather satisfactory. Figure 6.2 shows the images of the trial flashover test with the first prototype of BS. Moreover, important technical points (to make BSs more effective, etc) were distinguished during this initial test. It provided beneficial insights and technical experience to go toward the main tests.

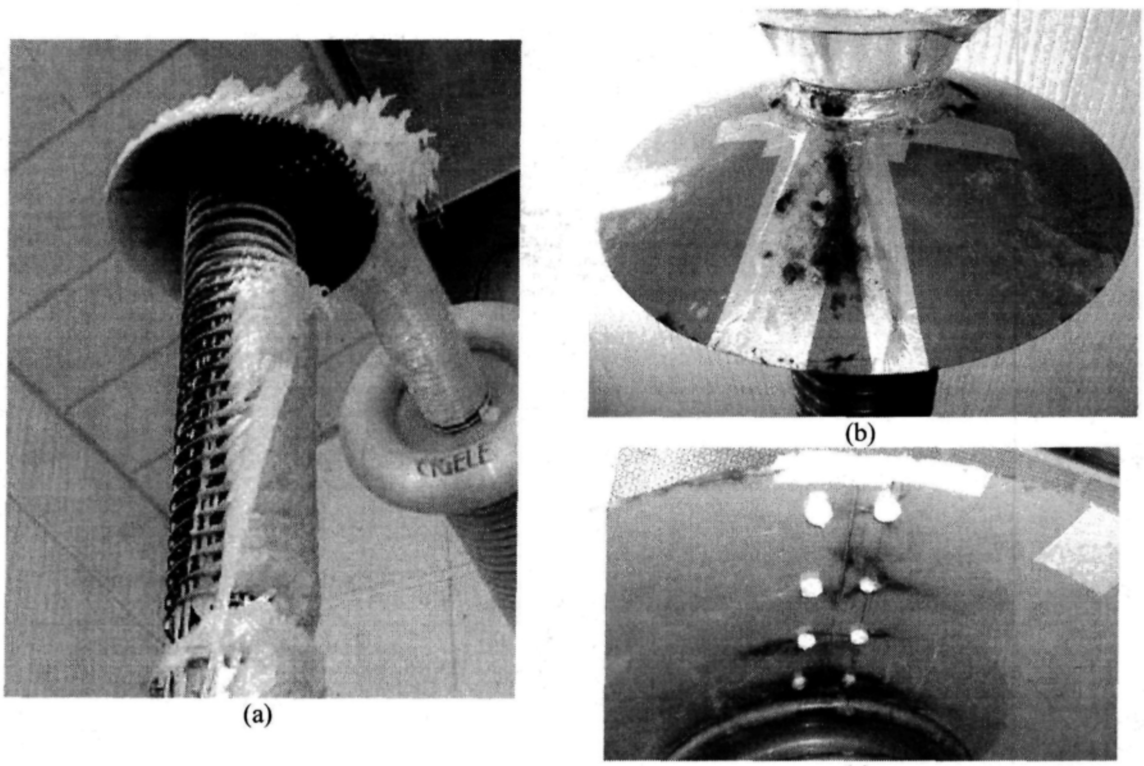

(a) (b) (c)

Figure 6.2- Trial flashover test with the first prototype of BS
a) ice-covered insulator with BS before flashover,
b) and c) the condition of BS after flashover period (upper side and underside of BS)

6.3.2 Trial tests with previous 6-BS configuration

This series of tests was carried out to master the facilities and to assure the correctness of the applied test procedure. The experimental procedure was the same as defined in [50], and considering the conditions of the previous BS tests in [2], [18]–[20]. Figure 6.3 illustrates the test procedure. Figure 6.4 shows the images of this test in the heavy ice conditions.

The flashover occurred after approximately 7 min application of 330kV. For the first time in the BS tests, arc propagation was recorded (Figure 6.5) by an ultra high-speed camera. The camera, Fastcam SA1, has the capacity of recording up to 675,000 frames per second. These observations can help to understand the formation of arcs when there are several air gaps in the flashover path.

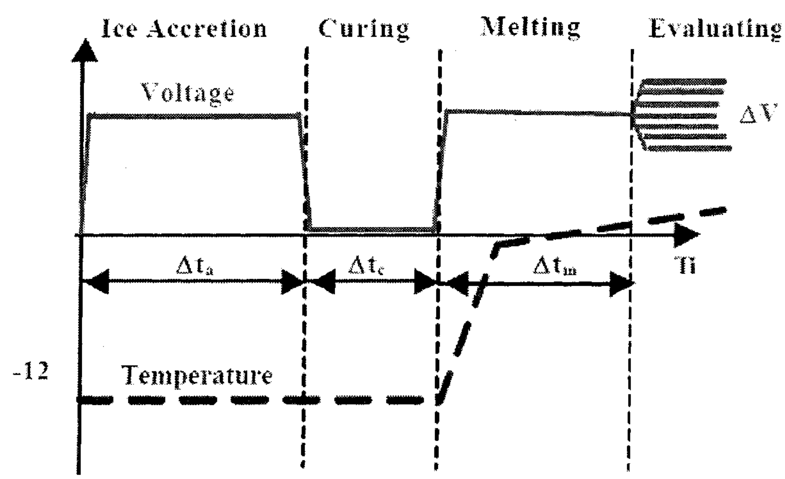

Figure 6.3- Different sequences during BS tests Δt_a=140 min, Δt_c=20 min

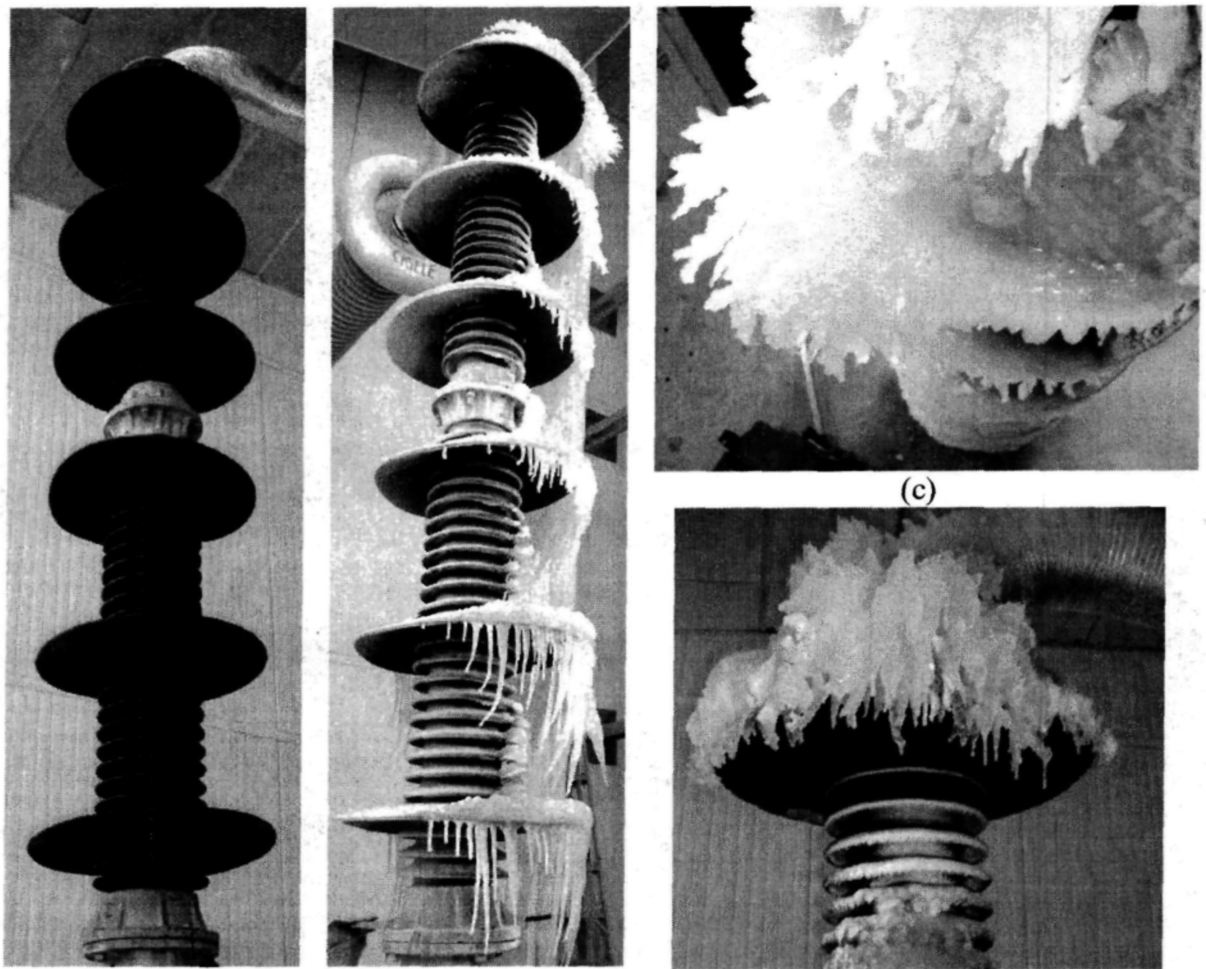

(a) (b) (c) (d)

Figure 6.4- Trial test with 6-BS configuration under heavy ice condition:
a) before ice accretion, b), c), and d) after 30 mm/140min ice accretion from different views

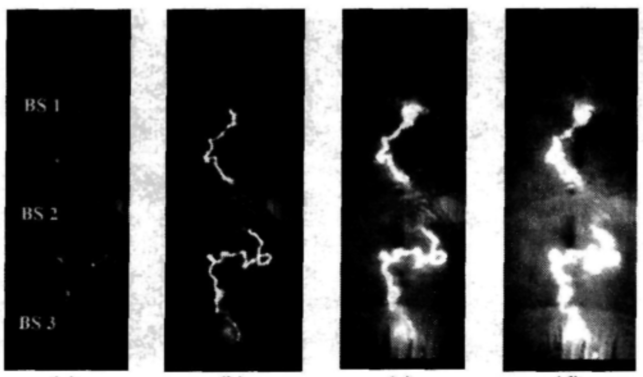

(a) (b) (c) (d)

Figure 6.5- Arc propagation pattern during the flashover along 6-BS configuration stages (a) to (d)

6.4 Classification of the BS parameters

The main parameters of BSs in this study are as follows: number, inclination angle, permittivity, diameter, and position. These parameters were classified as fixed and variable parameters compare to the previous BS tests in [2].

6.1.1. Fixed parameters of BSs

1) *Optimum Number of BSs (N_{opt}):*

   As explained in section 4.4 (Figure 4.18), the ice bridging may happen for 6-BS configuration. In fact, the previous BS test results with 30 mm ice accretion shows that to prevent ice bridging the maximum feasible number of BSs is six. In other words, as soon as another BS is added to the 6 BSs, ice bridging is unavoidable. In short: $N_{opt} = 6$

2) *Optimum inclination angle of BSs ($Angle_{opt}$):*

   The S/N ratio analysis (Figure 5.7) showed that the best inclination angle of BSs that can create the largest ice-free zones is 24.5° (24.5° is the upper angle of shed of the post insulator). So: $Angle_{opt} = 24.5°$

3) *Optimum relative permittivity of BS ($\varepsilon_{r\text{-}BS\text{-}opt}$):*

   As explained in section 4.3.3, the variation in the relative permittivity of BS ($\varepsilon_{r\text{-}BS}$= 2-15) has no significant effect on the potential and electric-field distributions along the EHV insulator in the wet-grown ice regime. Thus: $\varepsilon_{r\text{-}BS\text{-}opt} = arbitrary\ (2\text{-}15)$.

6.1.2. Variable parameters of BSs

The remaining parameters that can be changed to reach a V_{WS} higher than V_{WS} of the previous BS tests are the *diameter* and *position* of the BSs.

To make the prototypes of BSs, two PVC sheets (size: 121.9×243.8, thickness: 0.3 cm) were used. Figure 6.6 shows the drawing on the PVC sheets in order to extract 6 BSs with no sharp edges and fingers. The dimensions of the BSs are summarized in Table 6.1.

Table 6.1-.Diameters (cm) of the BS prototypes

	d_{BSi}	D_{BSi}
BS_1	21	89
BS_2	21	89
BS_3	21	84
BS_4	24	84
BS_5	24	84
BS_6	24	84

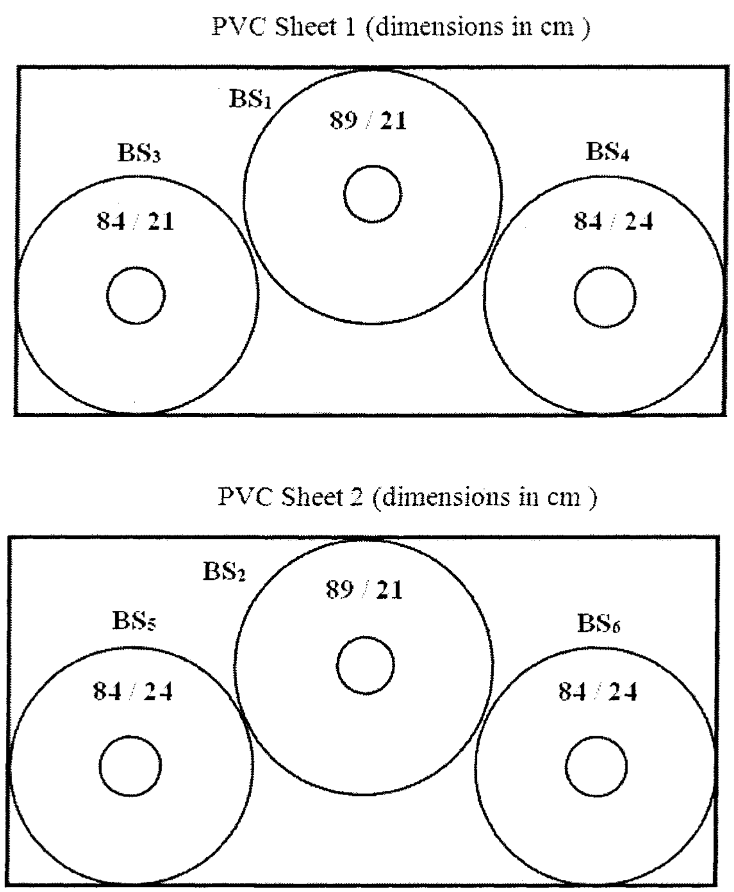

Figure 6.6-. Simplified drawing of BS prototypes on PVC sheets (size: 121.9×243.8, thickness: 0.3 cm)

The inner diameters of the BS prototypes were selected simply to fit the insulator core and nothing else. So, in this context, when BS diameter is mentioned, it means the outer diameter unless otherwise specified.

Considering the simulation results (Table 4.5), the majority of the voltage drops appears along the first and second air gaps. So, BS_1 and BS_2 have the most determinant role in the electrical performance of the ice-covered insulator. For this reason, the largest outer diameters were selected for the first and second BSs (Table 6.1-.Diameters (cm) of the BS prototypes

) to create the largest ice-free zone beneath them. Table 6.2 shows the position (shed number) and diameters of the BSs on the post insulator in the optimized BS test versus the previous 6-BS test.

Table 6.2-.The position (shed number) and diameters of BSs on the post insulator (proposed test versus 6-BS test)

	Previous 6-BS test		Optimized BS test	
BS No.	Position	D_{BS} (cm)	Position	D_{BS} (cm)
1	2	65.5	1	89
2	13	65.5	12	89
3	23	65.5	22	84
4	2	65.5	1	84
5	12	65.5	11	84
6	22	65.5	22	84

Considering the improved hypothesis of the BS effect (section 4.4), $IFLD_{tot}$ indicator was used to estimate the V_{WS} of the optimized configuration. More precisely, around 22.1% [i.e. the average value of 21.3 % and 23.0 % ($IFLD_{tot}$ variations in Table 4.15] increase in $IFLD_{tot}$ is considered as 15-kV increase in V_{WS}. That is:

$$V_{WS}(kV) \approx 285\,kV + \left(\frac{IFLD_{tot}(\%) - 100}{22.1}\right) \times 15\,kV \tag{6.1}$$

Equation (6.3) can be expressed in metric system as (6.4):

$$V_{WS}(kV) \approx 285kV + 1.207(IFLD_{tot}(m) - 3.75) \times 15kV \,. \tag{6.2}$$

Table 6.3 compares the previous 6-BS configuration and the optimized one from an electrical viewpoint. The positions of the BSs were optimized to prevent any ice bridging i.e. to maximize the $IFLD_{tot}$ as a first priority. Moreover, maximizing the DAD was the second main concern in selecting the BS positions.

Table 6.3-.Comparison of the optimized BS test and the previous 6-BS test

	Previous 6- BS test	Optimized BS test
$IFLD_{tot}$ (m)	5.41	*7.66
DAD_{tot} (m)	3.07	3.26
V_{WS} (kV_{rms})	315	**(355)
***$IFLD_{tot}$ (%)	144.3	204.2
DAD_{tot} (%)	102.0	108.3
V_{WS} (%)	110.5	(124.6)

*From BS-geometric model (Figure 5.2-b)
**The numbers in parentheses are the predicted values by equation (6.1).
***Using the similar approach in the improved hypothesis section, all values are normalized based on the 4-BS test values. So, 100% means: $IFLD_{tot}$ = 3.75 m, DAD_{tot} = 3.01 m and V_{WS} = 285 kV_{rms}.

6.5 Validation test results

The maximum withstand voltage was determined using the same method explained briefly in the trial (Section 6.2.2). The tests are complete when three withstands in four tests are observed at one voltage level, and two flashovers are observed at 5% higher voltage level. The V_{WS} is the test level that gives three withstands out of four tests [97]. Figure 6.7 shows the test results of the optimized configuration. So, 345 kV< V_{WS} and it is in a good agreement with the predicted value obtained by the geometric model and the improved hypothesis of BS effect. In fact, 345 kV was the maximum possible voltage to perform the tests in CIGELE laboratory considering the HV Transformer rating and the security circuit limitations. Figure 6.8 displays the physical appearance of the ice-covered post insulator with BSs after ice accretion sequence in the validation tests. Leakage current never reached more than 3 mA during the evaluation period.

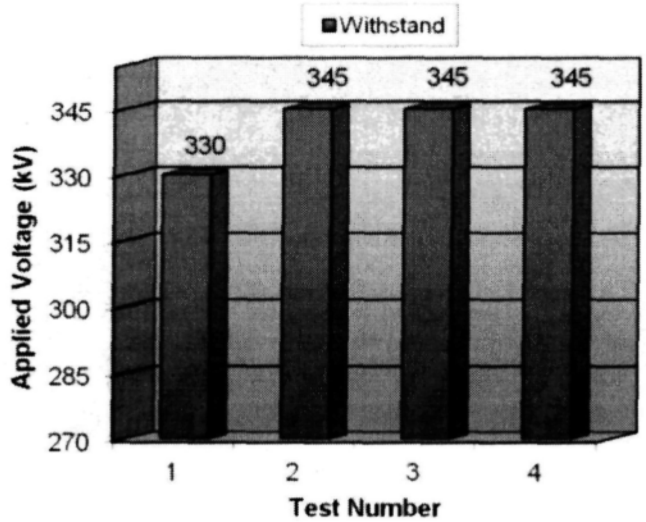

Figure 6.7- The results of V_{WS} of the optimized configuration

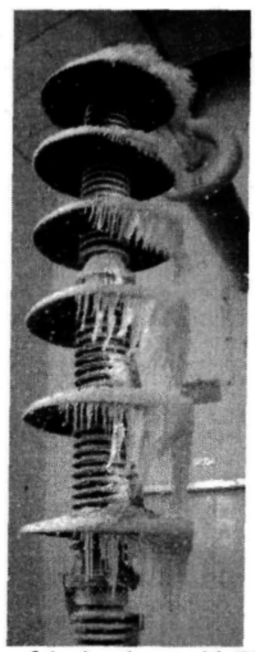
Figure 6.8- Physical appearance of the insulator with BSs after ice accretion sequence

Figure 6.9 displays the corona discharges and violet arcs during the evaluation period.

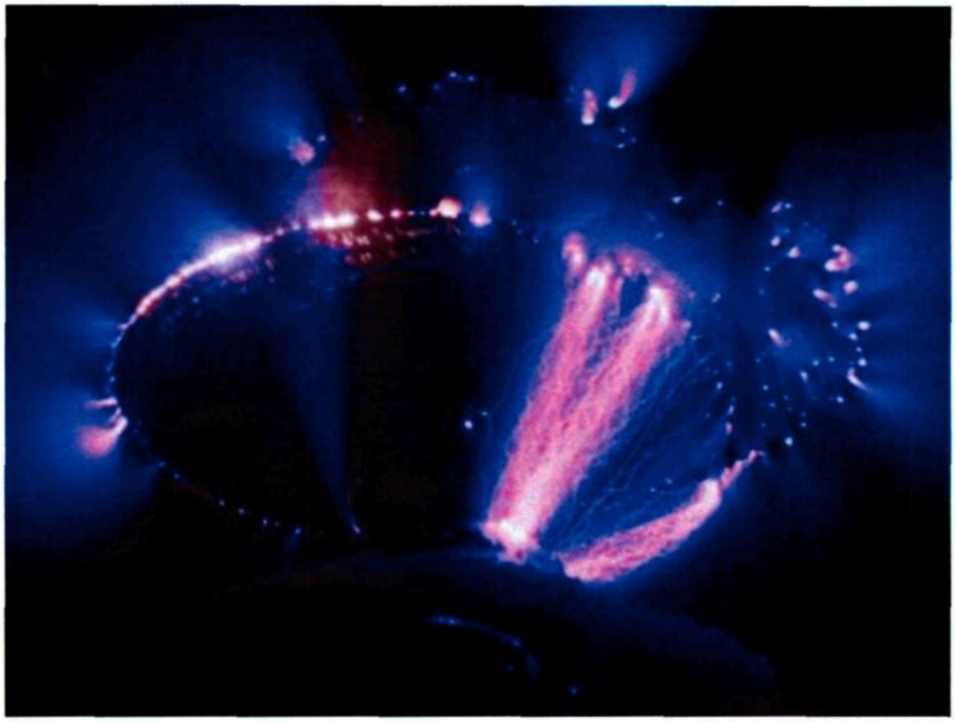

Figure 6.9-. Corona discharge appearance in the vicinity of the first BS

As was predicted by the simulations, special attention was required to the first BS because it bears the highest electric field stress and voltage drop (around 50% of the applied voltage). Hence, the first BS was repaired after each test. Figure 6.10 and Figure 6.11 exhibit two conditions of the BS_1 during the tests. After finishing test no. 2, a commercial BS was added on top of BS_1 to prevent more severe damages on BS_1 caused by partial arcs (Figure 6.11).

Figure 6.10- The first BS condition after test no. 2.

Figure 6.11- The first BS repaired after test no. 3

Figure 6.12 presents the optimization and design procedure clearly by a flowchart.

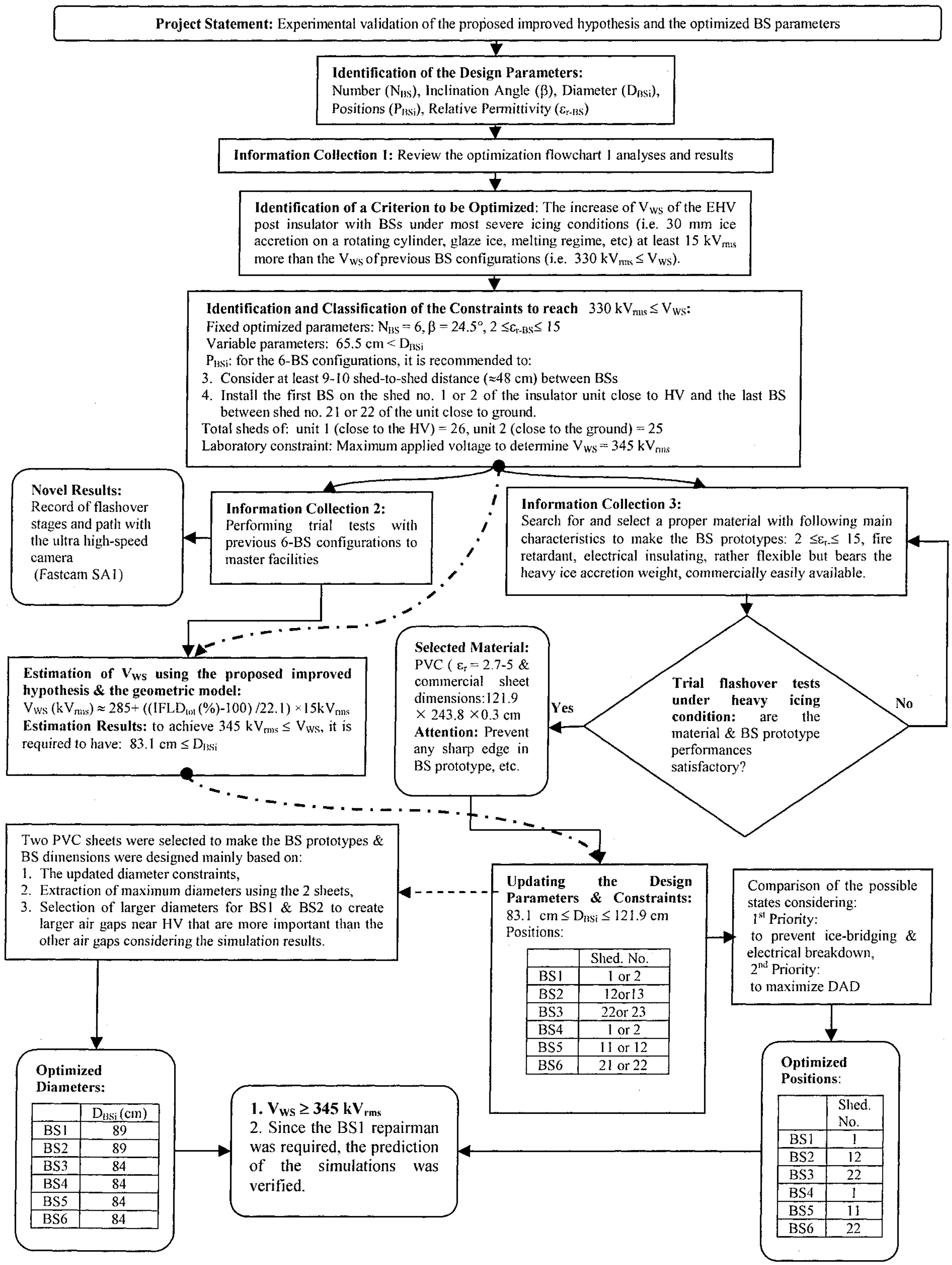

Figure 6.12- Optimization flowchart 2 (validation tests)

6.6 Experimental tests on icicle growth of BSs

In addition, to the validation tests described in the previous section, two extra tests were carried out without application of voltage. The duration of ice accretion, curing and melting period were kept as same as the earlier validation tests. The main objective of these tests was analyzing the effect of applied voltage and electric field on the icicle growth of BSs from top to bottom. This study provides a better prediction of ice-bridging with BS configuration. Consequently, it will be helpful to select better positions for BSs in practical applications.

Figure 6.13 compares the icicle growth along the air gaps with and without applied voltage. In without-voltage state, ice-bridging along all of the air gaps is clearly observable at t = 105 min (Figure 6.13-d′). Moreover, the inclination angles of the icicles are approximately identical. On the other hand, in the hot line condition (with-voltage), no ice-bridging appeared till t=140 min. Furthermore, the inclination angles are not identical, especially for the icicles on BSs no. 1 to 3 which were installed on the insulator unit close to the HV electrode.

Figure 6.14 compares dripping water conductivity for the two conditions. The high conductivity of the water film is due to the rejection of impurities onto the ice surface through the crystallization of water droplets during the accumulation period. As the impurities on the ice surface collected gradually, the conductivity decreased gradually as well. Higher conductivity of with-voltage condition is probably due to extra pollution of the ice surface from by-products of corona discharges and BS_1 damages.

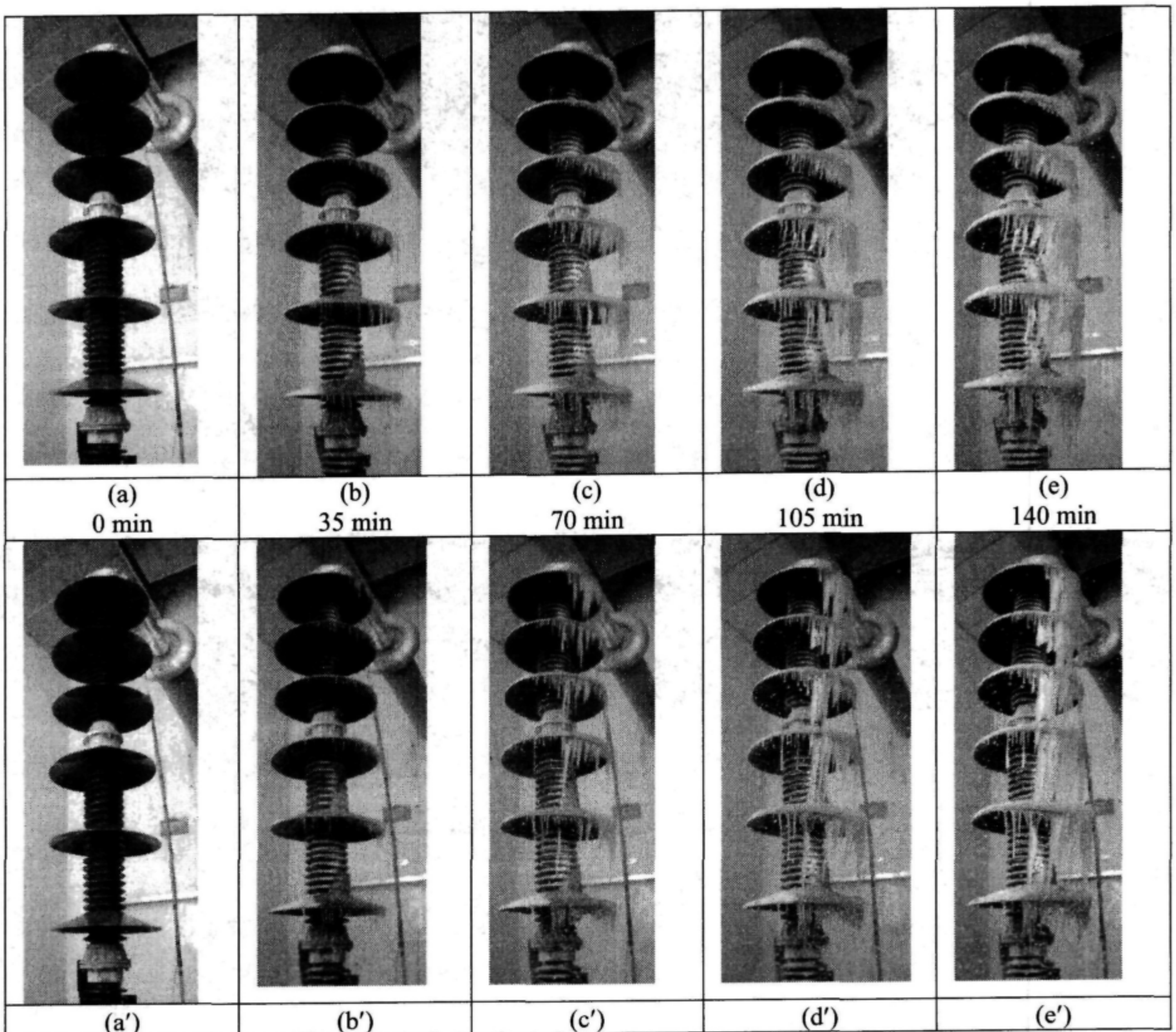

Figure 6.13- Comparison of the icicle growths along the air gaps to study the effect of applied voltage (a)-(e) with voltage (V_{app}= 285 kV), (a′)-(e′) without voltage

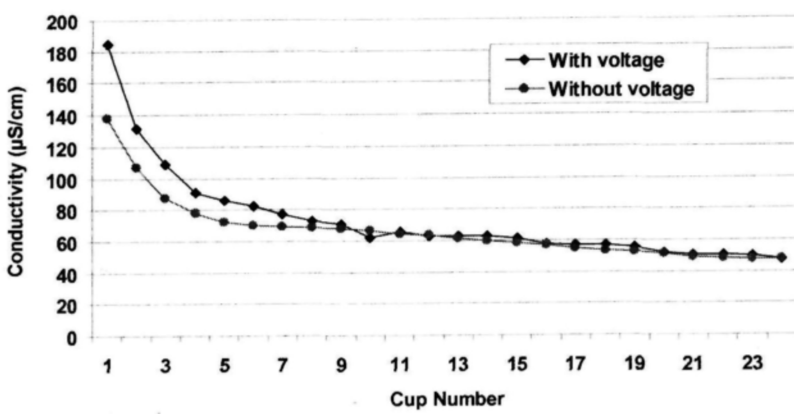

Figure 6.14- Dripping water conductivity comparison for with- and without-voltage conditions

6.7 Conclusions

This chapter reviewed the theoretical validation of the simulations of BS configurations. Moreover, it presented an experimental validation of the simulations and the improved hypothesis of BS effects under heavy icing conditions. The experimental results were in good agreement with the numerical analyses and the improved hypothesis.

Before the main validation tests, a series of trials was carried out. The first trial demonstrated that PVC sheets are good enough to fabricate the prototypes of BSs for research purposes under extra high voltage and heavy icing conditions. The second trial test obtained for the first time the electric arcing path by an ultra high speed camera and during the flashover period on the 6-BS configuration. To clarify the whole procedure of the validation tests, it was summarized in a flowchart (Figure 6.12).

Moreover, after the main validation tests, the icicle growth of BSs under the heavy icing conditions were analyzed experimentally. It was demonstrated that the electric field has a significant effect upon the growth of the icicles on BSs. The results are useful for better estimating ice-bridging of the air gaps as well as better positioning of BSs in practical applications.

CHAPTER 7

CONCLUSIONS AND RECOMMENDATIONS

CHAPTER 7

CONCLUSIONS AND RECOMMENDATIONS

7.1 Conclusions

The present study concerns the optimized design of BS parameters (diameter, inclination angle, position, number, and relative permittivity) for icing protection of post insulators. The explained methodology consists of elaborating simulation analysis, geometric models, and their validation based on comparison with confirmed simulation results in the literature, experimental results previously obtained at CIGELE, as well as new test results on BS prototypes whose design is based on the models and computer aided analysis. According to the presented study, the following conclusions are drawn:

1) Since the main objective of the BS installation is the improvement of the electrical performance under heaviest icing conditions, it is necessary to optimize BS parameters mainly under the most severe anticipated conditions; for example: melting regime and 30-mm radial ice accretion on a rotating cylinder.

2) Based on the simulation studies of the electrical field distributions by Comsol Multiphysics™ regarding the standard post insulators with BSs under melting regime:

a) the optimized value of relative permittivity of BS ($\varepsilon_{r\text{-}BS}$) is an arbitrary value in its feasible variation range ($\varepsilon_{r\text{-}BS}$= 2-15).

b) The total voltage drop distributed along the air gaps (ΔV_{tot}) is almost 99% of the applied voltage. This value ($\Delta V_{tot} \approx 99\%$) is independent of the number, lengths, positions of the air gaps, inclination angles and diameters of the BSs, or the inclination angle of the icicles on BSs. The results of 2D-axisymmetric simulation are in good agreement with previous validated 3D simulations in [59], [60].

c) The closest air gap (AG_1) and BS (BS_1) to the HV electrode have the most important roles in the electrical performance of the ice-covered insulator. It is due to the largest value of the voltage drop (i.e. around 50% of the applied voltage) along AG_1. Hence, the installation of a larger BS to create a wider air gap close to HV electrode seems to be useful. However, to prevent any damage (puncture, etc.) under the high electric field stresses close to HV electrode on BS_1, using a modified grading ring [49] or a creepage extender instead of BS might be recommended. Another solution is the installation of BS_1 further from HV electrode, e.g. on 2nd or 3rd shed of the insulator instead of 1st shed. However, this latter solution leads to the negative result of a slight decrease in dry arcing distance.

3) The upgraded model of BS dimensioning concerns the proper calculation of diameter and position of BSs on two sections of a standard post insulator. It shows that in order to determine the proper diameters and positions of the BSs, the electric-field stress is the main factor for the BSs close to the HV electrode. Moreover, ice bridging (icicle length) is the main factor for the BSs close to the ground electrode. This guideline would be used for the application of BSs on full-scale post station insulators on 735-kV Hydro-Quebec network as well.

4) The improved hypothesis regarding the positive effects of BSs on standard post insulators under heavy icing conditions consists of the following:

a) Qualification of BS effects:

- The major effect is the creation of ice-free zones (unbridged ice zones).
- The minor effect is the increase in dry arcing distance.

b) Quantification of BS effects:

Among dry arcing distance, the total length of the air gaps, and the total ice-free leakage distance ($IFLD_{tot}$), the best indicator to quantify the electrical performance ranking (i.e. the variation of V_{WS}) is $IFLD_{tot}$.

5) A comprehensive computer aided study using Matlab and Minitab was carried out. Based on this study:

a) A geometric model was proposed to calculate $IFLD_{tot}$ on a standard post insulator with BSs considering the precipitation angle. The results were in good agreement with the previous BS tests in [2], [18]–[20]. Moreover, its effectiveness was confirmed by its successful application in the required calculations of the final validation tests. Thus, it is a robust model that also can be used in other applications.

b) A novel index ($y_i = \Delta V_{tot\ i}/IFLD_{tot\ i}$) was proposed to quantify the electrical performance of the virtual experiments in the Taguchi method. Then, after systematic analyses (summarized in a flowchart in Figure 5.8.), the optimal values of the BS parameters and their importance rankings were obtained as:

N_{BS}=6, $Angle_{BS}$=24.5°, and D_{BS}= 70.5 cm, (laboratory and wind storm conditions)

1. N_{BS}, 2. D_{BS}, 3. $Angle_{BS}$; (in the laboratory conditions, $\theta = 51°$)

1. N_{BS}, 2. $Angle_{BS}$, 3. D_{BS}. (in winter storm conditions, $\theta = 0°$)

c) Optimization of the positions should be accomplished for various possibilities by comparison of the $IFLD_{tot}$ and dry arcing distance as the major and minor concern, respectively. The presented geometric model of dry arcing distance can be used as an effective tool for analysis and quantifications in this regard.

d) Response surface methodology was used to provide various selections of BS parameters for a specific $IFLD_{tot}$. It also was used to analyze the correlation between the design parameters of BSs and no local maximum was observed on the response surface of $IFLD_{tot}$.

6) The results of the final validation tests (summarized in a flowchart in Figure 6.12) were in good agreement with the simulation analyses and the improved hypothesis. Moreover, another original experimental study was performed concerning the effect of the electric field on the icicle growth of BSs. It can improve the estimation of ice-bridging of the air gaps which is important for proper positioning of BSs.

7) The presented generic approach is not only Taguchi method. In fact, it is an innovative combination of the improved hypothesis, virtual experiments defined by the geometric modeling, and the Taguchi technique (Figure 7.1). Table 7.1 shows the different stages in the novel design approach which leads to considerable time saving. In this approach, 128 states (2×4×4×4) were analyzed. IEEE Task Force recommendations [50] call for at least 5 to 6 icing tests to determine the maximum withstand voltage of each of the states. In addition, during every working day only one icing test can be performed. The orthogonal arrays in Taguchi method reduce the number of states to 32. Finally, the improved hypothesis and the geometric model helped to obtain only one optimized configuration for the final validation test. Moreover, much more time and cost have been saved indeed, because the required time should also considered for the repairs of equipment, fabrication of many BSs, the availability of a well-equipped laboratory, etc. Above all of these advantages, the proposed modern approach is a generic design approach that can be applied for many other insulators and configurations.

Table 7.1-. Different stages in the novel design approach leading to considerable time saving

	Tests	Required time (year)
All states	128×5-6	≈ 3
Orthogonal selection (Taguchi method)	32×5-6	$\approx 3/4$
Geometric model calculations and final validation test	1×5	0.02

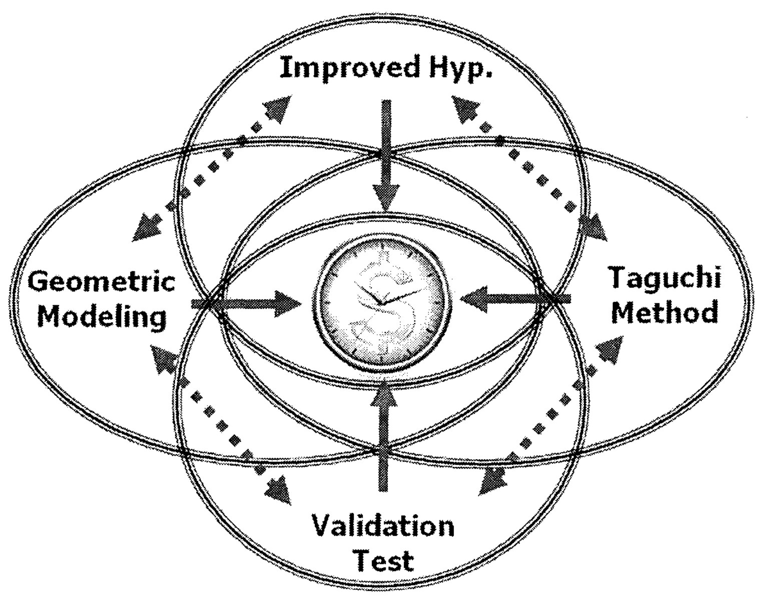

Figure 7.1- Interaction of the scientific methods used in the novel design approach leading in time and cost saving

7.2 Recommendations for future work

The following technical and practical issues deserve further investigation:

1) Booster sheds prevent ice bridging by the creation of ice-free zones along ice-covered insulators. Moreover, regular/modified grading rings lead to significant improvements of the electric field stress on EHV insulators [49] . Thus, an effective design to make use of these mitigation options simultaneously can lead to a practical guideline in order to benefit their positive effects altogether. A primary simulation analysis concerning the combined effects of BSs and grading rings under heavy icing conditions can be found in our paper [98]. However, more numerical and experimental studies are required in this regard.

2) Design and optimization of the BSs considering other weather conditions (rain, fog, ice, pollution build-up, etc.). Most importantly:

a) Experimental analysis of the effect of wind with strong speeds on $IFLD_{tot}$ and the V_{WS} of the insulators equipped with BSs.

b) Since pollution problems of BSs have reported more frequently, further research concerning this challenge is in greater demand than the other conditions. For example, using anti-contamination and self-cleaning coatings [99] as well as application of micro/nano fillers [46], [100] for BSs seems feasible solutions that deserve more investigations. Superhydrophobic surfaces are generally considered as self-cleaning, because water droplets roll-off on them easily and remove any contamination [101], [102].

3) Since PVC sheets were adequate to fabricate the prototypes of BSs for this study, their application for the future research regarding the design of BSs for other configurations and type of insulators is recommended. For example:

a) Suspension, bushings, V-type, etc., and especially parallel post insulators on 0.5-m spacing that are often used for air-break disconnect switches.

b) Alternating BS configurations. In each configuration, the $IFLD_{tot}$ can be calculated as an effective index to quantify the total ice-free zones. Then, based on the improved hypothesis, generally a higher $IFLD_{tot}$ indicates a better configuration. Their dry arcing distance should be considered in the analysis as well. Moreover, the possibility of the ice bridging between the BSs should be estimated. This estimation can be realized using the presented experimental test studies of icicle growth on BSs.

4) A comprehensive study of the effect of electric field on the icicle growth of BSs with a good support of mathematical models is recommended. This study can provide a better estimation of ice-bridging along the air gaps and thus, better positioning of BSs in practical applications.

5) In the following, a new test is suggested considering the criteria of R3 (representative, repeatable, and reproducible) and cost-effectiveness for future research, essentially in the area of BS applications under heavy icing conditions. The air gaps formed during the first minutes of ice accumulation in a wet regime can be assimilated to rod-plane configurations. The configuration in Figure 7.2 is proposed to make the modeling as representative as possible. The main objective of this test is to obtain a better estimation of the breakdown voltage as a function of air gap length. Hence, its results can lead to a better understanding of BS effects under icing conditions.

In Figure 7.2, the vertical (semi-cylinder) and horizontal (semi-BS shape) ground electrodes represent the accumulated ice surface along the post insulator and along the upper surface of the next BS, respectively. Actually, Figure 7.2 shows the cross section of the proposed configuration (the mounting of the icicle, BS, and the ground electrodes). A comparison of the proposed configuration (Figure 7.2) and the post station insulator with BSs under heavy ice accretion (Figure 7.3) helps to better understanding of the representative characteristic of the proposed configuration.

The vertical ground electrode is a semi-cylinder with a diameter ($d_{s\text{-}cy}$) and a height ($H_{s\text{-}cy}$) matching the average dimensions of the iced-covered insulator and BSs in the icing tests of BSs. As well, the horizontal ground electrode is a semi-circular plane with a radius ($R_{s\text{-}BS}$) similar to the shape of BS in the BS tests. The electrodes can be made from a proper conductor, such as copper or aluminum. The electric field near a sharp edge or point is intensive, and it can cause a breakdown of the air and electric discharges. Thus, it is important to avoid sharp edges or points on ground electrodes used in the test (Figure 7.2).

The icicles used in the experiments can be formed by a freezing method at a temperature of -12 °C and using several aluminum or wooden molds particularly shaped to achieve the average form of the icicles. The conductivity of freezing water adjusts to a desired value by adding sodium chloride (NaCl) to de-ionized water. The high voltage is applied to the molded icicle through a metal copper electrode incorporated into the center of icicle during its freezing formation in the mold. The molded icicle must be changed after each test, since breakdown alters its form. The breakdown voltage, V_b, can be obtained by recording the voltage signal and the breakdown time (t_b).

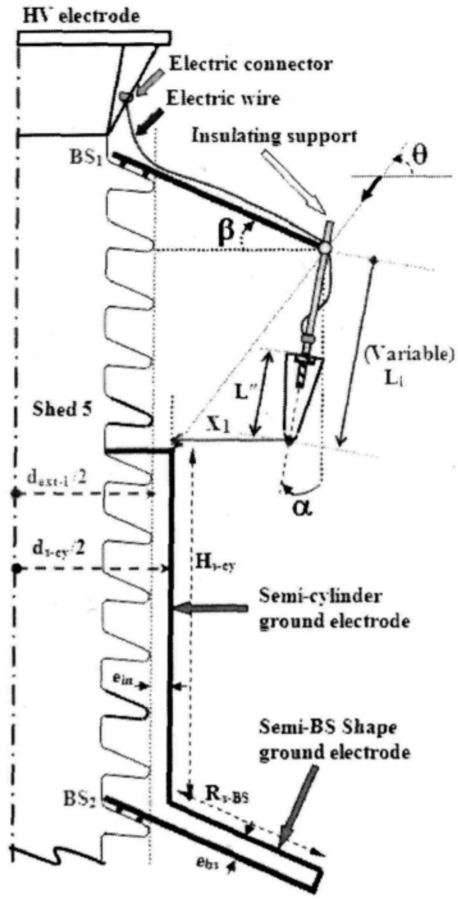

Figure 7.2- Cross section of the proposed experimental test; typical values (ds-cy/2≈16 cm, $H_{s\text{-}cy}\approx$ 30 cm, $R_{s\text{-}BS}\approx$16 cm, $e_{in}\approx e_{bs}\approx$3cm, L″=3.6 cm, 20 cm $\leq x_1 \leq$ 27cm, θ = 53, $\alpha \approx$ -15°)

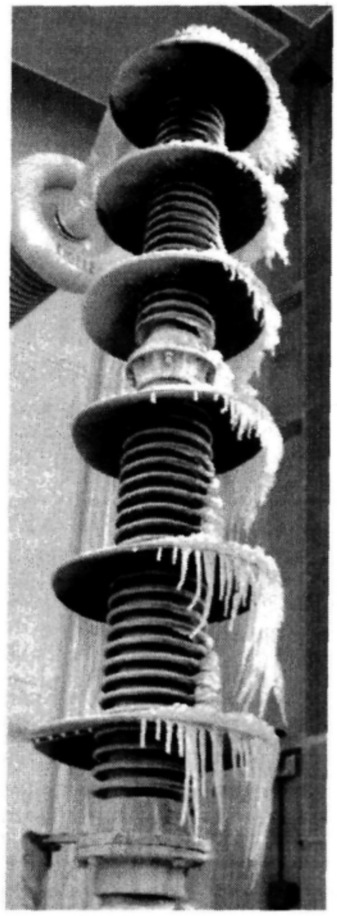

Figure 7.3- Trial test of 6-BS configuration under 30-mm ice accumulation on a rotating cylinder

The cold room and facilities are described in the previous investigations [80]. Typical values and dimensions of the proposed test (Figure 7.2) correspond to the first air gap range during the previous BS tests in [2]. However, to achieve a better understanding of the breakdown voltage of the air gaps in the BS tests, these typical values may be changed. Moreover, it is recommended to study the effect of inclination angle (α) variation of the icicle. The proposed test can be used not only in the area of BS designs and applications under icing conditions but also for other designs of ice-covered insulators with similar large air gaps. For example, it may provide better estimation of the breakdown voltage along the large air gaps for modified grading rings in [49]. Using equation (3.35) as a primary approximation, a transformer in the range of 198 kV or higher is required to perform the proposed test for its typical values (Figure 7.2).

Any artificial test method for insulators must meet the criteria of R3 (representative, repeatable, and reproducible) and cost-effectiveness [2], [97]. This test is representative as it is carried out based on the study of ice accretion configurations on BSs. Moreover, the icicles are formed from the water conductivity of σ_{20} = 340 µS/cm, which is selected on the basis of field experiences in Quebec [80]. For simulating ice near the seacoast or industrial region, a higher value of σ_{20} may be appropriate [2]. In addition, the proposed test can be repeated and reproduced in other conventional HV laboratories. Also, it is similar to finding the breakdown voltage of icicle-plane configuration for previous cost-effective investigations in [80].

REFERENCES

[1] M. Farzaneh, T. Baker, A. Bernstorf, J. T. Burnham, T. Carreira, E. Cherney, W. A. Chisholm, R. Christman, R. Cole, and J. Cortinas, "Selection of station insulators with respect to ice and snow-part II: methods of selection and options for mitigation," *IEEE Trans. Power Deliv.*, vol. 20, no. 1, pp. 271–277, 2005.

[2] M. Farzaneh and W. A. Chisholm, *Insulators for icing and polluted environments*. IEEE Press Series on Power Engineering, John Wiley, 2009.

[3] A. Nekahi and M. Farzaneh, "Excitation temperature determination of an arc formed over an ice surface using optical emission spectroscopy," *IEEE Trans. Dielectr. Electr. Insul.*, vol. 18, no. 6, pp. 1829–1834, 2011.

[4] Y. Sun, X. Wang, Z. Bie, and X. Wang, "Characteristics Analysis and Risk Modeling of Ice Flashover Fault in Power Grids," *IEEE Trans. Power Deliv.*, vol. 27, no. 3, pp. 1301–1312, 2012.

[5] X. Wei, Z. Jia, Z. Sun, W. Liao, Y. Qin, Z. Guan, Z. Xu, and X. Peng, "Study of anti-icing performance of insulator strings bottom-coated with semiconductive silicone rubber coating," *IEEE Trans. Dielectr. Electr. Insul.*, vol. 19, no. 6, pp. 2063–2072, Dec. 2012.

[6] I. A. Metwally, A. Al-Maqrashi, S. Al-Sumry, and S. Al-Harthy, "Performance improvement of 33kV line-post insulators in harsh environment," *Electr. power Syst. Res.*, vol. 76, no. 9, pp. 778–785, 2006.

[7] E. H. El-Zohri, M. Abdel-Salam, H. M. Shafey, and A. Ahmed, "Mathematical modeling of flashover mechanism due to deposition of fire-produced soot particles on suspension insulators of a HVTL," *Electr. Power Syst. Res.*, vol. 95, pp. 232–246, 2013.

[8] N. A. Al-geelani, M. A. M. Piah, and R. Q. Shaddad, "Characterization of acoustic signals due to surface discharges on HV glass insulators using wavelet radial basis function neural networks," *Appl. Soft Comput.*, vol. 12, no. 4, pp. 1239–1246, 2012.

[9] C. H. A. Ely, P. J. Lambeth, and J. S. T. Looms, "The booster shed: prevention of flashover of polluted substation insulators in heavy wetting," *IEEE Trans. Power Appar. Syst.*, vol. PAS-97, no. 6, pp. 2187–2197, 1978.

[10] P. J. Lambeth, "Laboratory tests to evaluate HVDC wall bushing performance in wet weather," *IEEE Trans. Power Deliv.*, vol. 5, no. 4, pp. 1782–1793, 1990.

[11] O. Oliveira Filho, J. A. Cardoso, D. R. de Mello, R. M. de Azevedo, and S. G. Carvalho, "Use of booster sheds to improve performance of 800 kV multicone type insulators under heavy rain," *J. High Volt. Eng.*, vol. 37, no. 011, pp. 2772–2779, 2011.

[12] L. Tang and M. R. Raghuveer, "Numerical evaluation of the efficacy of booster sheds and RTV coating in improving the performance of HVDC wall bushings," in *IEEE Conference on Electrical Insulation and Dielectric Phenomena*, 1997, vol. 2, pp. 410–413.

[13] O. Oliveira Filho, J. A. Cardoso, D. R. de Mello, R. M. de Azevedo, and S. G. Carvalho, "The use of booster sheds to improve the performance of 800 kV multicone type insulators under heavy rain," in *International Conference on High Voltage Engineering and Application (ICHVE)*, 2010, pp. 485–488.

[14] V. Sklenicka and J. Vokale, "Insulators in icing conditions: selection and measures for reliability increasing," in *7th Int. Workshop Atmospheric Icing Structures (IWAIS)*, 1996, pp. 72–76.

[15] J.-F. Drapeau, M. Farraneh, and M. J. Roy, "An exploratory study of various solutions for improving ice flashover performance of station post insulators," in *10th Int. Workshop Atmospheric Icing Structures (IWAIS)*, 2002, p. paper 4–06.

[16] M. Farzaneh and J. Zhang, "A multi-arc model for predicting AC critical flashover voltage of ice-covered insulators," *IEEE Trans. Dielectr. Electr. Insul.*, vol. 14, no. 6, pp. 1401–1409, 2007.

[17] C. Volat and M. Farzaneh, "Method of sizing the sheds of post insulators in view of improving their electrical performance under cold atmospheric conditions," in *IEEE Canadian Conference on Electrical and Computer Engineering (ICCECE),*, 2003, vol. 1, pp. 647–650.

[18] M. Farzaneh and C. Volat, "Étude de la tension de tenue des isolateurs de postes en présence de glace atmosphérique en vue d'un choix approprié de type et configuration d'isolateurs de postes à 735 kV," *Vol. 9 Résultats complémentaire relatifs aux Impuls. manoeuvre appliquées à un Isol. poste Stand. avec sans jupes Aux. Sci. Rep.*, pp. 1–12, 2007.

[19] M. Farzaneh and C. Volat, "Étude de la tension de tenue des isolateurs de postes en présence de glace atmosphérique en vue d'un choix approprié de type et configuration d'isolateurs de postes à 735 kV.," *Vol. 3 Étude en vue l'amélioration la tenue diélectrique des Isol. poste Stand. par l'ajout jupes Aux. Sci. Rep.*, pp. 1–40, 2005.

[20] M. Farzaneh, C. Volat, and C. Tavakoli, "Étude de la tension de tenue des isolateurs de postes en présence de glace atmosphérique en vue d'un choix approprié de type et configuration d'isolateurs de postes à 735 kV.," *Vol. 4 Étude sous Impuls. manoeuvre d'une colonne isolante avec trois jupes Aux. Sci. Rep.*, pp. 1–14, 2006.

[21] M. Farzaneh, J. T. Burnham, T. Carreira, E. Cherney, W. A. Chisholm, R. Christman, R. Cole, J. Cortinas, C. De Tourreil, J. F. Drapeau, S. Fikke, R. Gorur, T. Grisham, I. Gutman, J. Kuffel, A. Phillips, G. Powell, L. Rolfseng, M. Roy, T. Rozek, D. L. Ruff, A. Schwalm, V. Sklenicka, G. Stewart, R. Sundararajan, M. Szeto, R. Tay, J. Zhang, T. Baker, and A. Bernstorf, "Selection of station insulators with respect to ice and snow-part I: technical context and environmental exposure," *IEEE Trans. Power Deliv.*, vol. 20, no. 1, pp. 264–270, 2005.

[22] A. Nekahi and M. Farzaneh, "Local thermodynamic equilibrium of an arc over an ice surface," *IEEE Trans. Dielectr. Electr. Insul.*, vol. 20, no. 3, pp. 727–730, 2013.

[23] J. C. Pohlman and C. R. Davis, "Cracked insulators create hazardous working conditions during restoration after extreme ice storm," in *Seventh International Conference on Transmission and Distribution Construction and Live Line Maintenance (ESMO-95),*, 1995, pp. 143–149.

[24] Q. Hu, L. Shu, X. Jiang, C. Sun, Z. Zhang, and J. Hu, "Effects of shed configuration on AC flashover performance of ice-covered composite long-rod insulators," *IEEE Trans. Dielectr. Electr. Insul.*, vol. 19, no. 1, pp. 200–208, 2012.

[25] X. Jiang, Y. Chao, Z. Zhang, J. Hu, and L. Shu, "DC flashover performance and effect of sheds configuration on polluted and ice–covered composite insulators at low atmospheric pressure," *IEEE Trans. onDielectrics Electr. Insul.*, vol. 18, no. 1, pp. 97–105, 2011.

[26] Z. Xu, Z. Jia, Z. Li, X. Wei, Z. Guan, M. MacAlpine, Y. Zhao, and Y. Li, "Anti-icing performance of RTV coatings on porcelain insulators by controlling the leakage current," *IEEE Trans. Dielectr. Electr. Insul.*, vol. 18, no. 3, pp. 760–766, 2011.

[27] Q. Yang, W. Sima, J. Deng, C. Sun, and J. Hu, "Shed Configuration Optimization for Ice-Covered Extra High Voltage Composite Insulators," *J. Adhes. Sci. Technol.*, vol. 26, no. 4–5, pp. 575–591, 2012.

[28] S. Berlijn, K. A. Halsan, A. T. Olsen, M. Runde, M. Hinteregger, T. Judendorfer, and M. Muhr, "Voltage upgrading-An insulation coordination challenge," in *IEEE Trondheim PowerTech*, 2011, pp. 1–8.

[29] H. Matsuda, H. Komuro, and K. Takasu, "Withstand voltage characteristics of insulator string covered with snow or ice," *Power Deliv. IEEE Trans.*, vol. 6, no. 3, pp. 1243–1250, 1991.

[30] A. B. Dehkordi and M. Vakilian, "Simulation and analysis of electric field distributions of ice-covered insulators using finite element method," in *(Persian), 17th International Power System Conference (PSC), Iran*, 2002.

[31] M. Farzaneh, *Atmospheric Icing of Power Networks*. Springer, 2008.

[32] M. Farzaneh, "Ice accretions on high–voltage conductors and insulators and related phenomena," *Philos. Trans. R. Soc. London. Ser. A Math. Phys. Eng. Sci.*, vol. 358, no. 1776, pp. 2971–3005, 2000.

[33] Z. Xu, Z. Jia, Z. Guan, L. Wang, R. Zhang, Y. Zhao, and Y. Li, "Anti-icing performance of RTV coating with different resistivity on insulators," in *IEEE Conference on Electrical Insulation and Dielectric Phenomena (CEIDP),*, 2010, pp. 1–4.

[34] Z. Zhang, X. Jiang, C. Sun, J. Hu, H. Huang, and D. W. Gao, "Influence of insulator string positioning on AC icing flashover performance," *IEEE Trans. Dielectr. Electr. Insul.*, vol. 19, no. 4, pp. 1335–1343, 2012.

[35] M. Farzaneh, J. Kiernicki, and J.-F. Drapeau, "Ice accretion on energized line insulators," *Int. J. Offshore Polar Eng.*, vol. 2, no. 3, pp. 228–233, 1992.

[36] M. Farzaneh and J. F. Drapeau, "AC flashover performance of insulators covered with artificial ice," *IEEE Trans. Power Deliv.*, vol. 10, no. 2, pp. 1038–1051, 1995.

[37] M. Farzaneh and J. Kiernicki, "Flashover performance of IEEE standard insulators under ice conditions," *IEEE Trans. Power Deliv.*, vol. 12, no. 4, pp. 1602–1613, 1997.

[38] V. Jaiswal, M. Farzaneh, and D. A. Lowther, "Impulse flashover performance of semiconducting glazed station insulator under icing conditions based on field calculations by finite-element method," *IEE Proceedings-Generation, Transm. Distrib.*, vol. 152, no. 6, pp. 864–870, 2005.

[39] Z. Zhang, X. Jiang, J. Hu, and C. Sun, "AC electric characteristics of 110 kV post insulators covered with ice or snow," *J. High Volt. Eng.*, vol. 35, no. 10, pp. 2528–2534, 2009.

[40] V. Jaiswal and M. Farzaneh, "Modelling of flashover performance of an ice-covered resistive glazed post station insulator in presence of an air gap," *J. Phys. D. Appl. Phys.*, vol. 39, no. 1, p. 227, 2006.

[41] M. Farzaneh, J. Zhang, and C. Volat, "Effect of Insulator Diameter on AC Flashover Voltage of an Ice-covered Insulator String," *IEEE Trans. Dielectr. Electr. Insul.*, vol. 13, no. 2, pp. 264–271, 2006.

[42] M. Farzaneh and S. Brettschneider, "É tude de la tension de tenue des isolateurs de postes en pr é sence de glace atmosph é rique en vue d ' un choc appropri é de type et confi guration d ' isolateurs de poste à 735 kV," *Vol. 1, É tude en vue du choix d ' Isol. pour le Futur poste Mont é r é gie, " Sci. Rep.*, 2001.

[43] F. Meghnefi, C. Volat, and M. Farzaneh, "Temporal and frequency analysis of the leakage current of a station post insulator during ice accretion," *IEEE Trans. Dielectr. Electr. Insul.*, vol. 14, no. 6, pp. 1381–1389, 2007.

[44] C. Volat, F. Meghnefi, M. Farzaneh, and H. Ezzaidi, "Monitoring leakage current of ice-covered station post insulators using artificial neural networks," *IEEE Trans. Dielectr. Electr. Insul.*, vol. 17, no. 2, pp. 443–450, 2010.

[45] R. S. Gorur, E. A. Cherney, and J. T. Burnham, *Outdoor insulators*. Ravi S. Gorur Inc., Phoenix, Arizona, USA,, 1999.

[46] G. Momen and M. Farzaneh, "Survey of micro/nano filler use to improve silicone rubber for outdoor insulators," *Rev. Adv. Mater. Sci*, vol. 27, no. 1, pp. 1–13, 2011.

[47] X. Wei, Z. Jia, Z. Xu, and H. Su, "Thermal and Voltage distribution along insulator strings with semiconducting RTV coatings," in *IEEE Electrical Insulation conference (EIC)*, 2011, no. June, pp. 240–243.

[48] M. Farzaneh and W. A. Chisholm, "Insulator icing test methods, selection criteria and mitigation alternatives," *IEEE Trans. Dielectr. Electr. Insul.*, vol. 14, no. 6, pp. 1462–1473, 2007.

[49] H. Akkal, C. Volat, and M. Farzaneh, "Improving electrical performance of EHV post station insulators under severe icing conditions using modified grading rings," *IEEE Trans. Dielectr. Electr. Insul.*, vol. 20, no. 1, pp. 221–228, 2013.

[50] M. Farzaneh, T. Baker, A. Bernstorf, K. Brown, W. a. A. Chisholm, C. de Tourreil, J. F. F. Drapeau, S. Fikke, J. M. M. George, E. Gnandt, C. T. Baker, T. Grisham, I. Gutman, R. Hartings, R. Kremer, G. Powell, L. Rolfseng, T. Rozek, D. L. Ruff, D. Shaffner, V. Sklenicka, R. Sundararajan, and J. Yu, "Insulator icing test methods and procedures a position paper prepared by the IEEE task force on insulator icing test methods," *IEEE Trans. Power Deliv.*, vol. 18, no. 4, pp. 1503–1515, Oct. 2003.

[51] M. Farzaneh, J. Zhang, and X. Chen, "Modeling of the AC arc discharge on ice surfaces," *IEEE Trans. Power Deliv.*, vol. 12, no. 1, pp. 325–338, 1997.

[52] F. A. M. Rizk, "Mathematical models for pollution flashover," *Electra*, vol. 78, no. 5, pp. 71–103, 1981.

[53] T. Xu, H. Wang, L. Wang, Z. Xu, T. Yao, and L. Cai, "Flashover performance of 500kV ice-covered porcelain post insulators with composite assistant shed," *J. High Volt. Eng.*, vol. 38, no. 1, pp. 167–172, 2012.

[54] W. Sima, Q. Yang, C. Sun, and F. Guo, "Potential and electric-field calculation along an ice-covered composite insulator with finite-element method," in *IEE Proceedings-Generation, Transmission and Distribution*, 2006, vol. 153, no. 3, pp. 343–349.

[55] H. Javadi and M. Farzaneh, "Comparison of electrostatic field calculation in rod-plane electrode using analytical and finite element methods," *Int. J. Appl. Eng. Res.*, vol. 5, no. 4, pp. 573–582, 2010.

[56] F. Mirshafiei, G. McClure, and M. Farzaneh, "Modelling the Dynamic Response of Iced Transmission Lines Subjected to Cable Rupture and Ice Shedding," *IEEE Trans. Power Deliv.*, vol. 28, no. 2, pp. 948–954, 2013.

[57] P. Fu, M. Farzaneh, and G. Bouchard, "Two-dimensional modelling of the ice accretion process on transmission line wires and conductors," *Cold Reg. Sci. Technol.*, vol. 46, no. 2, pp. 132–146, 2006.

[58] M. Farzaneh, C. Volat, and A. Gakwaya, "Electric field modelling around an ice-covered insulator using boundary element method," in *IEEE International Symposium on Electrical Insulation*, 2000, pp. 349–355.

[59] C. Volat and M. Farzaneh, "Three-dimensional modeling of potential and electric-field distributions along an EHV ceramic post insulator covered with ice-part II: effect of air gaps and partial arcs," *IEEE Trans. Power Deliv.*, vol. 20, no. 3, pp. 2014–2021, 2005.

[60] C. Volat and M. Farzaneh, "Three-dimensional modeling of potential and electric-field distributions along an EHV ceramic post insulator covered with ice-part I: simulations of a melting period," *IEEE Trans. Power Deliv.*, vol. 20, no. 3, pp. 2006–2013, 2005.

[61] M. Farzaneh, C. Volat, and J. Zhang, "Role of air gaps on AC withstand voltage of an ice-covered insulator string," *IEEE Trans. Dielectr. Electr. Insul.*, vol. 13, no. 6, pp. 1350–1357, 2006.

[62] J. Arora, *Introduction to optimum design*. Academic Press, 2004.

[63] A. Saxena and B. Sahay, *Computer aided engineering design*. Springer, 2005.

[64] W. Sima, F. P. Espino-Cortes, E. A. Cherney, and S. H. Jayaram, "Optimization of corona ring design for long-rod insulators using FEM based computational analysis," in *IEEE International Symposium on Electrical Insulation*, 2004, pp. 480–483.

[65] W. Sima, Q. Yang, C. Sun, S. H. Jayaram, and E. A. Cherney, "Optimization of corona ring design for EHV composite insulator using finite element and neural network method," *Proceedings-Chinese Soc. Electr. Eng.*, vol. 25, no. 17, p. 115, 2005.

[66] P. Kitak, J. Pihler, I. Ticar, A. Stermecki, O. Biró, and K. Preis, "Potential control inside switch device using FEM and stochastic optimization algorithm," in *12th Biennial IEEE Conference on Electromagnetic Field Computation*, 2006, pp. 418–421.

[67] P. Kitak, J. Pihler, I. Ticar, A. Stermecki, O. Biro, and K. Preis, "Potential control inside switch device using FEM and stochastic optimization algorithm," *IEEE Trans. Magn.*, vol. 43, no. 4, pp. 1757–1760, 2007.

[68] I. Sebestyén, "Optimization for high voltage composite insulators using experimental design theory," in in *Computer Engineering in Applied Electromagnetism*, Springer, 2005, pp. 95–98.

[69] D. C. Domínguez, P. Gómez, C. Dominguez, and F. P. Espino-Cortés, "Optimized design of electric field grading systems in 115 kV non-ceramic insulators," *IEEE Trans. Dielectr. Electr. Insul.*, vol. 20, no. 1, pp. 63–70, 2013.

[70] S. Gunasekaran and M. W. Iruthayarajan, "Contour optimization of suspension insulators using real coded genetic algorithm with simulated binary crossover," in *IEEE Conference on Pattern Recognition, Informatics and Medical Engineering (PRIME),*, 2013, pp. 360–364.

[71] R. Jafari, L. F. Mobarakeh, and M. Farzaneh, "Water-Repellency Enhancement of Nanostructured Plasma-Polymerized HMDSO Coatings Using Grey-Based Taguchi Method," *Nanosci. Nanotechnol. Lett.*, vol. 4, no. 3, pp. 369–374, 2012.

[72] A. R. Khoei, I. Masters, and D. T. Gethin, "Design optimisation of aluminium recycling processes using Taguchi technique," *J. Mater. Process. Technol.*, vol. 127, no. 1, pp. 96–106, 2002.

[73] G. Taguchi, *Introduction to quality engineering: designing quality into products and processes*. Asian Productivity Organization, 1986.

[74] X. He, Z. Yu, and X. Lai, "Robust parameters control methodology of microstructure for heavy forgings based on Taguchi method," *Mater. Des.*, vol. 30, no. 6, pp. 2084–2089, 2009.

[75] C. Volat, "Calcul de la distribution du potentiel du champ électrique le long des surfaces de glace recouvrant les isolateurs haute-tension et dans les intervalles d'air entre celles-ci," Thesis of Ph. D. in Engineering, UQAC, 2002.

[76] C. Volat and M. Farzaneh, "A simple axisymmetric model for calculation of potential distribution along ice-covered post station insulators during a melting period," in *IEEE Conference on Electrical Insulation and Dielectric Phenomena (CEIDP)*, 2008, pp. 232–235.

[77] S. M. Ale-Emran, M. Farzaneh, and C. Volat, "Simulation analysis of the effect of booster sheds on post insulators under icing conditions," in *IEEEE Conference on Electrical Insulation and Dielectric Phenomena (CEIDP)*, 2012, pp. 749–752.

[78] C. Volat, S. M. Ale-Emran, and M. Farzaneh, "Numerical simulations of ice-covered EHV post station insulator performance equipped with booster sheds," in *IEEE International Symposium on Electrical Insulation (ISEI),*, 2012, pp. 91–94.

[79] L. S. M. Farzaneh, J. Zhang, D. Yu, C. Sun, W. Sima, "Characteristics of Corona Discharge in an Icicle/Iced-Plate Electrode System Under Negative DC Voltage," in *8th International Conference on Properties and Applications of Dielectric Materials (ICPADM 2006), Bali, Indonesia*, 2006, pp. 48–51.

[80] I. Fofana, M. Farzaneh, H. Hemmatjou, and C. Volat, "Study of discharge in air from the tip of an icicle," *IEEE Trans. Dielectr. Electr. Insul.*, vol. 15, no. 3, pp. 730–740, 2008.

[81] C. Volat, F. Farzaneh, and H. Akkal, "Influence of a grading ring on AC flashover voltage of an EHV post insulator covered with ice," in *IEEE Conference on Electrical Insulation and Dielectric Phenomena (CEIDP)*, 2009, pp. 250–253.

[82] M. Farzaneh and O. T. Melo, "Flashover Performance of Insulators in the Presence of Short Icicles," *Int. J. Offshore Polar Eng.*, vol. 4, no. 2, pp. 112–118, 1994.

[83] D. Yu, Z. Jia, X. Wei, H. Su, Z. Guan, T. Wang, and K. Wang, "Mechanism of salt migration in icicles during phase transition and its impact on ice flashover," *IEEE Trans. Dielectr. Electr. Insul.*, vol. 19, no. 5, pp. 1700–1707, 2012.

[84] N. Ravelomanantsoa, M. Farzaneh, and W. A. Chisholm, "A simulation method for winter pollution contamination of HV insulators," in *IEEE Electrical Insulation Conference (EIC)*, 2011, pp. 373–376.

[85] H. Javadi, M. Farzaneh, and A. Peyda, "Determination of Electric Field at Inception Based upon Current-Voltage Characteristics of AC Corona in Rod-Plane Gaps," *Iran. J. Electr. Electron. Eng.*, vol. 6, no. 2, p. 119, 2010.

[86] H. Javadi, A. Peyda, and M. Farzaneh, "Numerical study to determine Corona inception electric field using a rod-plane configuration," in *18th IASTED International Conference on Modelling and Simulation*, 2007, pp. 79–83.

[87] W. A. Chisholm, K. G. Ringler, C. C. Erven, M. A. Green, O. Melo, Y. Tam, O. Nigol, J. Kuffel, A. Boyer, I. K. Pavasars, F. X. Macedo, J. K. Sabiston, and R. B. Caputo, "The cold-fog test [for outdoor insulators]," *IEEE Trans. Power Deliv.*, vol. 11, no. 4, pp. 1874–1880, 1996.

[88] E. A. Cherney, "Silicone rubber dielectrics modified by inorganic fillers for outdoor high voltage insulation applications," *IEEE Trans. Dielectr. Electr. Insul.*, vol. 12, no. 6, pp. 1108–1115, 2005.

[89] I. M. de Alegría, J. L. Martín, I. Kortabarria, J. Andreu, and P. I. Ereño, "Transmission alternatives for offshore electrical power," *Renew. Sustain. Energy Rev.*, vol. 13, no. 5, pp. 1027–1038, Jun. 2009.

[90] J. Farzaneh-Dehkordi, J. Zhang, and M. Farzaneh, "Experimental study and mathematical modelling of flashover on extra-high voltage insulators covered with ice," *Hydrol. Process.*, vol. 18, no. 18, pp. 3471–3480, 2004.

[91] J. Farzaneh-Dehkordi, J. Zhang, and M. Farzaneh, "Exprimental and Mathematical Modeling of Flashover on EHV Insulators Covered with Ice," in *61th Eastern Snow Conference*, 2004, pp. 3–12.

[92] Y. Wang, J. Kim, and J. Song, "Optimization of plastic injection molding process parameters for manufacturing a brake booster valve body," *Mater. Des.*, vol. 56, pp. 313–317, Apr. 2013.

[93] P. Jongpradist, R. Rojbunsongsri, T. Kamnerdtong, and S. Wongwises, "Parametric study and optimization of a food can corrugation design using a response surface method," *J. Mech. Sci. Technol.*, vol. 27, no. 7, pp. 2043–2052, Jul. 2013.

[94] S. Ray, *Electrical power systems: concepts, theory and practice*. PHI Learning Pvt. Ltd., 2006.

[95] U. C. Hasar, "Permittivity measurement of thin dielectric materials from reflection-only measurements using one-port vector network analyzers," *Prog. Electromagn. Res.*, vol. 95, pp. 365–380, 2009.

[96] S. Ramesh, A. H. Yahaya, and A. K. Arof, "Dielectric behaviour of PVC-based polymer electrolytes," *Solid State Ionics*, vol. 152, pp. 291–294, 2002.

[97] M. Farzaneh, "IEEE standard 1783–guide for test methods and procedures to evaluate the electrical performance of insulators in freezing conditions," no. October. IEEE Press, New York, pp. 1–32, 2009.

[98] S. M. Ale-Emran and M. Farzaneh, "Numerical analysis of the combined effects of booster sheds and grading rings on an ice-covered EHV ceramic post insulator," in *IEEE Electrical Insulation Conference (EIC)*, 2013, pp. 346–350.

[99] V. A. Ganesh, H. K. Raut, A. Sreekumaran Nair, and S. Ramakrishna, "A review on self-cleaning coatings," *J. Mater. Chem.*, vol. 21, no. 41, pp. 16304–16322, 2011.

[100] R. Menini and M. Farzaneh, "Production of superhydrophobic polymer fibers with embedded particles using the electrospinning technique," *Polym. Int.*, vol. 57, no. 1, pp. 77–84, 2008.

[101] S. A. Kulinich and M. Farzaneh, "Effect of contact angle hysteresis on water droplet evaporation from super-hydrophobic surfaces," *Appl. Surf. Sci.*, vol. 255, no. 7, pp. 4056–4060, Jan. 2009.

[102] R. Jafari, S. Asadollahi, and M. Farzaneh, "Applications of Plasma Technology in Development of Superhydrophobic Surfaces," *Plasma Chem. Plasma Process.*, vol. 33, no. 1, pp. 177–200, Oct. 2012.

APPENDIX

STUDY OF ICE ACCRETION ON BOOSTER SHEDS

APPENDIX

STUDY OF ICE ACCRETION ON BOOSTER SHEDS

This appendix presents the detailed study of ice accretion on BSs. It is based mainly on the previous experimental tests in CIGELE [2], [18]–[20] to determine the characteristic of the artificial air gaps, the variation of Ice-Free Leakage Distance (IFLD), etc. under different configurations and conditions (Figure A. 1).

30-mm/140 min ice accretion on rotating cylinder			15-mm/70 min ice accretion on rotating cylinder		
4-BS test	5-BS test	6-BS test	4-BS test	6-BS test	0-BS test
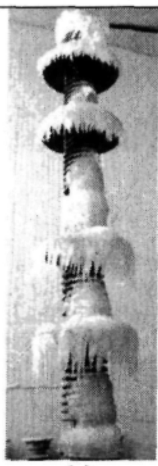 (a)	 (b)	 (c)	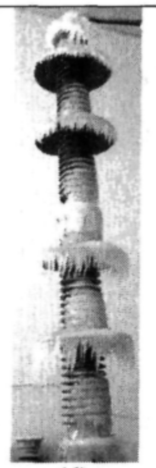 (d)	 (e)	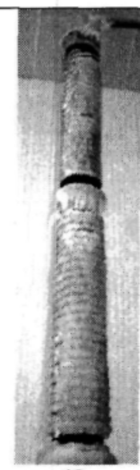 (f)
V_{WS} = 285 kV Improvement over untreated: 5.6%	V_{WS} = 300 kV Improvement over untreated: 11.1%	V_{WS} = 315 kV Improvement over untreated: 16.7%	V_{WS} = 330kV Improvement over untreated: 22.2%	V_{WS} > 350 kV Improvement over untreated: >29.6%	V_{WS} = 270 kV untreated

Figure A. 1- Test results of various configurations of standard post insulators in heavy icing conditions with 30-mm ice accretion a) 4 BSs b) 5 BSs c) 6 BSs and with 15-mm ice accretion d) 4 BSs e) 6 BSs f) 0 BS (untreated) [2], [18]–[20]

In previous experimental tests, an untreated EHV ceramic post insulator under heavy ice condition usually has an ice-free zone at the 1^{st} and 2^{nd} sheds close to the HV electrode (Figure A. 1-f). This phenomenon is because of the high electric field and consequent discharge activity close to the HV electrode zone that can produce enough heat dissipations to prevent ice bridging on the 1^{st} and 2^{nd} sheds. A similar pattern is seen at the junction from insulator to metal fitting of junction and also at the ground electrode.

Table A. 1 shows the shed numbers of the EHV ceramic post insulter units which the BSs were installed on them. Also in Table A. 2 the distances between the installed BSs are presented. Two sets of tests were carried out for six BS configurations [2], [18]–[20]. In Table A. 1 and Table A. 2, 6p-BS test represents the primary series of six BS tests. The problem in 6p-BS test was the appearance of ice bridging between BS_5 and BS_6. For this reason, BS_5 on shed 13 shifted to shed 12 (the bold numbers in Table A. 1 and Table A. 2).

Table A. 1- The position (shed number) of the installation of the BSs on the insulator

BS No.	4-BS test	5-BS test	6-BS test	6p-BS test
1	3	3	2	2
2	15	15	13	13
3	3	26	23	23
4	14	6	2	2
5	-	18	**12**	**13**
6	-	-	22	22

Table A. 2- Distances between the installed BSs (cm)

BS_{ij}*	4-BS test	5-BS test	6-BS test	6p-BS test
BS_{12}	60.5	60.5	56.5	56.5
BS_{23}	96	54	48.5	48.5
BS_{34}	57.5	56	51	51
BS_{45}	-	62.5	**52**	**57**
BS_{56}	-	-	**50.5**	**45.5**
Total	214	233	258.5	258.5
Average	71.3	58.25	51.7	51.7

*BS_{ij}: signifies the zone between BS_i and BS_j.

The number of ice-free, partly-bridged ice and fully-bridged ice sheds of the insulator under each BSs for an accretion of 30-mm and 15-mm on a rotating cylinder are presented in Table A. 3 and Table A. 4, respectively. These values are extracted from the images of the previous BS tests in [2], [18]–[20]. Since the area above the BS_I close to the HV electrode cannot be seen in the images, the ice condition of the sheds in this area is estimated after comparing with the untreated insulator of 15-mm ice accretion (Figure A. 1-f) and validation test results of 30-mm ice accretion (Figure 6.8).

Table A. 5 shows the values of the equivalent number of total ice-free sheds and the values of IFLD for both 30-mm and 15-mm ice accretion on rotating cylinder. To calculate the values in Table A. 5, the following relations are developed:

$$N_{\text{equivalent total ice free sheds}} = N_{\text{total ice-free sheds}} + 0.5 \times N_{\text{partly ice-bridged sheds}} \cdot \qquad \text{(A.1)}$$

It means the number of equivalent total ice-free sheds is equal to the number of total ice-free sheds plus the 50% of the number of partly ice-bridged sheds.

$$IFLD_{1\_t}\ (\text{cm}) \cong K \times N_{\text{equivalent total ice free sheds}} \times d_{\text{shsh}}\,(cm) \qquad \text{(A.2)}$$

Where,

$IFLD_{1\_t}$: is the sum of the equivalent IFLD along surfaces of the sheds of insulator in the BS tests.

K: is the ratio of total leakage distance of one unit of the post insulator to its dry arcing distance (DAD): 2.52 (3.5 m /1.39 m)

d_{shsh} : is the shed-to-shed distance of the post insulator ($d_{\text{shsh}} \approx 5cm$)

$$IFLD_2(\text{cm}) \approx IFLD_{\text{bBSi}} \times N_{\text{BS}} \qquad \text{(A.3)}$$

Where,

$IFLD_2$: is sum of the IFLD of bottom surfaces of BSs (cm)

$IFLD_{bBSi}$: is the IFLD of bottom surface of BS_i (cm) = 23.0 cm.

N_{BS}: is the number of installed BSs.

At the end, we obtain the total ice-free leakage distance ($IFLD_{tot}$) as follows:

$$IFLD_{tot}(\text{cm}) = IFLD_{I\text{-}t}(\text{cm}) + IFLD_2(\text{cm}) + IFLD_3(\text{cm}) \quad . \tag{A.4}$$

Where $IFLD_3$ is the ice-free distance of top surfaces of BSs.

Table A. 3- The ice condition of the insulator sheds under booster sheds
(**30 mm ice accretion** on rotating cylinder)

Shed Conditions / Region	4-BS test			5-BS test			6-BS test		
	ice-free sheds	partly bridged sheds	fully bridged sheds	ice-free sheds	partly bridged sheds	fully bridged sheds	ice-free sheds	partly bridged sheds	fully bridged sheds
HV-BS1	(0)*	(0)	(2)	(0)	(0)	(2)	(0)	(0)	(1)
BS_{12}	5	1	6	5	1	6	5	1	5
BS_{23}	5	1	8+Conj**	6	1	4	5	1	4
BS_{34}	6	0	5	1+Conj	0	5	4+0.6Conj	0	1+0.4Conj
BS_{4G}/BS_{45}	5	1	6+G**	5	1	6	5	1	4
BS_{5G}/BS_{56}	-	-	-	4	1	3+G	5	0	5
BS_{6G}	-	-	-	-	-	-	4	0	0
Total	21	3	27+Conj+G	21+Conj	4	26+G	29+0.6Conj	3	19+0.4Conj
Equivalent total sheds	21	3	31***	25	4	26	30.5	3	21.5

* The numbers in the parentheses are the estimated values.
** ''Conj'' signifies the conjunction floating electrode between the two units of the insulator. Also, ''G''is the Ground electrode.
*** To calculate the equivalent total sheds, the effective length of Conj and G is considered equal to around 4 and 0 sheds of the insulator, respectively.

Table A. 4- The ice condition of the insulator sheds under BSs (**15 mm ice accretion** on rotating cylinder)

Shed Conditions / Region	4-BS test			6-BS test			0-BS test (untreated insulator)		
	ice-free sheds	partly bridged sheds	fully bridged sheds	ice-free sheds	partly bridged sheds	fully bridged Sheds	ice-free sheds	partly bridged sheds	fully bridged sheds
HV-BS1	(1) *	(1)	(0)	(1)	(0)	(0)	-	-	-
BS_{12}	5	2	5	5	2	4	-	-	-
BS_{23}	5	2	7+Conj*	5	2	3	-	-	-
BS_{34}	6	0	5	4+0.6Conj	0	0.4Conj	-	-	-
BS_{4G}/BS_{45}	5	1	6+G*	5	1	4	-	-	-
BS_{5G}/BS_{56}	-	-	-	5	0	5	-	-	-
BS_{6G}	-	-	-	4	0	0	-	-	-
Total	22	6	23+Conj+G	29+0.6Conj	5	17+0.4Conj	1+0.75Conj	1	49+0.25Conj+G
Equivalent* total Sheds	22	6	27	31.5	5	18.5	4	1	50

* Refer to the explanations below Table 1 please. (Also, it is considered: 0.6Conj≈2.5 shed, 0.5Conj≈ 2 shed, 1Conj≈4 shed)

Table A. 5- Equivalent total ice-free sheds and ice-free leakage distances (IFLD) in BS configurations

IFLD \ Configurations	30 mm ice accretion on rotating cylinder			15 mm ice accretion on rotating cylinder		
	4-BS test	5-BS test	6-BS test	4-BS test	6-BS test	0-BS (untreated)
Equivalent total ice-free sheds	22.5	27	32	25	34	4.5
$IFLD_{1-t}$ (equivalent ice-free leakage distance along insulator sheds (cm))	283.3	339.9	402.9	314.8	428.1	56.7
$IFLD_2$ (ice-free leakage distance of bottom surfaces of BSs (cm))	92.0	115.0	138.0	92.0	138.0	0
$IFLD_3$ (ice-free distance of top surfaces of BSs (cm))	0	0	0	(15)*	(15)	0
$IFLD_{tot}$ (total ice-free leakage distance (test)	375,3	454,9	540,9	421.8	581.2	56.7

* The numbers in the parentheses are the estimated values.

Table A. 6 and Table A. 7 show the length of the air gaps and icicles for the different configurations of the post insulator equipped with BSs.

Table A. 6- The lengths of the **air gaps** (cm) in BS configurations

BS No. \ Configs	30 mm ice accretion on rotating cylinder										15 mm ice accretion on rotating cylinder					
	4-BS	5-BS test			6-BS test			6p-BS test			4-BS test			6-BS test		
-	ave	range	ave	*ΔLag*	range	ave	*ΔLag*	range	ave	*ΔLag*	range	ave	*ΔLag*	range	ave	*ΔLag*
1	(23.2)*	22-27	23.2	5	20-24	21,8	4	20-23	21.25	3	24-25	24.2	1	21-24	22.3	3
2	(16.2)	14-19	16.2	5	12-15	13,8	3	13-16	14	3	22-25	22.6	3	14-15	14.5	1
3	((9.6))*	7-11	9	4	5-10	8,4	5	8-12	10.5	4	12-18	16.2	6	10-12	11	2
4	((11))	7-11	9.6	4	4-9	7	5	8-10	9	2	11-13	12	2	9-12	10.3	3
5	-	10-12	11	2	0-6	2,6	6	**0**	**0**	**0**	-	-	-	11-12	11.3	1
6	-	-	-	-	8-10	9,2	2	8-9	8.75	1	-	-	-	9-16	12.3	7
Total (L_{AG-tot})	**((60.0))**	60-80	**69.0**	20	49-74	**62,8**	25	57-70	**63.5**	13	69-81	**75**	12	74-91	**84.3**	17

* The numbers in the parentheses are the estimated values.

Table A. 7- The lengths of the **icicles** (cm) in BS configurations

Configs / BS No.	30 mm ice accretion on rotating cylinder											15 mm ice accretion on rotating cylinder					
	4-BS	5-BS test			6-BS test			6p-BS test				4-BS test			6-BS test		
	ave	range	ave	*ΔLice*	range	ave	*ΔLice*	range	ave	*ΔLice*		range	ave	*ΔLice*	range	ave	*ΔLice*
1	(17.4)*	15-19	17.4	4	19-20	19.8	1	17-20	18	3		5-10	6.8	5	11-12	11.7	1
2	(20)	16-22	20	6	22-27	24	5	19-23	21.5	4		10-13	10.6	3	12-18	16	6
3	((30))*	27-38	32.2	11	28-32	29.8	4	23-30	25.75	7		20-24	21	4	22-22	22	0
4	((37))	27-33	29.6	6	31-35	33	4	30-34	31.5	4		20-26	22.4	6	23-27	24.3	4
5	-	24-29	26.8	5	33-40	37	7	30-36	33.25	6		-	-	-	31-32	31.3	1
6	-	-	-	-	40-50	44	10	28-37	33.5	9		-	-	-	29-32	31	3
Total ($L_{Icicle-tot}$)	**((104.4))**	109-141	**126**	32	173-204	**187.6**	31	147-180	**163.5**	33		55-73	**60.8**	18	128-143	**136.3**	15

* The numbers in the parenthesis are the estimated values.

It can be also observed from the experimental test images (Figure A. 1) that:

1. A small ring was installed in the top of the insulators during the BS test.
2. There is a possibility of the appearance of a small air gap between the mentioned top small ring and BS_1.

The icicle lengths of the BSs closely depend on the position of the BS along the two insulator units. As the BS comes close to the ground, icicle length increases. This is due to the fact that the potential distribution along the insulators is not uniform. In other words, the icicles along the BSs closer to HV electrode are growing in a stronger electric field. The appearance of corona discharges at the tip of icicles in a strong electric field lead to the reduction of icicle growing rate. As BS approaches the ground electrode, electric field strength decreases and icicles can grow without restriction.

In general, the icicles on a lower BS, have longer lengths. However, in some cases it was observed that a lower BS had a shorter icicle length. This occurred for the BSs installed on the bottom unit (close to ground) of the standard insulator. Since the electric field along the bottom unit is not strong and the potential differences are low, the electric field has a minor role in the icicle growth of the BSs on the bottom unit. Thus, a lower BS can have a shorter icicle length according to the random manner of the creation of the icicles.

The average length of the icicles between sheds of insulator, L, as a function of the accumulation time in the space of sheds of insulator is [75]:

$$L_t(\text{cm}) = 0.242 \times \text{t}\,(\text{min}) \tag{A.5}$$

Using (A.5) as a primary approximation for the icicle length on BSs results in:

L_{o15}(cm)=16.9cm (15-mm ice accretion on rotating cylinder, t =70 min) (A.6)

L_{o30}(cm)=33.9cm (30-mm ice accretion on rotating cylinder, t=140 min) (A.7)

Normalization of the lengths of the icicles in Table A. 8 based on the above values, can give us a good understanding of the effect of the electric field in the icicle growth from top to bottom. Actually, the values of each icicle length on $BS_{i=k}$ in 30-mm ice accretion test is normalized by its corresponding icicle length on $BS_{i=k}$ in 15-mm ice accretion test. For example, the value of icicle length on BS_1 in 30-mm ice accretion 6-BS test ("19.8" in Table A. 7) is divided by its corresponding icicle length on BS_1 in 15-mm ice accretion 6-BS test ("11.7" in Table A. 7) and it led to "1.69" (Table A. 8). Two interesting points are as follows:

1. Although the accumulation times of 30-mm versus 15-mm ice accretion are twice as duration (140 min vs 70 min), their corresponding icicle lengths are usually less than twice as long.
2. The average icicle length of BS_1 in 4-BS test of 30-mm ice accretion is even more than twice its corresponding icicle length in 4-BS test of 15 mm ice accretion test. This can be explained by referring to the random manner of the creation of icicles. In other words, it is the variation range of the icicle length (ΔLice, Table A. 7) that can cause this phenomenon.

Table A. 8- Normalization of the average lengths of the icicles of BSs in 30-mm ice accretion tests based on 15-mm ice accretion tests

BS No.	4 BS test	6 BS test
1	(2.56) *	1.69
2	(1.89)	1.5
3	(1.43)	1.35
4	(1.65)	1.36
5	-	1.18
6	-	1.42

* The numbers in the parentheses are the estimated values.

Apart from the average length of the icicle, it is necessary to know its geometrical characteristics, for example the inclination of the icicles forming on the different BSs. According the images of the experimental tests, the inclination of icicles on the first BS is different from the other BSs. It is due to the fact that these icicles are growing in the strong electric field strength and water molecules are bipolar. So, the icicles grow in the direction of the equipotential line distributions of the insulator.